MASS TRANSPORT CONTROL

OF

NON - FERROUS PYROMETALLURGICAL PROCESSES

by

C.L. HARRIS, B.Eng.(Met.)

A thesis submitted for the degree of Doctor of Philosophy of the University of London.

John Percy Research Group,
Department of Materials,
Royal School of Mines,
Imperial College,
LONDON.

June 1989.

ABSTRACT.

Two distinctly different non-ferrous pyrometallurgical processes were studied, namely the decoppering of lead and slag cleaning. Both were subjected to computer modelling based on coupled reaction multi-component transport control theory described by Robertson et al.(Iron and Steelmaking, Vol.11, No.1, 1984). A significant extension to the theory was added by considering the effect of diffusion in the solid phase as being rate limiting. In each, relevent bench scale experiments were carried out for comparison with model predictions. Comparison with experimental results of other authors was also performed. In all cases, good agreement was achieved.

From this, the validity of estimates of mass transfer and diffusion coefficients input into the model has been assessed, and the validity of a newly proposed mechanism for decoppering reinforced.

C O N T E N T S

	Page.
Abstract	ii
Contents	iii
List of Figures	vii
List of Tables	x
List of Plates and Appendicies	xi
Section One : The Reduction of Non-Ferrous Values From Slags.	1
1.0 Introduction	2
1.1 Slag cleaning	2
1.2 Multi-component Transport Control Theory for Kinetics for Coupled Metal/Slag/Gas Reactions	6
1.3 Idealized Slag Cleaning Conditions	7
1.3.1. Complex Slags	7
1.3.2. Simple Slags	10
2.0 Reactions at Interfaces and Mathematical Formulation	12
2.1 Metal/Slag Interface	12
2.2 Slag/Gas Interface	15
2.3 Metal/Gas Interface	16

Page.

3.0 Model Inputs 17

3.1 Thermodynamics 17

3.2 Phase Densities 17

3.3 Transport Properties 17

3.4 Interfacial Areas and Phase Volumes 21

3.5 Comparisons with "real" Conditions 22

3.5.1 Metallic Phase 22

3.5.2 Slag Phase 24

4.0 Experimental Procedure and Results 27

4.1 Production of Master Alloys and Slags 27

4.1.1 Alloy Production 27

4.1.2 Slag Production 28

4.2 Slag Cleaning Experiments 30

4.2.1 Experimental Apparatus 31

4.2.2 Experimental Procedure 33

4.3 Results 34

5.0 Model Output 37

5.1 Modelling Strategy 37

5.2 Application of the Model to Toguri's Experiments 37

5.3 Application of the Model to the Current Experiments. 40

5.4 Application of the General Model to Hypothetical Slag Cleaning Conditions. 43

5.5 Dimensionless Time 54

Page.

6.0 Discussion 57

6.1 Model Predictions 57

6.1.1 "Standard" Conditions 59

6.1.2 The Effect of Bulk FeO Activity 63

6.1.3 The Effect of High Gas Phase Oxygen Potential 65

6.1.4 The effect of increasing temperature 66

6.1.5 The effect of low initial iron activity 69

6.1.6 The effect of increasing metal/slag mass ratio 70

6.2 Model Validity 71

6.3 Model Development 73

Section Two : The Decoppering of Liquid Lead Bullion By Elemental Sulphur Additions. 75

7.0 Introduction 76

8.0 Theoretical Considerations 80

8.1 Basis of Model 80

8.2 The Effect of Silver 82

9.0 Kinetic Model for Decoppering 86

9.1 Decoppering 86

9.2 Reversion 88

9.3 Model Applicability 90

9.4 Mathematical Formulation 92

Page.

10.0 Experimental Procedure and Results 95

10.1 Aim of Experimental Programme 95

10.2 Determination of Diffusion Coefficients 95

10.3 Preparation of Pb/Ag Alloy Pellets 96

10.4 Sulphide Layer Growth Experiments 97

10.5 Initial Experimental Development 104

10.6 The Effect of Temperature 104

10.7 The Effect of Ag Concentration 105

10.8 Model Output 108

11.0 Discussion 112

11.1 The Effect of Silver 115

12.0 Conclusions. 120

12.1 Slag Cleaning 120

12.2 Decoppering 121

Bibliography 123

Appendicies 132

Acknowledgements 165

LIST OF FIGURES Page.

1. Schematic Diagram of Slag Cleaning Showing Flux Densities, Interfacial Activities, and Bulk Concentrations. 9

2. Slag Cleaning Experimental Apparatus 32

3. Copper Reduction Rate and Iron Transfer Rate Using a Cu-Fe Alloy Under a p_{O_2} of 10^{-7} atm. in Copper Bearing Fayalite Slag at 1200°C. 38

4. As for Figure 2, but under a p_{O_2} of 5.0×10^{-11} atm. 39

5. Nickel Reduction Rate, Iron Transfer Rate, Slag Copper Pick-Up Rate, and Metal Nickel Pick-Up Rate Using a Cu-Fe Alloy Under a p_{O_2} of 10^{-7} atm. in Nickel Bearing Fayalite Slag at 1200°C. 41

6. As for Figure 3, but under a p_{O_2} of 5.0×10^{-11} atm. 42

7. Concentration of Species in Slag and Metallic Phases versus Time Under " Standard " Conditions. 46

8. As for Figure 6, but with a_{FeO} set to 0.1. 48

9. As for Figure 6, but with a_{FeO} set to 0.6. 49

10. As for Figure 6, but with $p_{O_2} = 10^{-7}$ atm. 50

11. As for Figure 6, but with Temp. = 1500°C. 52

12. As for Figure 6, but with Initial Iron Concentration in the Metallic Phase = 0.1 Wt%. 53

13. As for Figure 6, but with Metal/Slag Mass Ratio = 1.0. 55

Page.

14. Flux of Species Being Reduced at the Slag/Gas Interface Under " Standard " Conditions. 60

15. Metal/Slag Interfacial Oxygen Activity versus Time for " Standard " Conditions. 60

16. Flux Densities of FeO and $FeO_{1.5}$ To and From the Metal/Slag Interface. 61

17. As for Figure 15, but To and From the Slag/Gas Interface. 61

18. Oxygen Activity at the Metal/Slag Interface versus Time for a_{FeO} = 0.1 and 0.6. 64

19. Fluxes of Species Being Reduced at the Slag/Gas Interface versus Time with Temp. = 1500^{o}C. 68

20. As for Figure 17, but with a_{FeO} = 0.4 and Initial Iron Concentration in the Metallic Phase = 0.1 and 5.0 Wt%. 68

21. Partial Gibbs Free Energy of Mixing in the Pb-S System. 81

22. Partial Gibbs Free Energy of Mixing in the Cu-S System. 83

23. The Effect of Ag Concentration in PbS on the Position in Layer of p-n Junction versus RT ℓn ($p_{S_2}^{1/2}$). 84

24. Schematic Model of the Early Stages of Decoppering. 87

25. Schematic Model of the Latter Stages of Decoppering. 89

26. Schematic Model of Reversion. 91

27. Steel Mould for Chill Casting Pb Pellets 98

Page.

28. Decoppering Experiment Vertical Tube Furnace. 100

29. Log Diffusion Coefficient of Pb in PbS versus Inverse Temperature. 106

30. Log Diffusion Coefficient of Pb in PbS versus Ag Concentration in Pb Pellet. 107

31. Copper Concentrations in Bulk Lead and Sulphide Layer Thicknesses versus Time. 110

32. Occurence of the p-n Junction as a Function of Temperature and Sulphur Potential. 116

LIST OF TABLES. Page.

1. Typical Analyses of Potential Slags Suitable For Slag Cleaning Treatment. 4

2. ΔG^{o} Model Input. 18

3. Activity Coefficients at Infinite Dilution (γ_{M}^{o}) in Liquid Copper. 19

4. Activity Coefficients at Infinite Dilution ($\gamma_{MO_{\sigma}}^{o}$) in Liquid FeO - SiO_2 Slags. 19

5. Interaction Parameters for Solutes in Metallic Copper at 1300°C. 23

6. Chemical Analyses of Master Alloys and Master Slag. 29

7. Experimental Conditions and Results. 35

8. Equilibrium Constants at 1200°C and 1500°C. 67

9. Published Diffusion Coefficients. 79

10. Chemical Analysis of Lead Pellets. 99

11. Pb in PbS Diffusion Coefficient versus Temperature. 106

12. Pb in PbS Diffusion Coefficient versus Silver Concentration. 107

LIST OF PLATES. Page.

1. Micrographs of Phases Present During Layer Growth 102
Experiments on Pure Lead and a Silver Doped Lead.

2. Micrograph of Phases Present During Layer Growth 103
Experiments on Pure Copper.

3. Micrograph of Phases Present 30 Seconds after the 111
Commencement of Decoppering in the Presence of Ag.

4. Micrograph of Phases Present 3 Minutes after the 111
Commencement of Decoppering in the Presence of Ag.

5. Micrograph of Phases Present at the Conclusion of 111
Decoppering in the Presence of Ag but Before Reversion
Commences.

LIST OF APPENDICIES

1. Slag Cleaning Model Mathematical Formulation. 132

2. FORTRAN Coding of Slag Cleaning Model. 138

3. Listing Of Data Input Files 145

a) Toguri Experiment Simulation

b) Current Experiment Simulation

c) Idealized Slag Cleaning Simulation

4. Decoppering Model Mathematical Formulation. 151

5. Typical Layer Thickness Measurements and 157
Explanation of Mathematical Manipulation.

6. Fortran Coding of Decoppering Model and Listing Of 159
Data Input File.

LIST OF SYMBOLS.

Symbol	Description	Fortran Name	
		Slag Cleaning. Model	Decop. Model
A	Interfacial Area (m^2)	AMS, ASG, AMG	AREA
a	Activity(dimensionless)	A	A
C	Bulk Molar Conc.(mol/m^3)	C1, C4, C6	C
c	Local Molar Conc.(mol/m^3)		
D	Diffusion Coeff.(cm^2/s)	D	-
ΔG^o	Gibbs Free Energy(cal/mol)		
$\Delta \bar{G}_M$	Partial Gibbs Free Energy of Mixing (cal/mol)		
J	Flux (mole/sec)	XJ	-
K	Equilibrium Const.	E	E
k	Mass Trans. Coeff. (m/s)	K	DK
M	Metal		
MO_σ	Metal Oxide		
N	Flux Density ($mol/m^2/s$)	-	XN
O	Oxygen		
p	pressure		
t	Time		
T	Temperature		
V	Volume		
V	Vacancy		
x	mole fraction		
[ ]	In Solution		

Symbol	Description	Fortran Name	
		Slag Cleaning. Model	Decop. Model
()	Gaseous		
γ	Activity Coefficient	AC	AC
Σ	Summation		
σ	Stoichiometric Constant	Z	Z
τ	Layer Thickness (m)	-	LT
μ	Chemical Potential		

SECTION ONE.

THE REDUCTION OF NON-FERROUS VALUES FROM SLAGS.

1.0 Introduction

1.1 Slag Cleaning

Reduction of non-ferrous metal values from slags is currently the subject of considerable research and development efforts in the extractive metallurgy industry. The growing importance of such "slag cleaning" operations can be attributed to the following factors.

1) The widespread introduction of flash smelting of sulphides and the trend to the production of higher grade mattes in the copper and nickel industries have led to increased metal losses to the slag phase during smelting. Furthermore, efficient recovery of values from converter slags by slag recycled to the smelting stage has also been effectively been prevented, thus necessitating separate slag cleaning treatments. Slag cleaning is also of crucial importance in all proposed processes for continuous production of copper and lead.

2) In many cases, recent attempts at the exploitation of complex ores have involved the production of complex multi-component slags that contain non-ferrous values demanding subsequent metal recovery procedures.

The technology, economics,and phyiochemical aspects of slag cleaning have been considered in a number of recent comprehensive review articles[1-3]. In pyrometallurgical slag cleaning, two mechanisms of metal recovery can be identified.

1) Chemical reduction of dissolved metal into either metallic or matte phases by means of a reductant.

2) Physical settling of dispersed or entrained metal and/or matte particles from the slag phase.

Electric furnaces heated via submerged electrodes , top blown rotary converters, and Sirosmelt submerged combustion reactors all have been employed for slag cleaning purposes. Optimization of the reactor conditions and metal recovery in such operations is obviously of prime importance in determining their economic viability.

Slag cleaning by reduction of values into the metallic phase will involve simultaneous oxidation into slag, reduction from slag and volatilization of species from metal and slag phases. Because of the complexity of the slags (see table(1)) and the multi-component nature of the metallic phases likely to be found in a slag cleaning reactor, at present little understanding of the interaction of the many coupled and competing reactions is held. Thus, it was considered important to develop a multi-component model, based on presently available fundamental data of chemical reactions involved.

The model specifically concentrates on conditions likely to be encountered towards the end of a slag cleaning operation where a copper rich metallic phase is in contact with an iron oxide rich slag. Even under idealized representations of such conditions, the model development process has highlighted the lack of some essential fundamental data.

Insights into the values of this missing data were gained by

Table 1. Typical Analyses of Potential Slag for Slag Cleaning Treatment. (Ref. (3) for Cu, Ni, and Pb; Ref. (1) for Zn and Complex Materials.)

Primary Metal Extracted	Process Source.	Compostition (Wt.%).						
Copper		Cu	Fe	SiO_2				
	Flash	1-2	30-45	25-40				
	Reverb	.2-.7	25-40	35-40				
	Electric	.3-.7	30-40	32-40				
	Noranda	11	34	20				
	Convert.	2-15	35-50	20-30				
Nickel		Ni	Cu	Co	Fe	SiO_2	CaO	MgO
	Flash							
	Inco	0.39	0.14	0.18	37	38	2.4	-
	Outokump	.7-1.2	-	0.05	43	30	-	-
	Reverb.	0.2	0.1	0.08	38	36	2.0	-
	Electric	0.16	-	-	21	45	-	21
Lead		Pb	Cu	Zn	Fe	SiO_2	CaO	
	Blast Fur	3-4	.2-.7	10-12	25-30	20-25	9-14	
	Electric	4	0.08	17	8	24	34	
	TBRC	1-2	-	15	22	23	20	
Zinc		Zn	Pb	Fe	Mn	SiO_2	CaO	Al_2O_3
	Fum. B.F.	25.3	2.3	22.0	3.0	20.8	14.0	5.9
Complex		Cu	Pb	Sn	Zn	Fe	SiO_2	CaO
To Metal	TBRC	-	35	1.3	16	22	33	20
To Matte	TBRC	7.5	11.3	-	9.7	40	-	-

studying simple systems related to slag cleaning conditions. Experimental results published in literature[54] were analyzed. Further experiments on simple systems not previously investigated were also carried out to aid in estimating the unknown but essential fundamental data. These estimates were implemented into the model, which was then applied to complex slags to arrive at conclusions applicable to industrial slag cleaning processes.

The model is, in its current state, not specific to any particular reactor. The principles involved can be extended with some modification to slag cleaning procedures involving the production of either a matte phase or of both matte and metallic phases. However, it should be noted that the account is only taken of the chemical reaction of dissolved metal in the slag as a means of slag cleaning. The physical settling of the dispersed metal and matte particles requires a separate model taking into account the effects of slag, matte and metal physical properties(such as composition, viscosity, density, and interfacial tension), the size of dispersed particles and the degree of stirring in the cleaning operations. Ultimately, combination of such models would be required for complete process modelling of commercial slag cleaning operations.

1.2 Multi-component Transport Control Theory for Kinetics for Coupled Metal/Slag/Gas Reactions

Robertson and co-workers[4] have presented a generalized theory for the kinetics of metal/slag/gas reactions, taking into account the coupled nature of such reactions, which may be applied to ferrous and nonferrous systems. The theory assumes that

1) the chemical reactions at the interfaces between the metal, slag, and gas phases are rapid and equilibrated at any time, and that

2) the reaction rates are determined by mass transfer kinetics in metal, slag, and gas phases.

The "thin film" diffusion model is applied where the bulk phases are assumed to be well mixed and of uniform concentration, whilst the gradient of concentration of the species is confined to a thin film facing the interface. Transport across such thin films is treated by defining mass transfer coefficients for each species in each phase, the value of which needs to be estimated, predicted, or experimentally determined. Consideration of species flux density equations, limitations of equilibria at interfaces, and mass balances permit simultaneous solution of fluxes of species to and from the interfaces at a given time. In principle, if sufficient fundamental information is available, chemical control of species reactions can be accounted for by the incorporation of "pseudo" mass transfer coefficients or functions for specific species by permitting

deviations from equilibrium to occur at interfaces. Models based on this multi-component transport theory have been developed for ferrous systems involving the simultaneous desulphurization and dephosphorization of pig iron by lime based fluxes[4-7] and the decoppering and detinning of pig iron and liquid steel via sodium sulphide additions[8] amongst other applications.

The purpose of this work was to investigate the possibility of the application of Robertson's multi-component transport theory to process modelling of the reactions involved in the reduction of non-ferrous metals from both slags of commercial interest and simple binary and ternary slags. As such, this work represents the first application to a complex non-ferrous system.

1.3 Idealized Slag Cleaning Conditions

1.3.1 Complex Slags

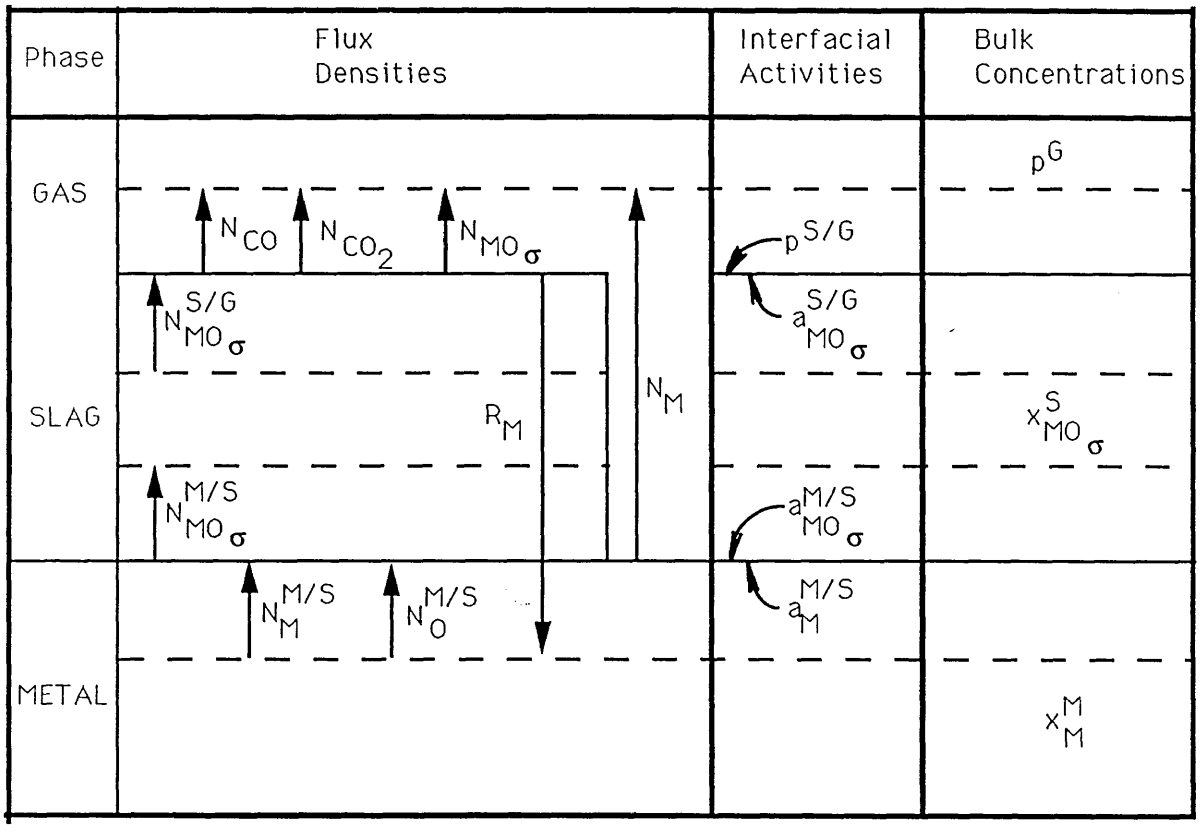
During the initial stages of industrial slag cleaning process of the kind to be modelled, a solid iron metallic phase is typically contacted with a $FeO-CaO-SiO_2$ based slag containing metal values(typically Cu, Pb, Zn,and Ni). The process proceeds via simultaneous oxidation of iron and dissolution of FeO into the slag phase, reduction of metallic values into a liquid metal phase and the vaporization of volatile species(typically SnO, PbO, Pb, Zn, Cu). During this early stage, the slags can be very concentrated in metal values and may therefore contain two or more phases, although

little is known of either the phase relationships or the solution thermodynamics of individual phases of such complex systems. As a result of the oxidation and the reduction of metallic values, by the later stages of the slag cleaning process, a liquid metallic copper based phase will be in contact with a slag dilute in non-ferrous metal values. Simultaneous oxidation into slag, reduction from slag, and volatilization will still be proceeding. This later stage of a slag cleaning operation provides the most convenient subject for process modelling and investigation as the presence of a solid metallic iron phase and a concentrated, possibly multi-phase slag are avoided. This stage is also of the most immediate practical concern as the ultimate degree of metal recovery and the time required to achieve such recoveries are major factors influencing process economics. However, in the long term, a complete understanding of slag cleaning will require that account is taken of the earlier stages of the process.

Idealized conditions meant to represent the later stages of slag reduction were chosen for model development as follows. The reaction between a copper based metallic phase dilute in Fe, Sn, Ni, Zn, and Pb in contact with a silica-saturated fayalite type slag containing dilute levels of SnO, Cu_2O, NiO, ZnO, and PbO, shown schematically in figure(1), was considered.

The developed model allows both direct contact between metal/gas and metal/slag/gas. The respective direct interfacial areas are required inputs. Because of

Figure 1. Schematic Diagram of Slag Cleaning Model Showing Flux Densities, Interfacial Activities and Bulk Concentrations.



limitations in available thermodynamic data, the modelling was limited to dealing with dilute solutions in metal and slag phases where Henry's Law can be considered a reasonable approximation and the relationship between chemical activity and species concentration can be estimated with some confidence. This approximation was achieved by limiting all non-ferrous oxides in the slag phase to mole fractions of less than 0.05. In order, therefore, to keep the metal values present at dilute levels on the liquid copper, limitations were placed on the range of slag/metal volume ratios that were investigated. For simplicity, the phase densities were assumed to remain constant throughout the process.

1.3.2 Simple Slags

Although industrially encountered non-ferrous slags which hold interest as feedstock to a slag cleaning process are generally complex, studies of simple slag systems will give insight into the more complex conditions. Toguri[54] has studied the kinetics of reducing copper from an $FeO-SiO_2$ slag into a copper rich metallic phase containing iron at $1200^{o}C$. These experiments were modelled using the method described earlier and comparisons drawn with the experimental results.

A more complex system where the slag phase contained nickel, replacing copper in Toguri's slag, was studied in this work. The constraints described in the previous section were also applied to the models, namely restricting solutions to high dilutions, limiting phase volume ratios and inputting

interfacial areas. In addition to the above assumptions, the species in these particular simple systems display little volatility, so metal and oxide volatilization was ignored.

2.0 Reactions at Interfaces and Mathematical Formulation

2.1 Metal/Slag Interface

It is assumed that coupled reactions of the type

$$[M]^M + \frac{1}{2}\sigma\,(O) = [MO_\sigma]^S$$

occur, and are at equilibrium. The metallic $[M]^M$ components as well as oxygen in solution in the metal are transferred to and from the interfaces, as are the oxides $[MO_\sigma]^S$ dissolves in the slag. Carbon/oxygen reactions at this interface are neglected at this stage, but should be considered at some later point in time, having a strong effect on the oxygen potential. Effectively, it has been assumed that no carbon, either from reducing gases or solid reductants, has dissolved into the metallic phase. The dissolution of carbon in the metallic phase can also cause further problems in process modelling as it then permits the nucleation of CO bubbles in the metal phase. Robertson(4) has considered this problem in his modelling of pig iron desulphurization/dephosphorization and, in principle, similar approaches could be used here.

Reactions and Equilibria Equations

$$[M]^M + \tfrac{1}{2}\sigma(O_2) = [MO_\sigma]^S$$

$$K_{MO\sigma} = a_{MO\sigma} / (a_M \cdot p_{O_2}^{(1/2.\sigma)})$$

$$[O]^M = \tfrac{1}{2}(O_2)$$

$$K_O = p_{O_2}^{(1/2)} / a_O$$

$$a_M = x_M \gamma_M$$

$$a_O = x_O \gamma_O$$

$$a_{MO_\sigma} = x_{MO_\sigma} \gamma_{MO_\sigma}$$

Flux Equations

$$J_M = A^{M/S} C^M k_M (a_M^b - a_M^i) / \gamma_M$$

$$J_O = A^{M/S} C^M k_O (a_O^b - a_O^i) / \gamma_O$$

$$J_{MO} = A^{S/G} C^S k_{MO_\sigma} (a_{MO_\sigma}^i - a_{MO_\sigma}^b)$$

Conservation Equations at Interfaces

Metals

$$J_M = J_{MO_\sigma}$$

Oxygen

$$J_O = \Sigma \sigma J_{MO_\sigma} = \Sigma \sigma J_M$$

Conservation Equations in the Bulk

$$J_M = dx_M / dt \cdot C^M \cdot V^M$$

$$J_O = dx_O / dt \cdot C^M \cdot V^M$$

$$J_{MO_\sigma} = dx_{MO_\sigma} / dt \cdot C^S \cdot V^S$$

At time, t equals zero, all bulk concentrations are known. Thus, all flux equations becomes functions of the unknown interfacial activities only.

Substitution of equilibrium equations can eliminate one set of interfacial activities a_M^i for example, and only introduce p_{O_2}. Substituting these modified flux equations into the metal conservation equations, followed by some manipulation, results in a set of equations giving interfacial activities as a function of p_{O_2}. Substituting for interfacial activities into the oxygen conservation equation will result in an equation in p_{O_2} only. This can be solved numerically.

Having the interfacial oxygen potential, one can back-calculate all other interfacial activities and thus fluxes at that point in time. Making a quasi-steady-state assumption, an incremental time step can be input into the bulk conservation equations to arrive at new estimates of bulk concentrations after this time interval. The entire solution procedure can be repeated to advance through time. An algebraic version of this explanation can be found in

appendix 1,Section(a).

2.2 Slag/Gas Interface

Two types of reaction occur at the interface. The first is the same as at the metal/slag,only differing in that ,

(1) oxygen is present as a gas and not dissolved in the metal phase, and

(2) metal, at a high activity is being produced by reduction.

The second type of reaction is the simple volatilization of metal oxides to the gas phase.

$$[MO_\sigma]^S = [MO_\sigma]^G$$

The solution technique for this interface is similar in principle to the metal/slag interface method, differing in only two ways,

(1) Volatilization of oxides results in the conservation equation being more complex, and

(2) there are no flux equations available for the fluxes of metals being produced by reduction at this interface. Thus, if reduction is occurring, the interfacial activities of the metals must be set (in our case, to unity). Details of this solution can be found in appendix 1,Section (b).

2.3 Metal/Gas Interface

Volatilization reactions of the following type only were considered.

$$[M]^M = (M)^G$$

Because of the reducing nature of the gas phases under consideration, reoxidation of the metallic phase was not included in this model.

This is a simple volatilization problem. Flux equations give unknown interfacial partial pressures and activities, which can be related by equilibrium equations. These equations are not coupled, so solution is trivial. Details are shown in appendix 1, Section(c).

A full listing of the FORTRAN coding is provided in appendix (2).

3.0 Model Inputs

3.1 Thermodynamics

Standard Gibb's free energies of reaction (ΔG^0) were taken from Turkdogan[9], JANAF tables[10], Nagamori[11] and are summarized in table(2). Values for the activity coefficients of species in metallic copper and silica-saturated $FeO-SiO_2$ slags, collected from literature and employed in the model, are summarized in Tables (3) and (4) respectively.

3.2 Phase Densities

The metallic phase was assumed to have a constant density of 7500 $kg.m^{-3}$ and the slag phase a constant density of 3500 $kg.m^{-3}$. This is quite a reasonable assumption to use within the model because it simulates the final stages of slag cleaning where we would not expect to see very large changes in bulk composition. However, larger composition changes nearer the commencement of an industrial slag cleaning process would invalidate this simple treatment, and require a much more elaborate method to estimate phase densities.

3.3 Transport Properties

Transport properties in the metal and especially in the slag phase are not well known. However, experience gained over recent years from kinetic studies in a wide range of

Table 2. ΔG^{o} Model Input (Ref. (9) unless otherwise stated).

Reaction	ΔG^{o} (cal)	
$CO = C + \frac{1}{2} O_2$	27340 + 20.50T	
$CO_2 = C + O_2$	94490 + 0.13T	
$CO + \frac{1}{2} O_2 = CO_2$	-67150 + 20.37T	
$Cu(l) + \frac{1}{4} O_2 = CuO_{0.5}$	-14190 + 4.72T	
$Cu(l) = Cu(g)$	73650 - 26.02T	
$Fe(l) + \frac{1}{2} O_2 = FeO$	-61200 + 12.83T	
$Fe(l) + \frac{3}{4} O_2 = FeO_{1.5}$	-97290 + 30.00T	
$Pb(l) + \frac{1}{2} O_2 = PbO(l)$	-43300 + 16.26T	
$Pb(l) = Pb(g)$	43490 - 21.54T	
$PbO(l) = PbO(g)$	51270 - 28.69T	ref. (10))
$Ni(l) + \frac{1}{2} O_2 = NiO(s)$	-60490 - 22.99T	
$Sn(l) + \frac{1}{2} O_2 = SnO(l)$	-62690 - 20.69T	
$SnO(l) = SnO(g)$	57990 + 32.27T	(ref(11))
$Zn(g) + \frac{1}{2} O_2 = ZnO(s)$	-110000 + 47.40T	
$Zn(l) = Zn(g)$	28230 - 23.96T	

Table 3. Activity Coefficients at Infinite Dilution (γ_M^0) in Liquid Copper. Ref(12)

Metal	RT $ln\ \gamma_M^0$ (cal)	γ_M^0 1300°C/1573K
Fe(l)	9300 - 0.41T	15.95
Ni(l)	2340	2.11
Pb(l)	8620 - 2.55T	4.37
Sn(l)	-8900	0.058
Zn(l)	-5640	0.165

Table 4 Activity Coefficients at Infinite Dil($\gamma^0_{MO_\sigma}$) in FeO-SiO_2 Slags. Ref(13)

MO_σ	$\gamma^0_{MO_\sigma}$	γ^0 1300°C/1573K
$CuO_{0.5}$(l)	$\gamma^0 = 3.0$	3.0
NiO(s)	$\log_{10}\gamma^0 = \frac{3050}{T} - 1.31$	4.26
PbO(l)	$\gamma^0 = 0.07$	0.07
SnO(l)	$\log_{10}\gamma^0 = \frac{8800}{T} - 5.70$	0.78
ZnO(s)	$\log_{10}\gamma^0 = \frac{400}{T}$	1.80

In FeO - SiO_2 saturated a_{FeO}(l) = 0.4 (Richardson (14))

pyrometallurgical systems enable fairly confident order of magnitude estimates of the required mass transfer coefficients. More accurate predictions of mass transfer coefficients of individual species are likely to be unreliable.

Mass transfer coefficients implemented in the simulation of the bench scale were more closely determined. Having collected information relating composition of the phases as a function of time, and having reasonably confident estimates of all other physical and chemical parameters, we are able to match predicted rates of reaction with observed rates to determine the mass transfer coefficients applicable to these circumstances. It must again be noted that these mass transfer coefficients are effective values, being defined as a parameter to describe movement of species to, across and away from phase boundaries, and have little bearing on the more rigorously defined transfer coefficients of ideal species travelling in perfectly homogeneous fluids with perfect interface contact and instantaneous reaction at these interfaces. Thus, these experimentally values are particular to the experimental conditions.

In industrial practice, the actual mass transfer coefficients achieved will be a function of the type of reactor employed, the mixing conditions achieved in the process and the slag and metal compositions.

Available data on mass transfer coefficients of species in liquid copper and fayalite type slags[1,13,15] indicate comparable values in the range of $D = 10^{-4}$ to 10^{-5} cm.s with

the metal phase diffusion coefficient normally a small but not insignificant amount larger. In any given phase, all species have initially been assumed to have the same mass transfer coefficient.

To minimize running time of the developed computer program, consideration of the gas phase was simplified by setting the slag/gas interfacial oxygen potentials. This procedure effectively assumes infinitely large oxygen gas phase mass transfer coefficients. The model can easily be developed to account for significant gas phase mass transfer resistances by numerical solution of the interfacial oxygen potentials from known bulk gas compositions and gas phase mass transfer coefficients.

3.4 Interfacial Areas and Phase Volumes.

As with the mass transfer coefficients, the interfacial areas present during industrial slag cleaning will be dependant upon the type of reactor employed and the mixing conditions achieved. For the simulations relating to the bench scale experiments, a planar interface between the slag and metal, which maintains perfect contact at all times, was assumed. This is justified by considering the large density difference between the two phases, and only the configuration where no stirring other than convection is occurring, as is the case of an unstirred radiation-heated crucible as used in all experiments considered. To arrive at the actual estimates used, the description of apparatus and burden given by Toguri

was used to calculate the interfacial areas of his experiments, whilst direct measurement was possible on the crucibles and burdens was possible in this current work. Estimates were used for modelling of industrial slag cleaning process simulations, these values being widely varied according to the process under consideration. Ultimately, for full process simulation, a mixing model must be employed to estimate the interfacial areas.

3.5 Comparison with "Real" Conditions

The idealized conditions chosen for this, an initial computer modelling development, contained some serious limitations compared to the real conditions they were meant to represent. These are discussed below.

3.5.1 Metallic Phase

The activity coefficients given in table (3) strictly only apply in dilute binary solutions of metallic copper (Henry's Law). An extension to slightly more concentrated and multi-component solutions can be made by use of interaction coefficients collected and compiled in table(5). In reality, however, final metal analyses in pilot plant slag cleaning trials indicate that the final metal phase can be typically a concentrated alloy of Cu-Sn-Pb or Cu-Sn-Ni containing Zn, Ni, Pb, and Fe at dilute levels. Some measurements[16,18] of Cu, Sn, and Pb activities in liquid ternary Cu-Sn-Pb alloys are available, but extrapolation would be required for

Table 5. Interaction Coefficients for Solutes in Metallic Copper at 1300°C (Ref. (12))

$$\varepsilon_i^i = \frac{\delta \, n \, \gamma^i}{\delta \, Ni}$$

$$\varepsilon_{Fe}^{Fe} = -5.7$$

$$\varepsilon_{Ni}^{Ni} = \text{unknown}$$

$$\varepsilon_{Pb}^{Pb} = -2.7$$

$$\varepsilon_{Sn}^{Sn} = 10$$

$$\varepsilon_{Zn}^{Zn} = 4.0$$

application to slag cleaning conditions. It would also be necessary to estimate coefficients of Zn , Ni, and Fe when present in Cu-Sn-Pb on the basis of their known activity coefficients at infinite dilutions in Cu, Pb, and Sn. A recent review of the phase diagrams and thermodynamic properties of ternary copper systems highlights the lack of fundamental data for some of the ternary systems liable to be of interest to slag cleaning operations, not even taking into account the uncertainties involved in considering higher component concentration systems of real concern.

3.5.2 Slag Phase

In reality, the slag phase present in actual slag cleaning operations will be in the complex FeO - Fe_2O_3 - Al_2O_3 - SiO_2 system, rather than the simple FeO - SiO_2 saturated fayalite type slags. There are some limited data available (Floyd and Mackey[1], Rankin and See[20] on the effect of CaO and Al_2O_3 on slag component activities but these refer mainly to Fe and Cu oxides. Activity/composition relationships for components such as ZnO, SnO, NiO, and PbO in these slags are not well known. The absence of such data seriously hinders the prediction of the potentially beneficial effects of flux additions on slag cleaning performance.

In the application of the model the iron oxide activity (a_{FeO}) has been held constant in the bulk slag. This consideration effectively assumes that the slag is always silica saturated, that there is an available reservoir of SiO_2 to instantaneously maintain the conditions of silica

saturation as more iron is oxidized into the slag phase, and that the reduction of other metal oxides does not produce changes in the iron oxide activity. An estimate of the value of a_{FeO} can be made on the basis of available data[14] for the simple binary FeO - SiO_2 slags(a_{FeO} = 0.4).

Although we are setting the activity of FeO to a constant value to reflect silica saturation, this simplification must be used in combination with allowances for the presence of both ferric and ferrous oxides. The oxygen transfer rate into and out of the slag phase to the gas phase is likely to be governed to a large extent by the rate at with FeO and Fe_2O_3 can arrive and leave the slag/gas interface. Similarly, the rate at which iron can enter the slag from the metallic phase to alter the bulk slag oxygen potential will be governed by ferric and ferrous oxide diffusion. Ohguchi[5] ignored the effect of Fe^{3+} when modelling dephosphorization / desulphurization.

The presence of Fe^{3+} in the slag encountered in processes subject to very to moderately low oxygen potentials (eg. ironmaking, dephosphorization/desulphurization) may not be significant, but the relatively less reducing atmospheres found in slag cleaning causes a significant concentration of Fe^{3+} to be present.

The model defines diffusing species in the slag phase as metal oxides (MO_σ) only. Thus, in its current form, diffusion of free ionic Fe cannot be directly accounted for. This may be a serious oversight, but can be partially countered by allowing rapid $FeO_{1.5}$ movement if it becomes

apparent that correction is required.

4.0 Experimental Procedure and Results

A series of experiments were performed to study a system in which a nickel laden fayalite slag was brought into contact with a liquid copper-iron solution to measure the kinetics of nickel removal from the slag and iron pick-up by the slag. The experiments were designed to conform as closely as possible to those performed by Toguri[54], varying only in that the fayalite slag was contaminated with nickel in our experiments rather than copper as in Toguri's. This meant that we can make direct comparisons of results, producing good estimates of the mass transfer parameters by finding those which apply well to both sets of experimental results, all other process parameters being held constant.

4.1 Production of Master Alloys and Slags

4.1.1 Alloy Production

A quantity of electrolytic pure iron powder(99.99 wt%Fe) was placed into a 250ml alumina crucible. On top of the powder, a 1 kg block of electrode purity copper(99.999 wt%Cu) was placed. The crucible was placed into a graphite susceptor, which in turn, was placed into a large ceramic holder. The assembly was inserted into the induction coil of a Leybold-Hereaus vacuum induction furnace. The pressure was gently lowered to 10^{-6} atmospheres, then the chamber back-flushed with nitrogen. It was then re-evacuated and sealed. The low oxygen potential was sought to avoid

oxidation of the Fe powder which was expected to float to the surface of the melt, and to avoid decomposition of the carbon susceptor.

The temperature was raised to 1400^{o}C and held for 15 minutes. Virtually no oxide was formed on the surface, that being present probable surface oxidation on the original additives. Induction stirring was considerable, the melt surface being highly domed while the electrical field was present. The molten alloy was now cast into a thermally massive room temperature steel mould to ensure rapid solidification, the ingot shape being bars approximately 15mm in diameter and 150mm in length.

These bars were sectioned at regular intervals, each section weighing about 20g, polished and micro-inspected to check for homogeneity. The specimens were then sent for chemical analysis via atomic absorption spectrometry to further check for homogeneity and to determine accurate composition. The analytical results are shown in table(6).

4.1.2 Slag Production

The aim was to produce a uniform batch of silica-saturated fayalite type slag containing approximately 4 wt% Ni. Stoichiometric quantities of Fe, Fe_2O_3, and SiO_2 powder were mixed together along with sufficient NiO to obtain the required composition. The powder was uniformly mixed and carefully placed in a 500ml pure silica crucible, which was then slid into a larger graphite crucible that was to act as a susceptor for the induction heating. The assembly was

Table 6. Chemical Analyses of Master Alloys and Master Slag.

Master.	Sample.	Wt% Cu	Wt% Fe	Wt% Ni
Cu-Fe Alloy	I(a)	-	4.01	<0.005
	(b)	-	4.02	"
	(c)	-	3.96	"
	Average	-	4.00	"
	II(a)	-	2.36	"
	(b)	-	2.31	"
	(c)	-	2.29	"
	Average	-	2.32	"
	III(a)	-	0.10	"
	(b)	-	0.13	"
	(c)	-	0.12	"
	Average	-	0.12	"
Slag	Slag(a)	0.01	-	3.92
	(b)	0.01	-	3.74
	(c)	<0.01	-	3.64
	Average	<0.01	-	3.77

placed into the furnace mentioned above. The chamber was gently evacuated so as to avoid any loss of powder due to "dusting"(as the air departs from between the powder particles, it can carry particles with it). Nitrogen back-flushing was again carried out, then the temperature was raised to 1350^{0}C and held for 30 minutes. It was necessary to shake the crucible to cause the slag to slop about to get all the powder to collapse into the melt and be dissolved.
The furnace was allowed to cool, more powder was added, and the melting procedure was repeated to ensure sufficient slag was produced. After final cooling, the crucible was broken away from the slag, the slag crushed and milled and sent for analysis. The results of this analysis of a few random powder sample are shown in table(6).

4.2 Slag Cleaning Experiments

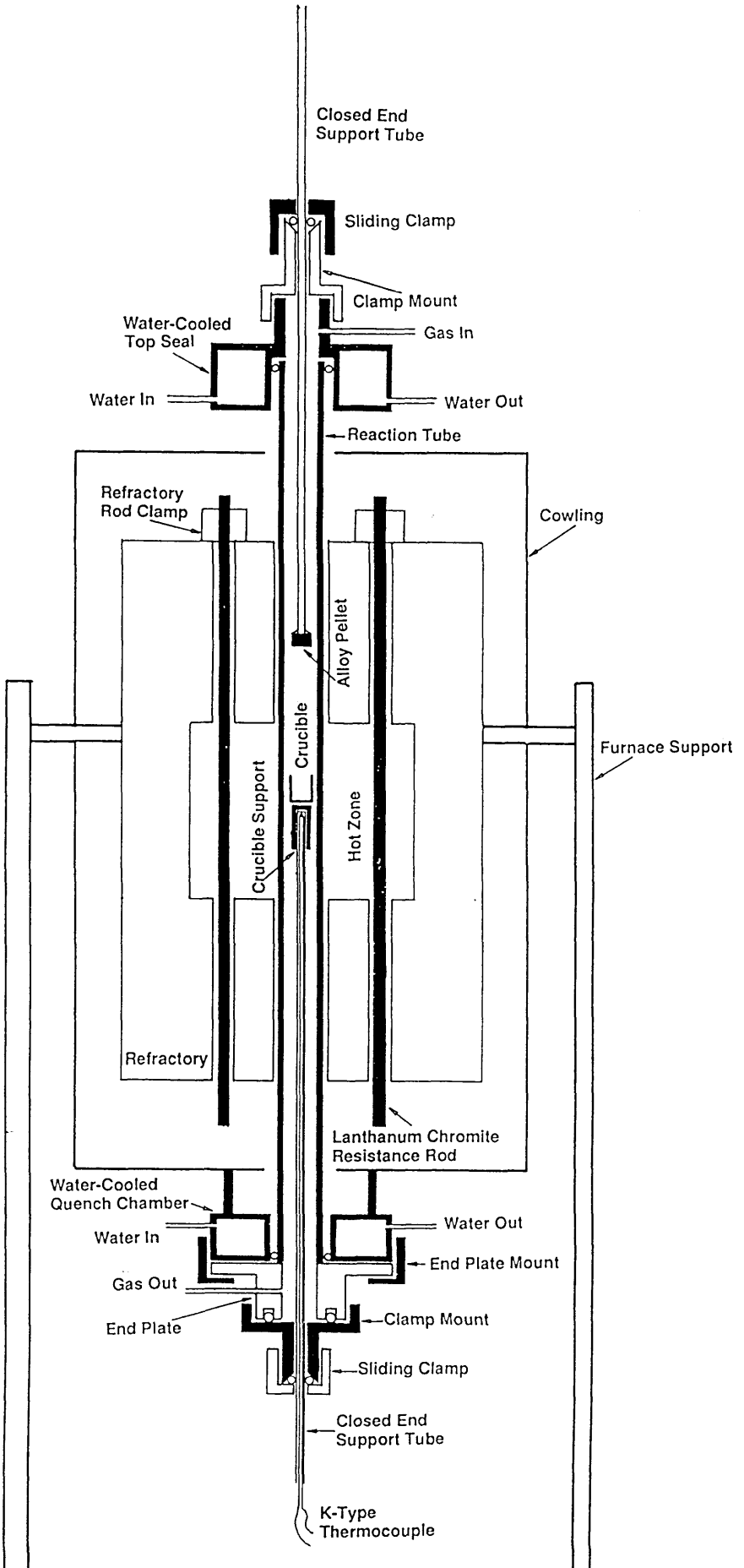
Slag cleaning experiments were designed to be as similar as possible to those of Toguri's so that direct comparison of results could be carried out. However, some small changes were implemented to improve on Toguri's rig. In his experiments, slag and metal were added to the crucible at room temperature, then heated to the reaction temperature. This means that the time at which reaction commenced(t=0) is somewhat imprecise. Obviously, it is desirable to have the time at which the reaction starts well known. To minimize, but not eliminate, this problem, the current apparatus allows the metal phase to be heated to 1000^{0}C before it is added to

the slag phase which is already at the reaction temperature. In this way, the metallic phase was completely liquid within a few seconds of the addition and the melt back to the desired reaction temperature within a few minutes.

4.2.1 Experimental Apparatus

The apparatus used for the present study is shown schematically in figure(2). A mullite reaction tube, 75mm internal diameter and 1000mm in length was placed in a vertical lanthanum chromite resistance furnace with P.D.I. control. Water cooled aluminium end caps, specially developed for these experiments, sealed both ends. Through the bottom cap, a hollow IAP(Impervious Aluminized Porcelain) closed end tube was inserted, closed end uppermost,up the centre of the reaction tube through a sliding seal that could be clamped to hold the tube in place and centrally aligned. On the end of this tube was placed an alumina crucible support on which rested the silica crucible. Little interaction was ever seen between the crucible, support,and tube because of poor surface contact. An alumel/chromel thermocouple was inserted up the inside of the tube to continuously monitor temperature. Gas was introduced through a port in the bottom cap. Through the top cap, another IAP closed end tube was mounted similar to the bottom. This tube had holes drilled in its end to facilitate the attachment of the copper alloy pellets with a very small length of pure Cu wire. The temperature profile of the furnace showed a uniform hot zone at the reaction temperature of 95mm in

Figure 2. Slag Cleaning Experimental Apparatus. Vertical Mullite Tube Resistance Furnace With Facility to Add and Remove Crucibles Through the Bottom and Add Samples From the Top. P.I.D Temperature Control. Two Stage Gas Mixing Provides Accurate pO2.



length with temperature variation of less that +/- $1^{0}C$. The oxygen potentials for this study were obtained by use of a mixture of CO and CO_2. Gas flows were regulated by manometer type venturi flow meters. Gases were dried with self indicating silica gel.

4.2.2 Experimental Procedure

Fayalite type slag containing nominally 4 wt%Ni was placed in a pure silica crucible(99.999wt%SiO_2) which was, in turn, placed on an alumina support. The support was lifted into the pre-heated hot zone by sliding the IAP tube up through the end seal. The atmosphere, which was initially argon, was now switched to the required CO/CO_2 mixture. Five minutes after the crucible was transferred, the metal pellet was lowered from the top to a location where it was heated to 1000°C. This took 10 minutes, by which time the crucible temperature had settled to $1200^{0}C$ and the slag was completely molten. The pellet was then lowered into the melt and the suspension tube withdrawn. After the desired reaction time, the crucible and mount were rapidly lowered to a quench zone. The crucible fractured during cooling. Metal and slag were easily separated manually, but much greater care was required to avoid fine shards of crucible becoming entrained in the slag sample.

The iron and nickel content of the copper and the copper and nickel content of the slag were analysed by atomic adsorption spectrometry. Total Fe and silica contents of the master slag were analysed by titration with $K_2Cr_2O_7$ and

gravimetrically respectably.

4.3 Results

The nickel content of the master slag was found to be 3.77wt% and the iron contents in the master alloys were analysed to be 4.00, 2.32, and 0.12 wt% . The experimental results are summarized in table(7).

A rough mass balance on nickel was performed for each sample. The final mass of metal and slag could not be easily measured. while separation of the metal from the slag and crucible was simple, the slag and crucible were strongly fused together. Assuming only small changes in metal and slag masses took place, the final concentrations gave mass balances within experimental and analytical error limits. A sample calculation is shown below.

$$\text{Initial Nickel Mass} = \frac{\text{Init.Wt\% Ni in Slag} \times \text{Init. Slag Mass}}{100}$$

(Taking as an example the reaction at 5×10^{-11} atm.,0.12 Wt%Fe in Alloy, reacted for 20 mins.)

$$= (3.77 \text{ Wt\% Ni} \times 5.00 \text{ g})/100$$

$$= 0.1885 \text{ g}$$

$$\text{Final Nickel Mass} = (\text{Final Wt\% Ni in Metal} \times \text{Final Metal Mass} + \text{Final Wt\% Ni in Slag} \times \text{Final Slag Mass}) / 100$$

$$\cong (\text{Final Wt\% Ni in Metal} \times \text{Init. Metal Mass} + \text{Final Wt\% Ni in Slag} \times \text{Init. Slag Mass}) / 100$$

Table 7. Experimental Conditions and Results. Initial Iron Content of Alloy, Oxygen Potential in the Gas Phase, Initial Phase Masses, Reaction Time and Chemical Analyses of Final Slag and Metallic Phases.

Wt% Fe in Alloy	p_{O_2} (atm.)	Time. (mins)	Alloy Mass (g)	Slag Mass (g)	Wt% Ni in Slag	Wt% Cu in Slag	Wt% Fe in Metal	Wt% Ni in Metal
0.12	5.0×10^{-11}	0	-	-	3.77	0.0	0.12	0.0
		20	16.13	5.0	1.48	1.50	0.49	0.64
		40	15.22	5.0	0.90	2.10	0.025	0.90
		90	17.15	5.0	0.28	2.01	0.020	1.03
		240	20.19	5.0	0.31	1.97	0.010	0.91
	10^{-7}	0	-	-	3.77	0.0	0.12	0.0
		20	20.39	5.0	1.01	1.47	0.04	0.63
		40	21.17	5.0	0.89	2.50	0.01	0.59
		90	20.43	5.0	0.61	2.70	0.01	0.80
		240	20.86	5.0	0.52	1.82	0.01	0.79
2.32	5.0×10^{-11}	0	-	-	3.77	0.0	2.32	0.0
		20	17.29	5.0	0.60	0.10	0.85	0.80
		40	19.16	5.0	0.13	0.21	0.71	0.91
		90	18.54	5.0	0.01	0.29	0.70	1.01
		240	16.20	5.0	0.03	0.30	0.70	1.10
	10^{-7}	0	-	-	3.77	0.0	2.32	0.0
		20	20.44	5.0	0.77	0.28	1.51	0.64
		40	20.72	5.0	0.22	0.33	1.01	0.90
		90	20.13	5.0	0.10	0.28	0.39	0.90
		240	18.89	5.0	0.03	0.35	0.50	1.05
4.00	5.0×10^{-11}	0	-	-	3.77	0.0	4.00	0.0
		20	19.53	5.0	1.00	0.09	2.29	0.61
		40	15.96	5.0	0.20	0.16	1.55	1.02
		90	16.14	5.0	0.01	0.19	2.01	1.20
		240	18.01	5.0	<0.01	0.14	2.01	1.11
	10^{-7}	0	-	-	3.77	0.0	4.00	0.0
		20	21.44	5.0	0.50	0.20	2.25	0.80
		40	20.82	5.0	0.08	0.30	1.96	0.87
		90	16.08	5.0	0.01	0.15	2.00	1.20
		240	18.90	5.0	0.01	0.20	2.58	1.05

$$= (\ 0.64\ \text{Wt\% Ni} \times 16.31\ \text{g}$$

$$+\ 1.48\ \text{Wt\% Ni} \times 5.00\ \text{g}\ ) \ /\ 100$$

$$= 0.1784\ \text{g}$$

This represents a 5.4 % error. Note that the slag mass is very likely to be greater than 5.0 g due to crucible dissolution. This would further reduce the error. If the slag mass was, say, 5.5 g , the error becomes only 1.4 %. Larger errors were apparent when the nickel concentrations in the slag were high, which is where the calculation is most sensitive to the assumption of constant slag mass.

5.0 Model Output

5.1 Modelling Strategy.

The first step taken was to develop the general model, capable of simulating mass transport to, across, and away from the metal/slag, slag/gas, and metal/gas interfaces for up to 10 species. The input parameters of this model were set to describe the experimental conditions described by Toguri[54]. Fine tuning of the model (that is adjusting the mass transfer coefficients within reasonable limits to give good agreement with observations) was carried out. This "fine tuned" model was then used to predict the results of the current experiments. When reasonable to excellent agreement was found, further modelling of more complex systems was undertaken.

5.2 Application of General Model to Toguri Experiments.

Figures (3) and (4) show the output of the general model when provided with parameters describing the experiments performed by Toguri and co-workers[54]. A very high level of agreement can be seen, the points being experimental results, the lines are the model output. The mass transport model provides as comparable agreement with observation as the "step-wise" equilibrium model applied by Toguri. However, the current model removes the need to define and set "rate constants" for oxygen, copper and iron transfer between phases, although it

Figure 3(a). Copper Reduction Rate Using Cu -Fe Alloy Under a pO2 of 10^{-7} atm.in Fayalite Slag at 1200°C.

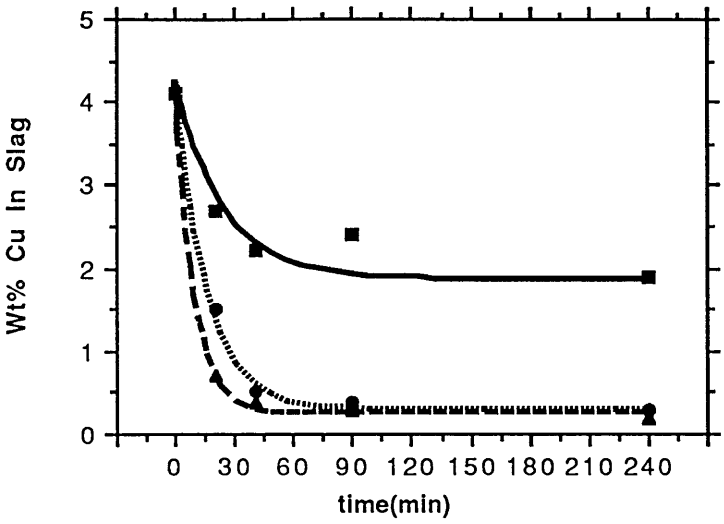
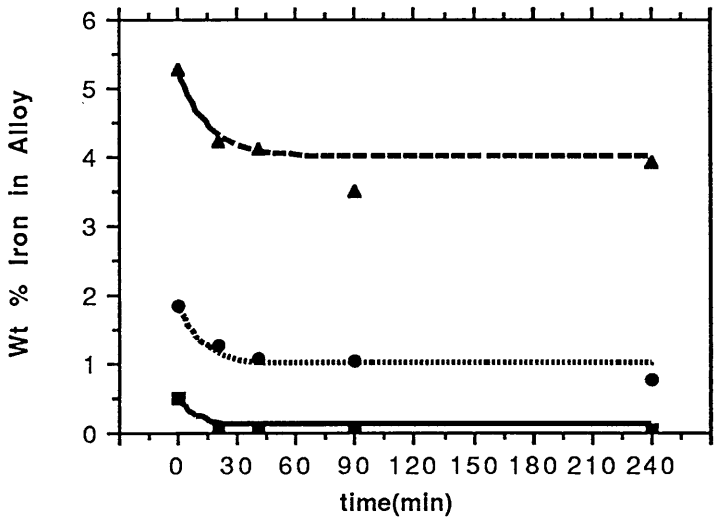


Figure 3(b). Iron Transfer In Cu-Fe Alloy Under a pO2 of 10^{-7} atm.in Fayalite Slag at 1200°C.



1. Cu- 0.50Wt% Fe Alloy (Calculated)
" (Experimental)
2. Cu- 1.86Wt% Fe Alloy (Calculated)
" (Experimental)
3. Cu- 5.27Wt% Fe Alloy (Calculated)
" (Experimental)

Mass Trans. Coeff. in Metal = 1.5×10^{-5} cm^2/s

Mass Trans. Coeff in Slag = 1.0×10^{-5} cm^2/s

Figure 4(a). Copper Reduction Rate Using Cu-Fe Alloy Under a pO2 of $5x10^{-11}$ atm in Fayalite Slag at 1200°C.

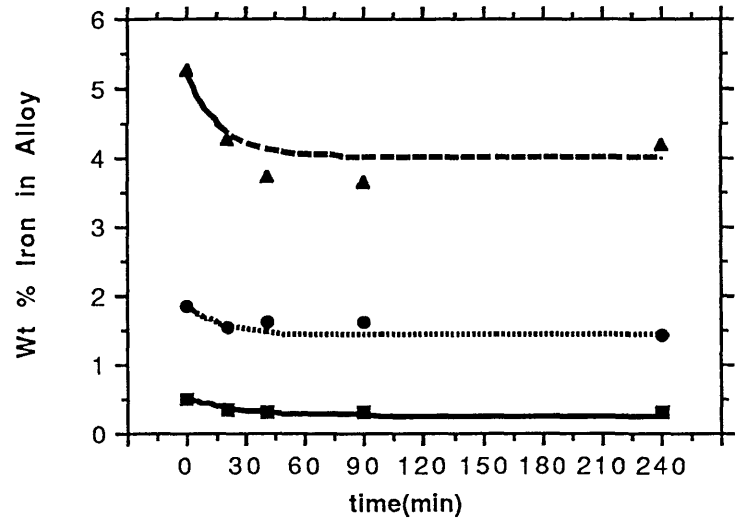
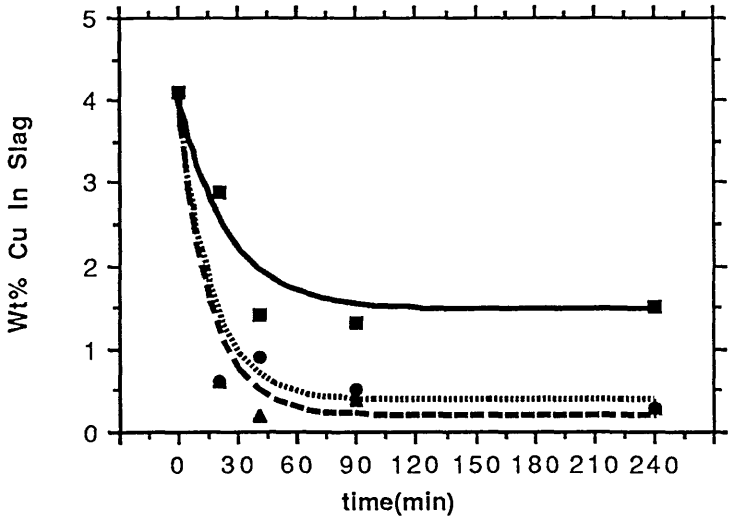


Figure 4(b). Iron Transfer in Cu-Fe Alloy Under a pO2 of $5x10^{-11}$ atm. in Fayalite Slag at 1200°C.



1. Cu- 0.50Wt% Fe Alloy (Calculated)
" (Experimental)
2. Cu- 1.86Wt% Fe Alloy (Calculated)
" (Experimental)
3. Cu- 5.27Wt% Fe Alloy (Calculated)
" (Experimental)

Mass Trans. Coeff. in Metal = 1.5×10^{-5} cm^2/s

Mass Trans. Coeff in Slag = 1.0×10^{-5} cm^2/s

is necessary to define mass transfer coefficients. Nonetheless, a general feel for these mass transfer coefficients is held, whilst the values of the rate constants are not directly related to any physically measured value. Values of the various mass transfer coefficients used to give the above agreement with experiment are given in the listing of the input file in Appendix(3).

5.3 Application of the General model to the Current Experiments.

Now that the model was tailored to the experimental conditions of Toguri's study, it was only necessary to estimate a small number of values to simulate the current experiments, all other parameters being the same. Specifically, these parameters were,

1)Mass Transfer Coefficient of Ni in the metallic phase (1.5×10^{-5} cm/s)

2)Mass Transfer Coefficient of NiO in the slag phase (1.0×10^{-5} cm/s)

3)Activity Coefficients of Ni and NiO (2.11 and 4.26 respectively)

Figures(5) and (6) show the model output again as lines, whilst points represent the results of analysis of samples produced by the current series of experiments. Values of the mass transfer coefficient of Ni in the metallic phase and NiO in the slag phase, along with all other values are again given in the input file listed in Appendix(3).

Figure 5. Nickel Reduction Rate, Iron Transfer Rate , Nickel Pick-Up Rate, and Copper Pick-Up Rate .

$pO2 = 10^{-7}$ atm.
Metal Mass Trans. Coeff. = 1.5×10^{-5} cm /s.
Slag Mass Trans. Coeff. = 1.0×10^{-5} cm /s.

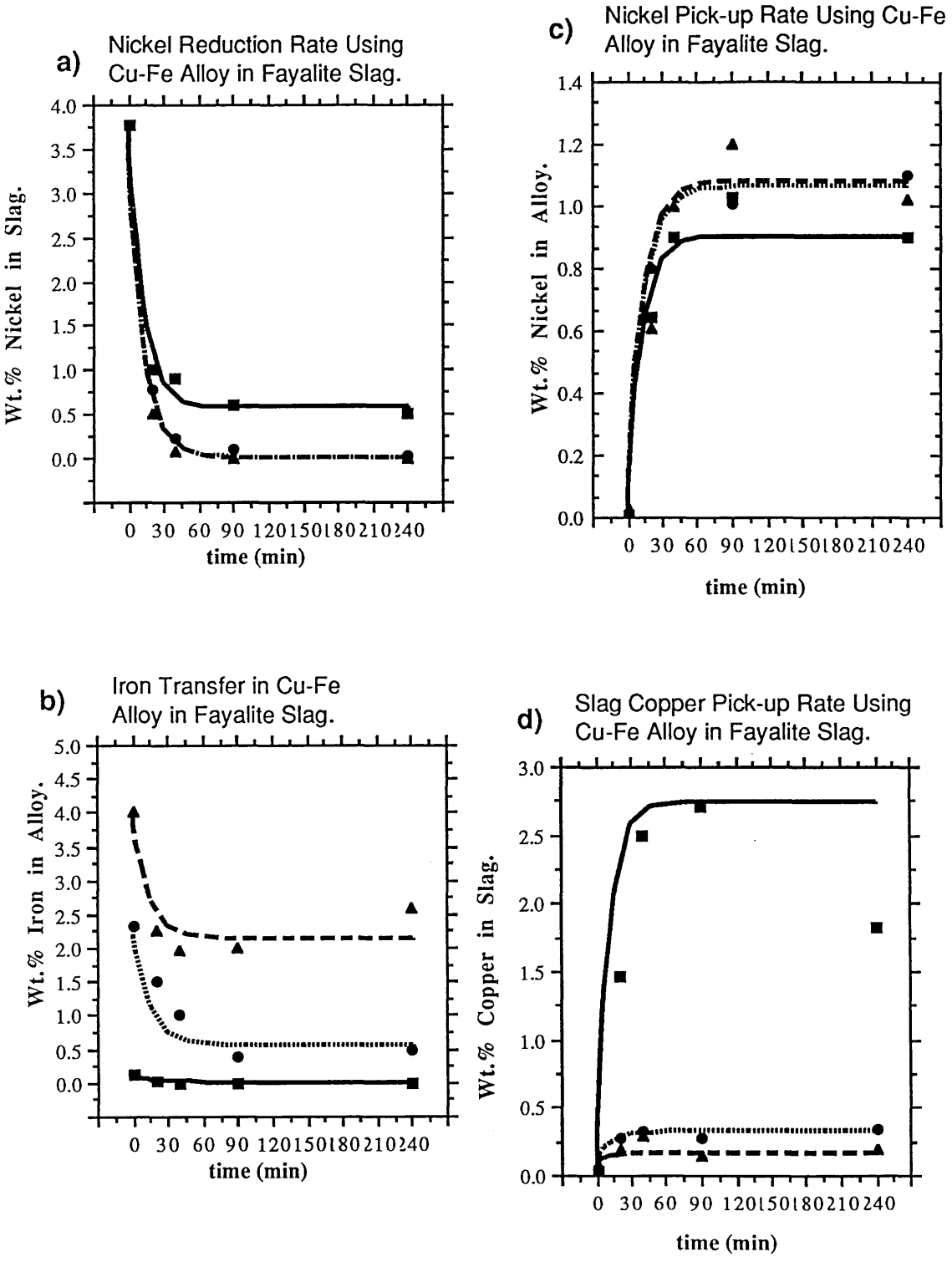
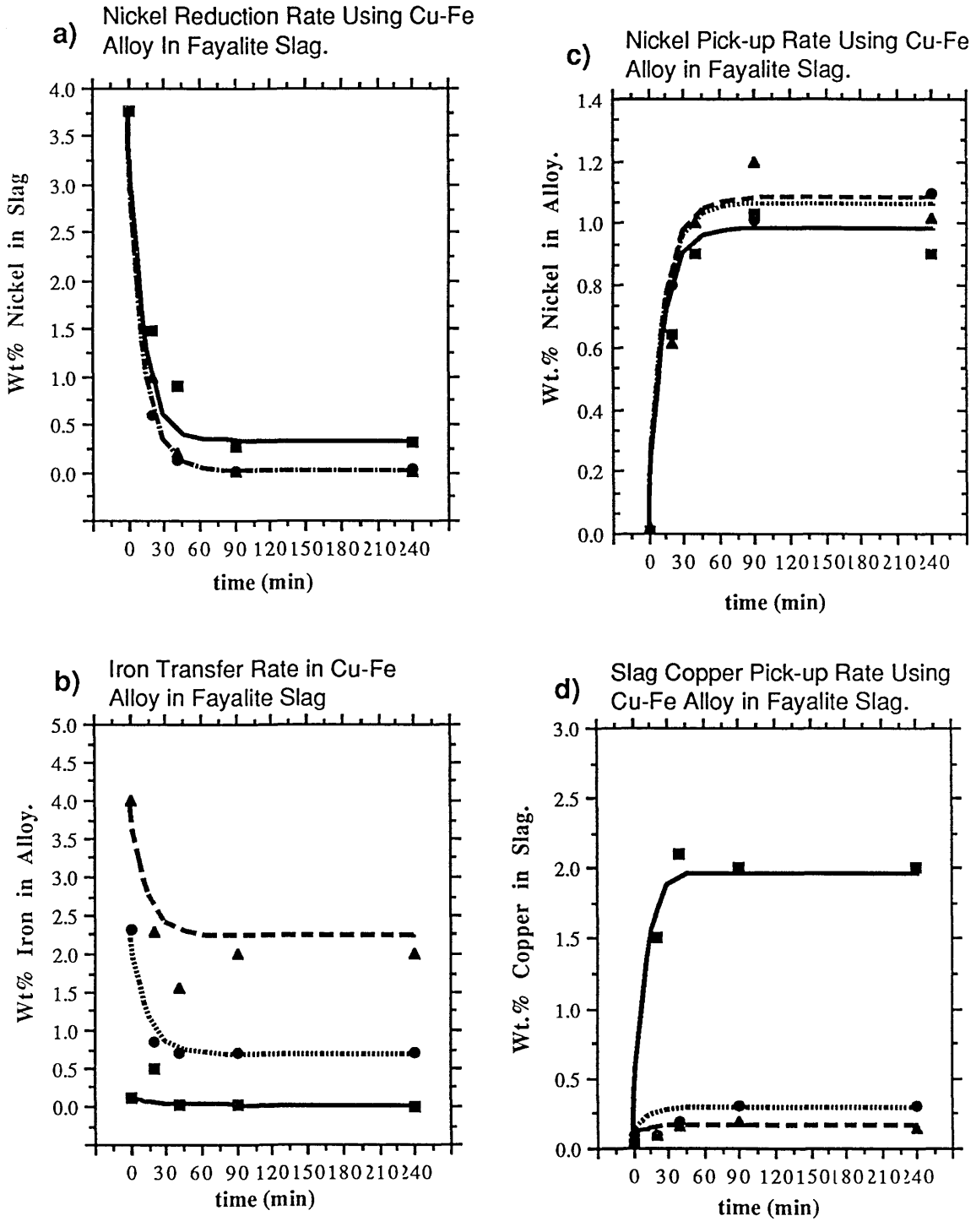


Figure 6. Nickel Reduction Rate, Iron Transfer Rate , Nickel Pick-Up Rate, and Copper Pick-Up Rate .

pO2 = 5.0 x 10^{-11}atm.
Metal Mass Trans. Coeff. = 1.5 x 10^{-5}cm /s.
Slag Mass Trans. Coeff. = 1.0 x 10^{-5}cm /s.



5.4 Application of the General Model to Hypothetical Slag Cleaning Conditions.

Now that reasonable estimates for mass transfer coefficients of some species are known, a much more complex system can be modelled with cautious confidence.

The general model is capable of producing an output of the following parameters,

- bulk and interfacial species activities and concentrations for metal, slag, and gas phases
- flux densities of species to and from interfaces
- mass balances on individual metals
- mass of any species in any phase and distribution of any species between phases
- phase masses and volumes
- fume masses and compositions.

Various slag cleaning conditions will be discussed, based on variation of reducing conditions and model parameters around a set of "standard" inputs. A full listing of the standard set of parameters can be found in Appendix (3). Determination of many of the inputs has been discussed before. The most important values are shown here.

Mass Transfer Coefficients in the Metallic Phase = 1.5×10^{-5} cm/s.

Mass Transfer Coefficients in the Slag Phase = 1.0×10^{-5} cm/s.

Note that these values are determined from bench-top scale experiments, so to maintain consistancy, the physical

dimensions of the reactor must again correspond to those in the current experiments and those of Toguri's. Metal/slag and slag/gas interfacial areas were set to 4 cm^2, the metal mass to 25g and the slag mass to 10g. Temperature again was $1200^{o}C$.

Any other consistant group of parameters that describe other reactors may be input. If mass transfer coefficients, interfacial areas, and phase masses for industrial processes are input, simulation of these processes, within the constraints described earlier, will be achieved.

Little has been said about the initial metal composition that is a sensible input to a model attempting to display similar behaviour to the final stages of slag cleaning. Early simulations that contacted nearly pure Cu containing 5wt% Fe with a fayalite slag bearing 5wt% of $CuO_{0.5}$, NiO, SnO, PbO, and ZnO revealed that Cu, Ni, and Sn readily left the slag and entered the metal phase, whilst Pb and Zn were not as easily reduced. It is likely that the final metal composition will be high in Cu, Ni, and Sn, (this being confirmed at pilot plant scale). Holding this in mind, the metallic phase composition selected to best represent that occurring towards the later stages of slag cleaning was predominantly Cu as the solvent holding small quantities of Ni, Sn, Pb, and Zn, with various amounts of Fe. Larger proportions of Ni and Sn would be desirable, but the complexity of the solution thermodynamics limits the model to dilute solutions.

The bulk of the results output from this simulation will be

presented as graphs of species concentration (wt%) versus time (mins.). Increases and decreases in concentration are closely proportional to the actual masses of species leaving or entering each phase as the total phase masses vary little from their initial values.

The slag/gas interfacial oxygen activity has a sensible lower limit set by the desire to avoid reduction of FeO. The actual value of this limit depends on the temperature and the slag/gas interfacial FeO activity. For example, with interfacial FeO activity (a_{FeO}) of 0.4 at 1200°C,

$$p_{O_2} = (a_{FeO} / K^{FeO}_{1473} a_{Fe})^2$$

$$= 4.5 \times 10^{-14} \text{atm.}$$

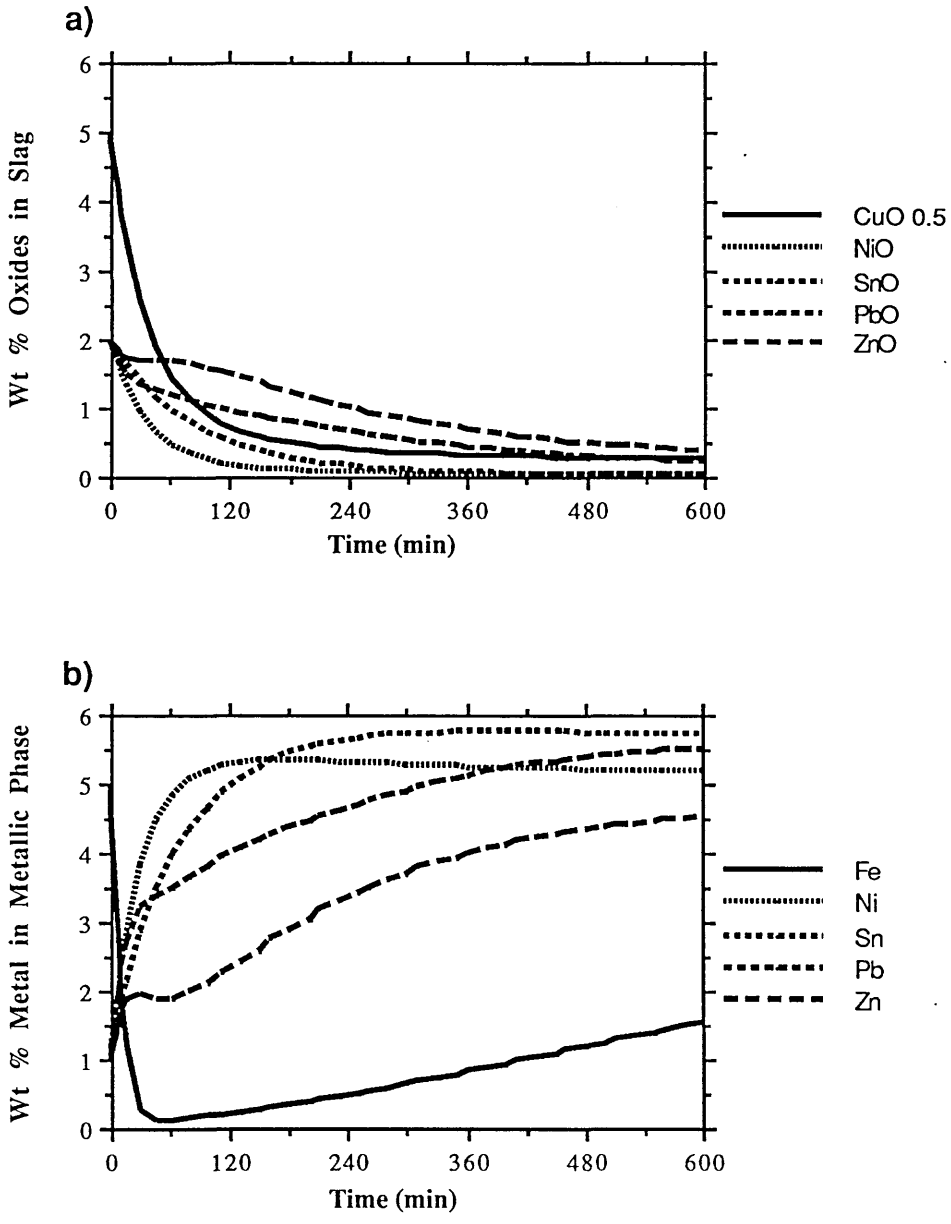
Similarly, with a_{FeO} at 0.4 and at 1500°C,

$$p_{O_2} = 5.3 \times 10^{-11} \text{atm.}$$

It is not possible to know the interfacial FeO activity to calculate the associated minimum p_{O_2} because it is necessary to set the p_{O_2} to find a_{FeO}. The value selected to approximate the interfacial FeO activity was that of the bulk. This guarantees no FeO reduction, the bulk FeO activity always being equal or higher than that at the interface.

Figure (7) shows the output resultant from the standard set of parameters. Initially, iron is rapidly taken up into the slag whilst other metal values move from the slag phase to the metal. Copper, tin, and nickel are cleaned to low levels, while lead and zinc travel to the metallic phase less completely. Note an intermediate period of zinc reversion

Figure 7. Concentration of Species Vs. Time.
"Standard" Conditions.
Metal Mass Trans. Coeff. = 1.5 x 10^{-5} cm /s.
Slag Mass Trans. Coeff. = 1.0 x 10^{-5} cm /s.
Temperature = 1200°C.
Metal/Slag Interfacial Area = 4 cm^2.
Slag/Gas Interfacial Area = 4 cm^2.
Initial Metal Mass = 25g.
Initial Slag Mass = 10g.
Initial Fe Concentration = 5.0 Wt%.
FeO Activity = 0.4
Oxygen Pressure = 4.5 x 10^{-14} atm.



followed later by continued cleaning. After a time of rapid reduction of value concentration in the slag bringing most values into the metallic phase, cleaning slows but does not stop entirely. Also at this time, iron reverts to the metal recontaminating it.

The effect of bulk activity of the FeO was considered very important. This parameter was varied with the following results. Figure (8) shows the output of the model when run with all inputs the same as for figure (7), excepting only in that the value of FeO activity was set at 0.1 rather than 0.4. Little change to the overall thoroughness of cleaning results. It can be seen that the initial rate of cleaning is increased, especially for tin. The intermediate reversion of zinc is much more pronounced, as is the final reversion of iron. Note that the lead also displays a small revertive stage. The most marked difference is that iron reversion is greatly reduced.

If the FeO activity is raised to 0.6 as in figure (9) , little change to the rate or extent of cleaning of any species is seen. Tin and nickel are cleaned slightly better. The revertive behaviour of zinc is very minor, but very significant quantities of iron return to the metallic phase.

Obviously, the overall reducing potential of the gas phase is the most important variable. The standard conditions looked at the maximum sensible reducing conditions. Figure (10) shows what happens if the gas phase is allowed to become much more oxidizing (from 4.5×10^{-14} to 1.0×10^{-7}). There is an initial period where some cleaning takes place, but this is

Figure 8. Concentration of Species Vs. Time.
As For "Standard" Conditions But With
FeO Activity Set To 0.1
Oxygen Pressure = 2.8 x 10^{-15}atm.

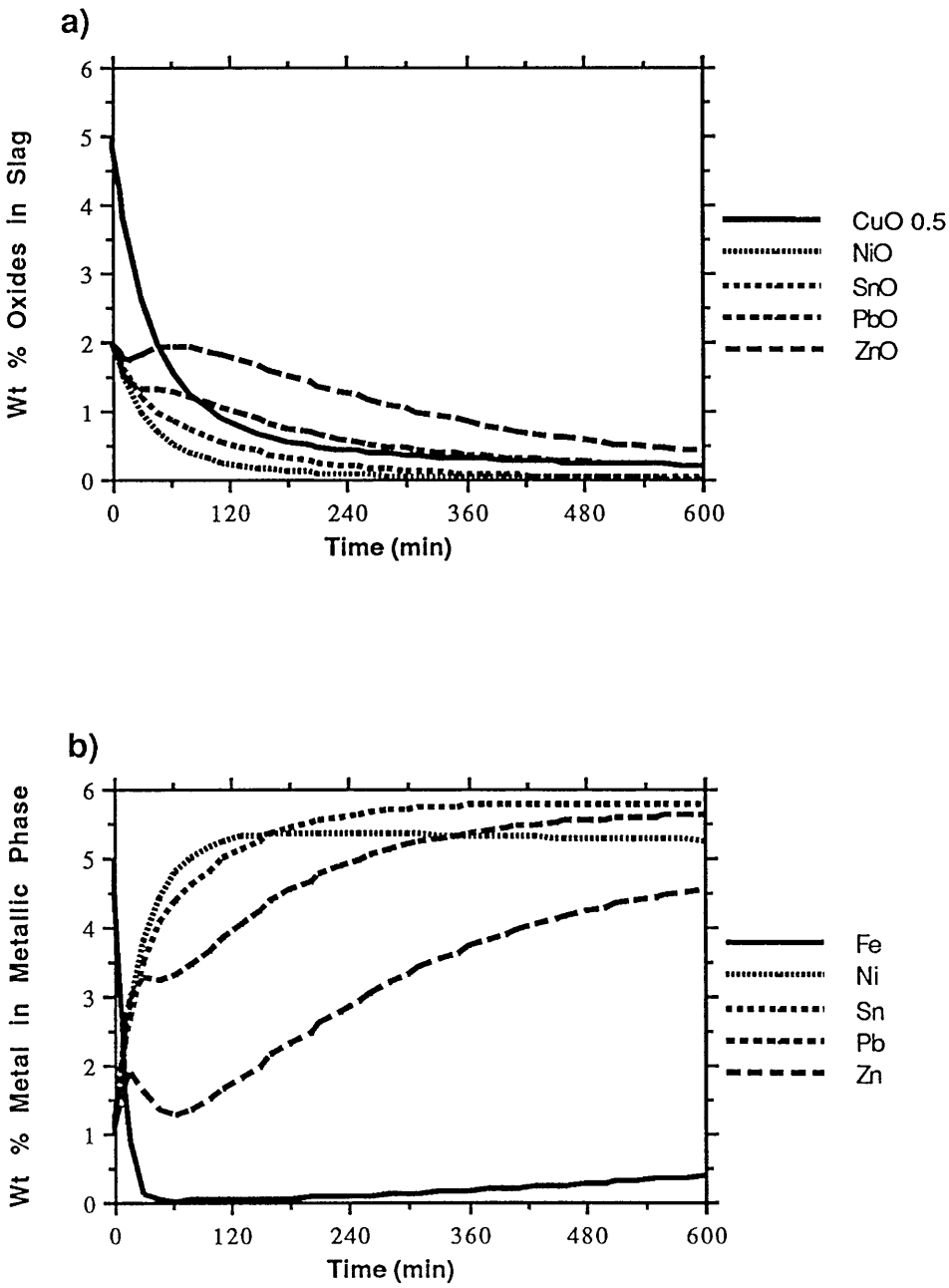


Figure 9. Concentration of Species Vs. Time.
As For "Standard" Conditions But With
FeO Activity Set To 0.6
Oxygen Pressure = 1.0 x 10^{-13}atm.

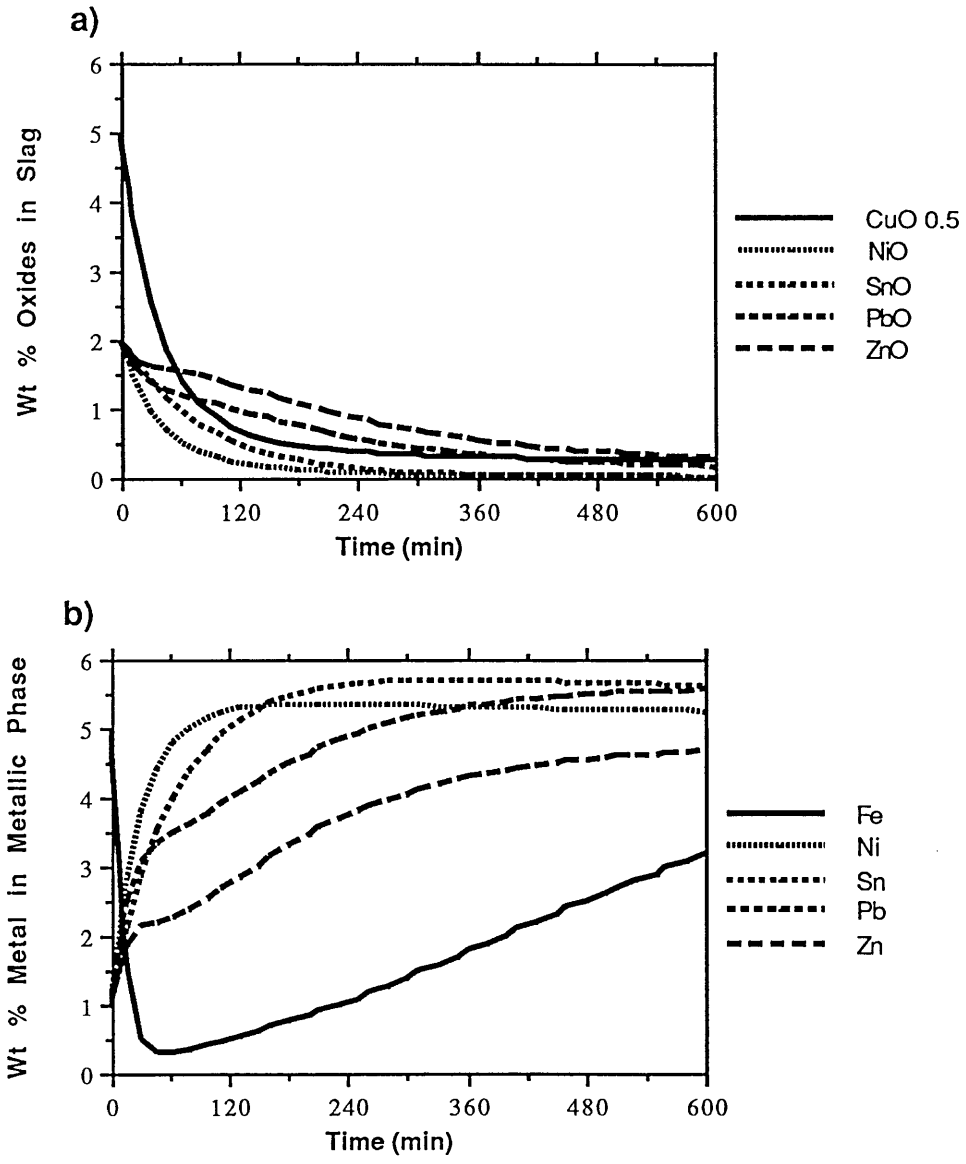
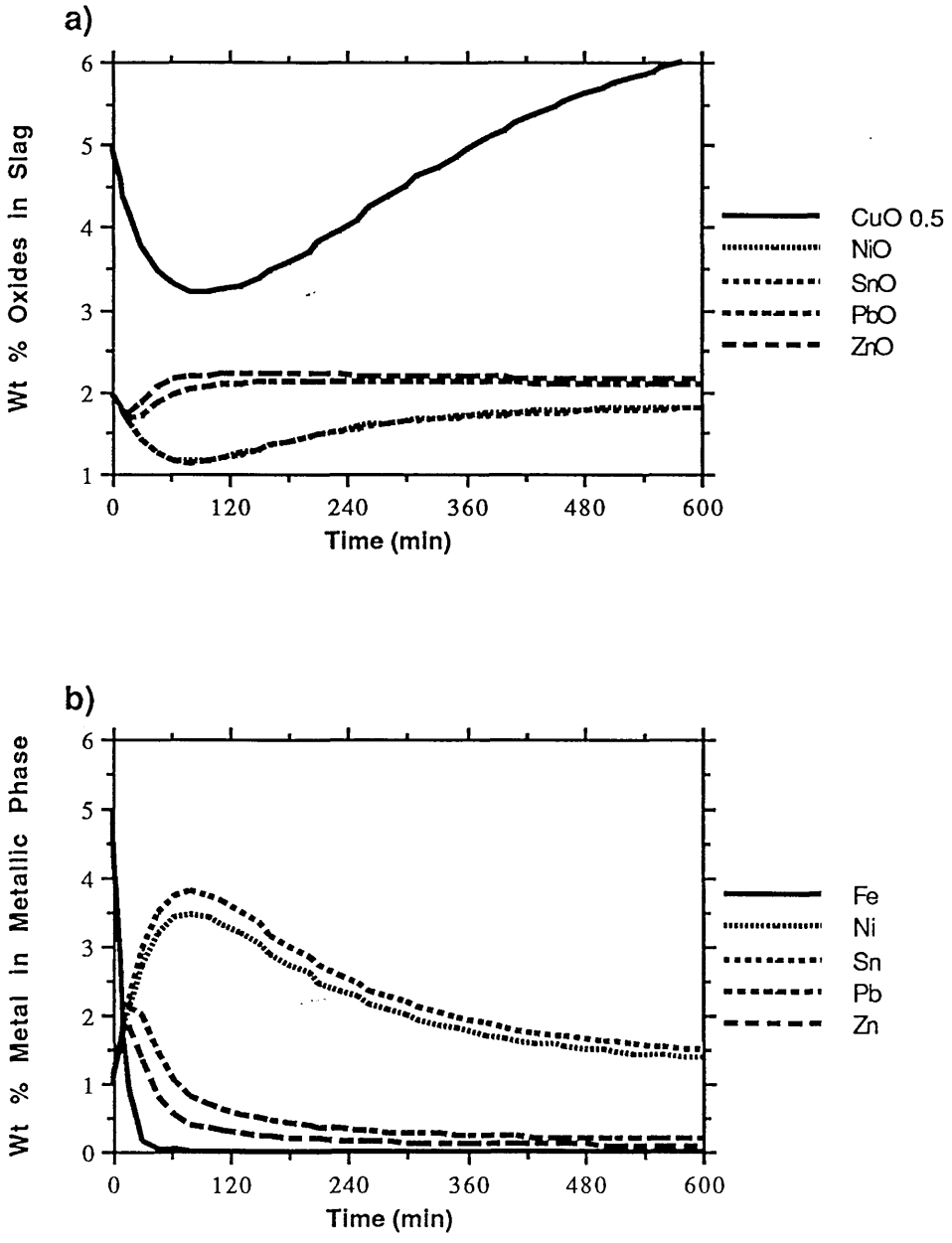


Figure 10. Concentration of Species Vs Time. As For "Standard" Conditions But With Oxygen Pressure = 1.0×10^{-7} atm.



short-lived. Soon, all the values return to the slag. Indeed, the concentration of copper oxide increases past its initial value, indicating a movement of bulk copper to the slag phase.

The effect of increasing temperature is shown in figure (11). The standard condition temperature of 1200^{o}C was increased to 1500^{o}C. This change does not directly relate to the effect that one would see in reality. Increased temperature would alter mass transfer coefficients, slag viscosities, surface tensions, and possibly interfacial areas, none of which is taken into account by making the appropriate associated changes to the other input parameters. Increasing the input temperature merely alters the position of each species equilibria. This aids the removal of zinc from the slag to a considerable extent, but at the expense of poorer Cu and Pb cleaning and more severe iron recontamination. Note that zinc shows almost no revertive behaviour, while strong reversion is displayed by lead.

Plotting the species concentrations against dimensionless time (defined and commented on in section 5.5) avoids the difficulties associated with changes in mass transfer coeffients and interfacial areas by normalizing these influences. However, care must be taken in interpreting these results because the two lines will relate to different real times.

The presence of iron in the metal phase has been shown to strongly affect the early stages of this simulation. Figure (12) shows what would be expected if only a little iron is

**Figure 11. Concentration of Species Vs Time.
As For "Standard" Conditions But With
The Input Value for Temperature Set To 1500°C.
Oxygen Pressure = 5.3 x 10^{-11} atm.**

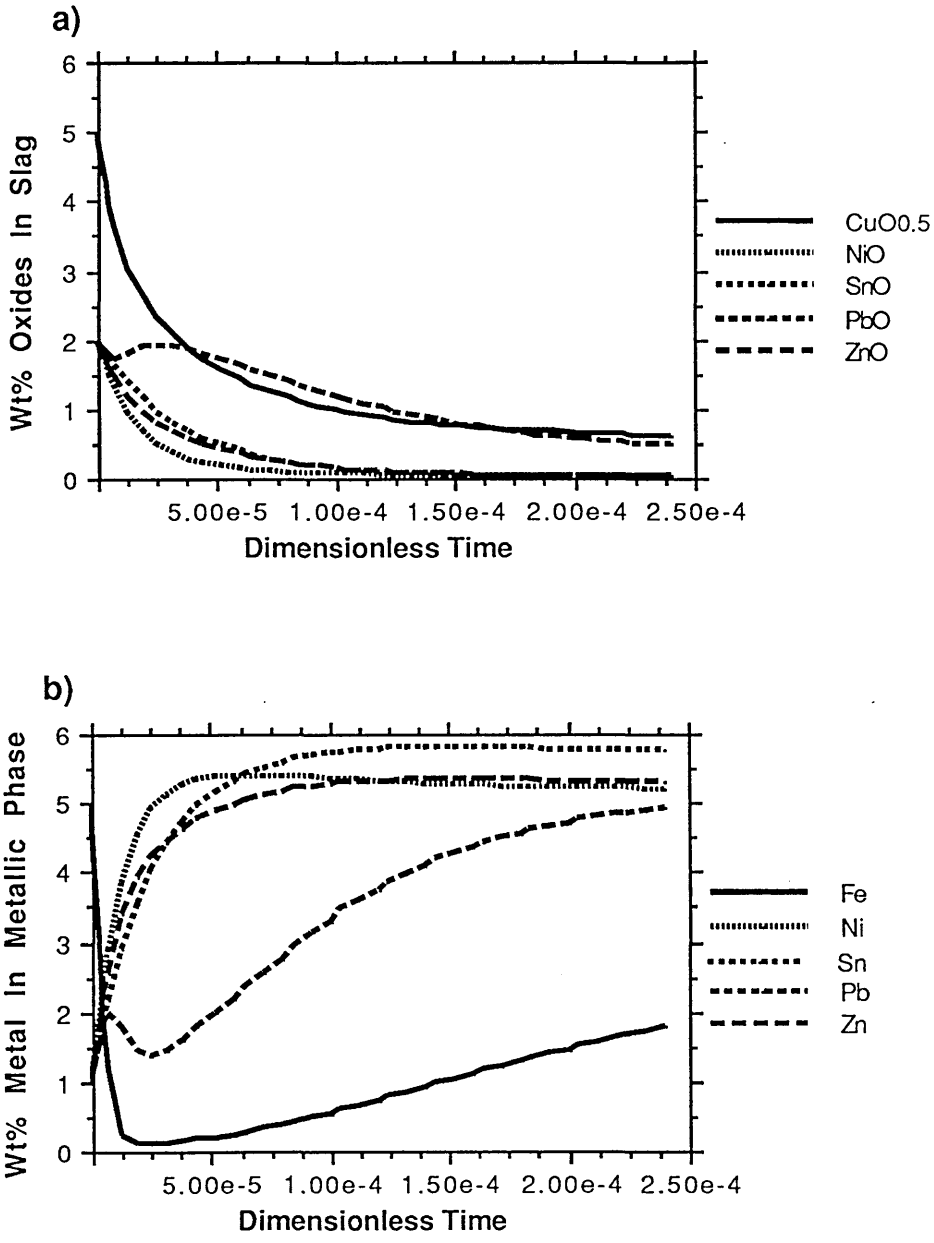
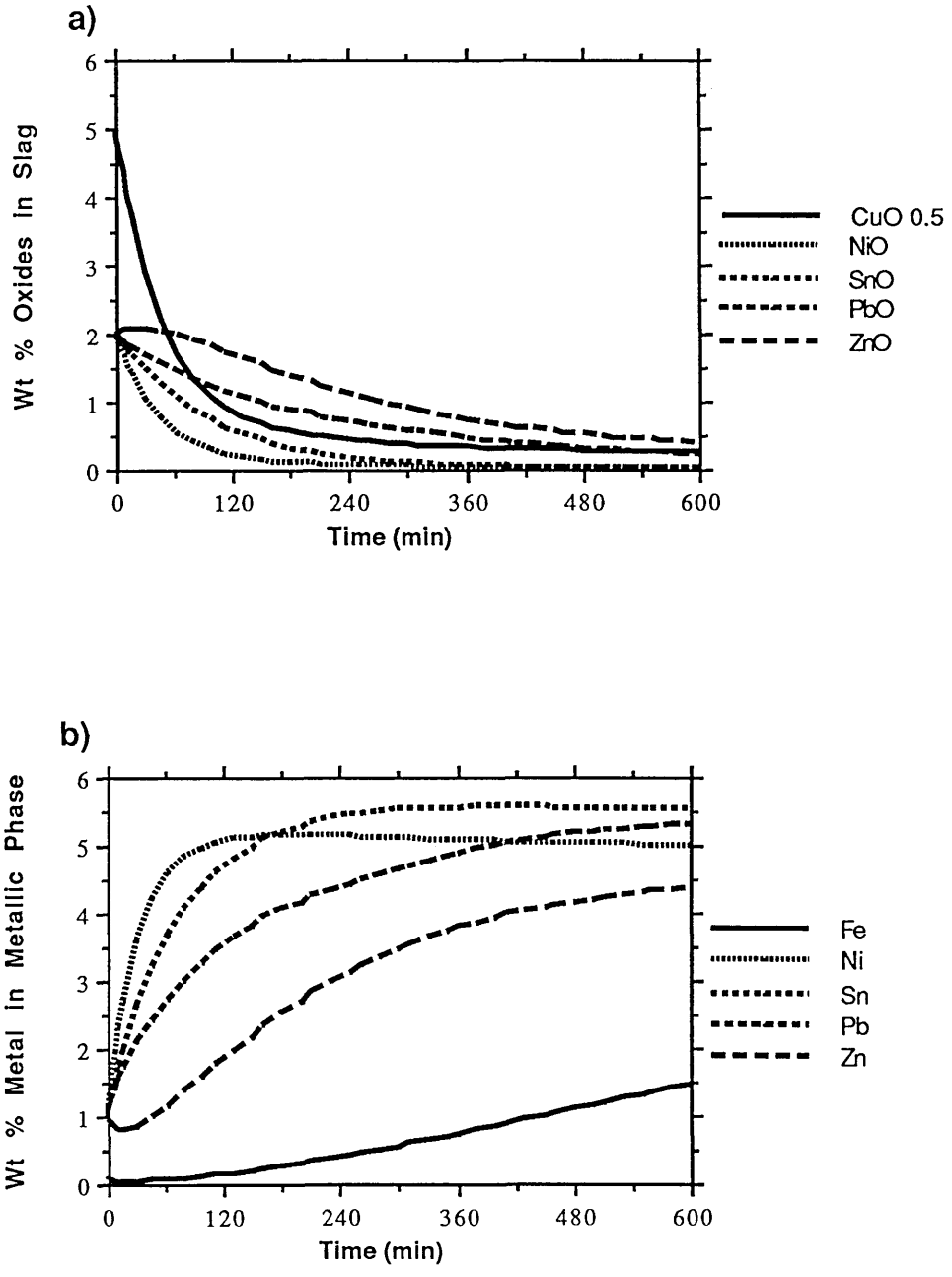


Figure 12. Concentration of Species Vs Time. As For "Standard" Conditions But With Only 0.1 Wt% Fe Initially In The Metallic Phase.



initially present in the metal phase. The rate of reduction is significantly reduced, although the final extent of cleaning is not greatly affected. No revertive behaviour of zinc is observed and the final level of Fe contamination is similar to that found when Fe is initially present.

One way in which it is possible to study the effect of a larger supply of Fe would produce good cleaning is to increase the metal/slag mass ratio, the giving more Fe in metal per unit mass of slag. Figure (13) shows the effect of increasing the metal/slag mass ratio from 0.25 to 1.0. Very good cleaning of all species is seen, with rapid kinetics. However, Fe contamination of the metallic phase is serious, and the actual concentration of species in the product metal is low.

5.5 Dimensionless Time.

The formula used to relate 'real' time to dimensionless time was :-

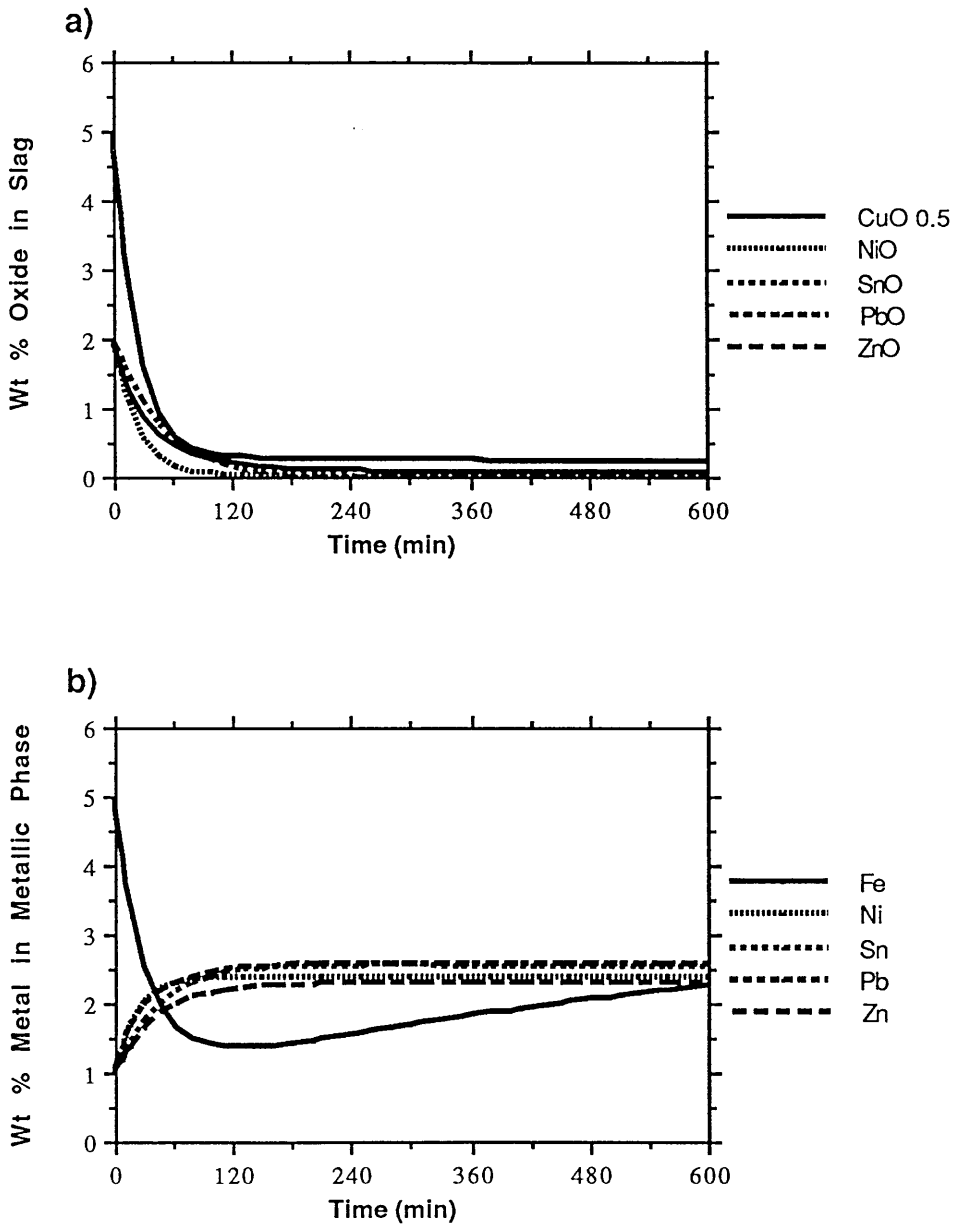
$$t\ (\text{dimensionless}) = \frac{k^M \ V^M(\text{initial})}{A^{M/S}} \times t\ (\text{real})$$

For the current standard set of input values,

$$t(\text{dim.less}) = 6.67 \times 10^{-9}\ t(\text{real})$$

Results plotted against dimensionless time give a means of showing the rate of change of species concentration expected for any set of mixing and mass transfer conditions. This is why these units were applied to figure 11 (and later in figure 19). Although the model predicted the relative changes in all the species concentrations, the lack of

**Figure 13. Concentration of Species Vs Time.
As For "Standard" Conditions But With
Initial Metal / Slag Mass Ratio Decreased To 1.0.**



information regarding mass transfer at 1500^{o}C prevented predictions in real time.

6.0 Discussion

It should be stressed immediately that the work presented here represents only the early stages of the total effort required to arrive at a versatile and reliable model of industrial slag cleaning. However, it is felt that the work shows promise in providing a framework and approach from which important features of the process can be better grasped.

The work will be discussed in relation to the following contexts:

1) Predictions obtained from the model in its current state, stressing the importance or otherwise of some process and chemical parameters

2) Applicability and validity of these predictions

3) Further model development.

The current model suffers from simplification of reactions and processes used, idealization of the conditions likely to be present, and lack of relevant fundamental thermodynamic and kinetic data. Within these limitations, it displays an impressive ability to predict the results of two sets of experiments, and is capable of full simulation of the effect of varying model parameters and reducing conditions.

6.1 Model Predictions

The results of the model simulations presented in previous sections illustrates its ability to predict the experimental

results of laboratory scale slag cleaning trials using simple slags. Although adjustments to mass transfer coefficients were made, agreement with Toguri's experiments were excellent for both sets of reducing conditions. Following this, the same set of parameters, plus estimates of some further required inputs were used to model the current set of experiments. Once again, good agreement was seen.

Note that the presence of iron in the current experiments did not enhance cleaning to any great extent. This is because the very low initial Ni activity in the metallic phase acts as a nickel "sink" into which any nickel reduced from the slag can go. Thus, only a moderate oxygen potential is required at the metal/slag interface to effect cleaning. However, it is important that Fe is present to avoid the slag phase taking in some of the bulk copper.

It is highly unlikely that one set of kinetic and chemical parameters could satisfactorily describe both groups of experiments over a range of oxygen potentials and not be good estimates. Thus, under the assumption that the early experimental and simulation process has given us confidence in our physio-chemical inputs, and a feel for other similar values, simulations were run looking at slags closer to slag cleaning feedstock and conclusions drawn. The actual composition of slag considered was subject to many constraints described earlier, but within these constraints, a standard sets of parameters were arrived at that would resemble the phases present towards the end of the slag cleaning process.

6.1.1 "Standard" Conditions.

Looking at the output resultant from a simulation with the standard set of inputs, an initial period of rapid cleaning of all species is easily understood when the metal/slag and slag/gas interfacial oxygen potentials are taken into consideration. Figure (14) shows the fluxes of species that are being reduced at the slag/gas interface. Copper, nickel and lead are reduced over a period to a level at which their activities in the slag are no longer high enough to react with the gas (the oxygen potential of which is set at this interface) to form metal at unit activity. Tin and zinc are already below this level at the start of the simulation. The interfacial oxygen potential is set to avoid FeO reduction in all trials, so no Fe fluxes from the slag/gas interface returning to the metallic phase will be seen.

Thus, any other cleaning must occur at the metal/slag interface. This means that the metal/slag interfacial oxygen potential is also of great importance. Figure (15) shows this oxygen potential plotted against time. During the early stages of the simulation, the p_{O_2} is kept low by the presence of a high iron activity at the interface. As can be seen by the rapid transfer of iron from the metal to the slag, considerable oxygen must be consumed by Fe. This aids the reduction of $CuO_{0.5}$, NiO, SnO, PbO, and ZnO, which are all being reduced at these early stages. Indeed, looking at figure(16), the Fe is holding the oxygen potential so low as to reduce $FeO_{1.5}$ to FeO, resulting in a small flux of $FeO_{1.5}$

Figure 14. Flux Densities of Metals being Reduced at the Slag/Gas Interface vs Time. "Standard" Conditions.

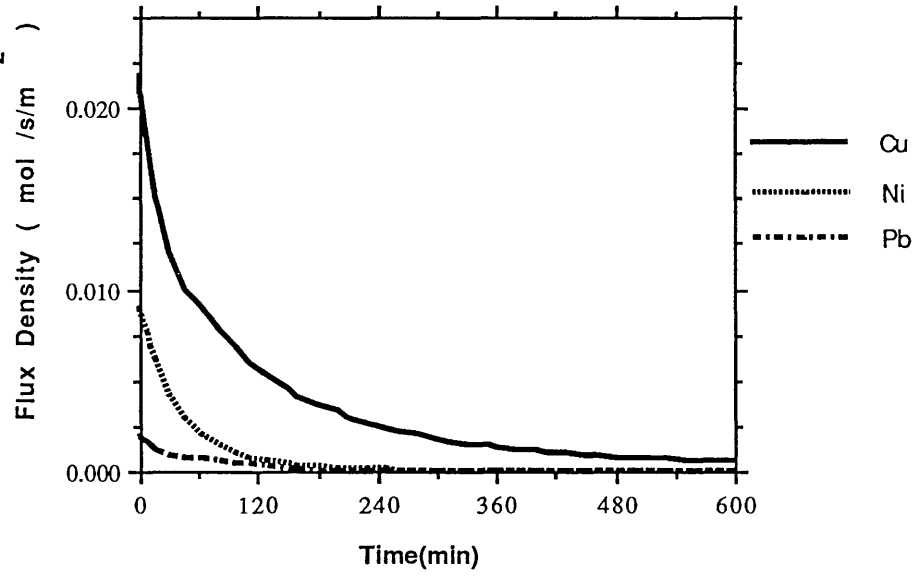


Figure 15. Oxygen Activity at the Slag/Metal Interface vs. Time. "Standard" Conditions.

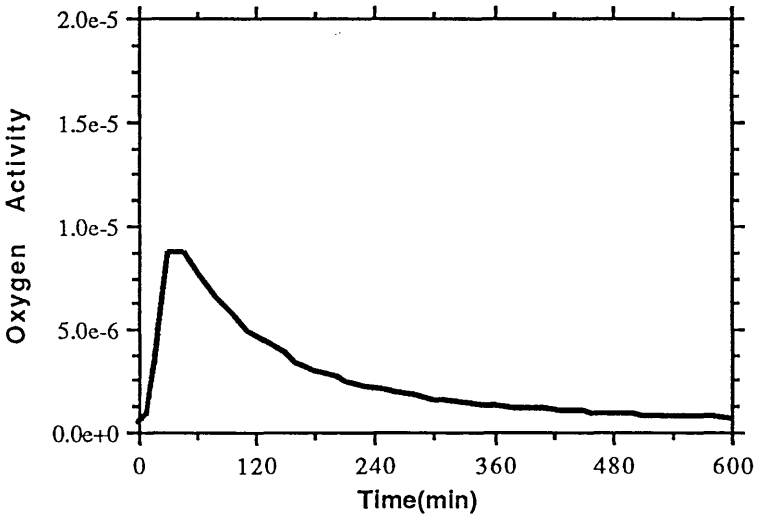


Figure 16. Fluxes of Iron Oxides To and From The Metal/Slag Interface. "Standard Conditions".

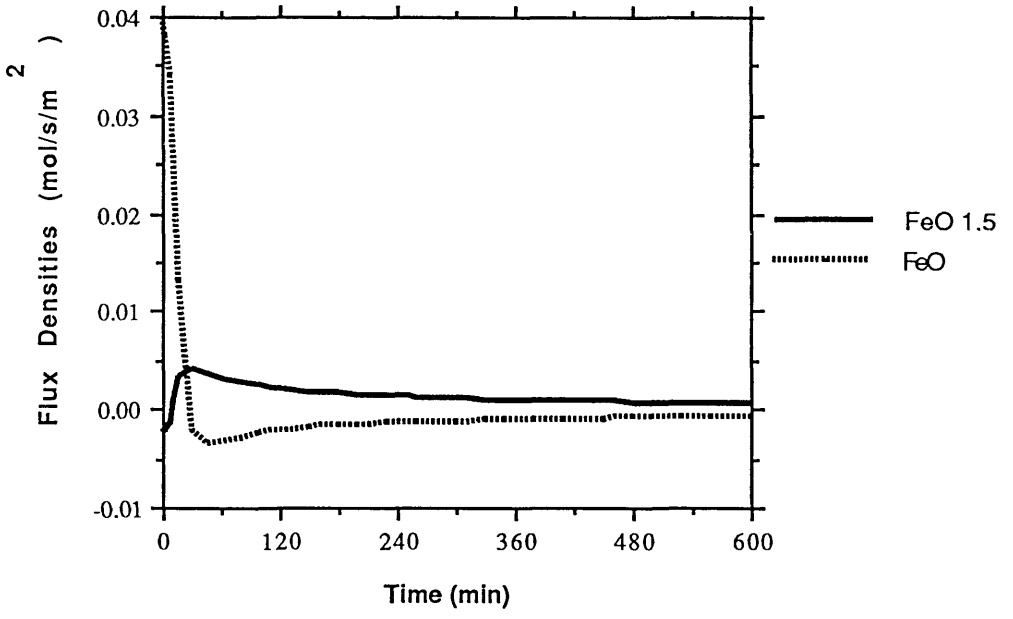
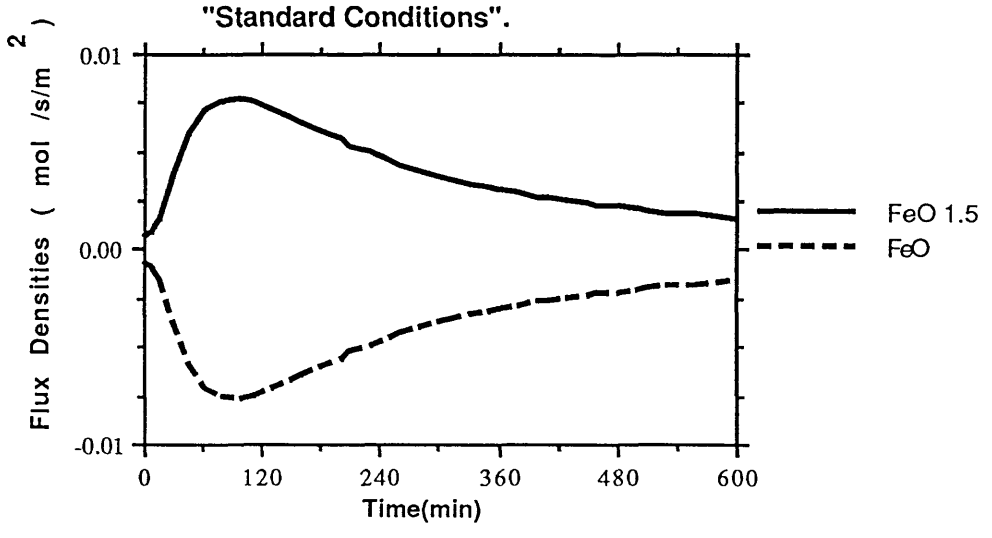


Figure 17. Flux Densities of FeO and FeO 1.5 To and From Slag/Gas Interface. "Standard Conditions".



towards the slag interface (ie. negative on the diagram) with a very large positive flux of FeO into the bulk slag, the FeO flux being the summation of the Fe arriving at the interface going to FeO and the $FeO_{1.5}$ being reduced to FeO. As the Fe is depleted, the interfacial oxygen potential begins to rise. Reduction of $CuO_{0.5}$, NiO, and SnO slows, that of PbO more considerably. ZnO reduction ceases, and some Zn taken into the metallic phase by the early low interfacial p_{O_2} returns to the slag phase. The FeO flux away from the interface decreases to zero and $FeO_{1.5}$ begins to diffuse away into the slag. FeO then starts to travel towards the metal/slag interface to pick up oxygen and travel away as $FeO_{1.5}$. This process is much slower than the previous Fe driven reduction. The metal/slag interface is steadily removing FeO from the slag and adding $FeO_{1.5}$. The simulation includes in its conditions a very small concentration of $FeO_{1.5}$ in the slag. This accounts for the small initial $FeO_{1.5}$ flux towards the metal/slag interface. This low initial concentration also explains the magnitude of the iron oxide fluxes travelling towards and away from the slag/gas interface (See figure (17)). The low initial flux of both $FeO_{1.5}$and FeO are due to the low bulk activity of $FeO_{1.5}$ providing a low driving force for $FeO_{1.5}$diffusion to the slag/gas interface and thus a low flux of FeO away, a simple mass balance here showing that the two fluxes must be equal and opposite.

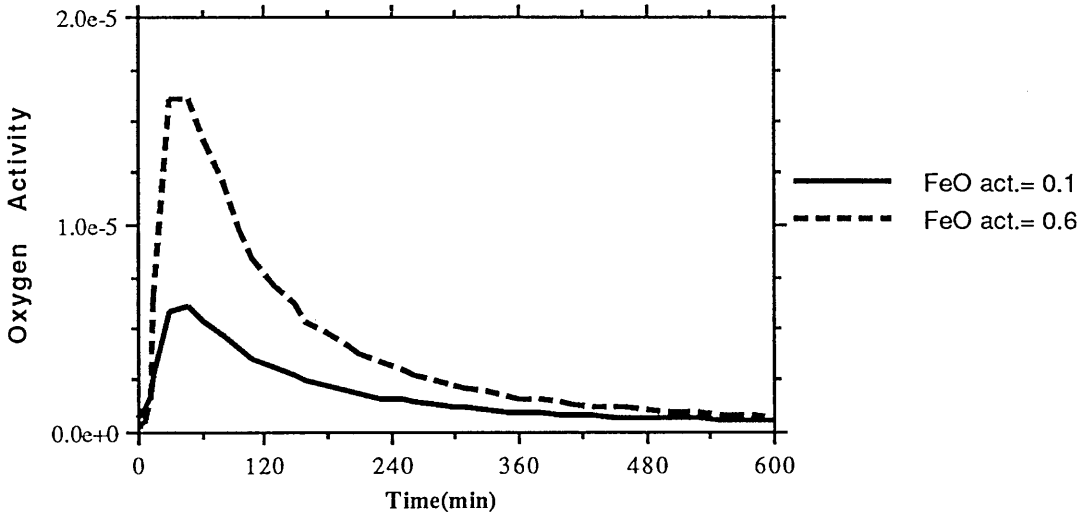
Now, as the metal/slag interface produces more $FeO_{1.5}$, the fluxes at the slag/gas interface increase, removing $FeO_{1.5}$

from the slag and replenishing FeO as quickly as they are produced and consumed respectively. As cleaning continues, the concentration of the valuable oxides decreases and the fluxes at which they arrive at the metal/slag interface decreases. This means that less and less oxygen is available for the $FeO/FeO_{1.5}$ reaction, thus lowering the fluxes of these species. However, the slag/gas interface will continue to form FeO and consume $FeO_{1.5}$. The resultant lowering of bulk slag oxygen potential will continue until all phases reach equilibria and cleaning ceases. This continued lowering of oxygen potential explains the reversion of Fe to the metal and the recommencement of ZnO reduction. The Fe activity in equilibrium with the bulk FeO activity and the final overall oxygen potential is approximately one. This is the final Fe activity one would expect to find throughout. To achieve this, Fe must return to the metallic phase. Similarly, the final ZnO activity is lower than that achieved by the rapid Fe driven reduction and certainly lower than the intermediate concentration seen after reversion.

6.1.2 The effect of bulk FeO activity.

Lowering the bulk FeO activity was seen to improve early cleaning rates while raising it had little effect. Looking again at the metal/slag interfacial oxygen potentials (figure (18)), lowering the bulk FeO activity encourages FeO diffusion into the bulk, firstly aiding the early Fe driven reduction and keeping the metal/slag interfacial oxygen potential low, and secondly, aiding diffusion of FeO away

Figure 18. Oxygen Activity at the Slag/Metal Interface versus Time For aFeO = 0.1 and 0.6.



from the slag/gas interface increasing the rate at which the overall oxygen potential is lowered. Most importantly, the lower bulk FeO activity will come into equilibrium with a said oxygen potential with a lower Fe activity. This means that much less Fe recontamination of the metal phase will occur. Note that even though the bulk oxygen potential of the slag will drop more rapidly, the rate of slag cleaning will not be greatly enhanced due to the lowering of driving force for FeO to travel to the metal/slag interface, thus limiting the rate at which oxygen can be removed from there. Also note that the very low oxygen potential that is seen in the initial stages causes much more Zn and Pb removal, but the slow kinetics of the $FeO/FeO_{1.5}$ reduction mechanism that follows allows significant reversion of Zn and a small amount of reversion of Pb.

As expected, raising the bulk FeO activity results in the opposite effects. The metal/slag interfacial oxygen potential is higher, initial cleaning slower, reversion much less marked, and severe Fe recontamination apparent.

6.1.3 The effect of high gas phase oxygen potential.

If the oxygen potential at the slag/gas interface is high, no reduction to metal occurs here. Any cleaning must result from Fe lowering the metal/slag interfacial oxygen potential. Once the Fe is taken up by the slag, any metal present will begin to oxidize. All values return to the slag and the bulk copper itself begins to oxidize.

6.1.4 The effect of increasing temperature.

As discussed in the model output section, changing the value of the input for temperature merely changes the position of the equilibria, any physical or kinetic effects being ignored. The slag/gas interfacial oxygen potential is set to just avoid FeO reduction. Increasing the temperature means that FeO can be reduced at higher oxygen pressures. To avoid FeO reduction, the p_{O_2} of the gas must be raised from 4.5 x 10^{-14} (standard conditions) to 5.3 x 10^{-11} atm. Table(8) shows the changes in equilibrium constants. Increasing temperature has very little effect on the equilibria of $CuO_{0.5}$ and PbO. The changes in NiO, SnO, and FeO are similar, while the high entropy of the formation of ZnO reaction causes a large change in the position of its equilibrium. Very little change in the cleaning of NiO and SnO is expected. Although their equilibria have moved favourably, the similarity of the change in FeO equilibrium means that the necessary change in p_{O_2} to avoid FeO reduction effectively cancels out any advantage gained. Because the equilibria of $CuO_{0.5}$ and PbO change little, the increased p_{O_2} will hinder cleaning of these oxides. Indeed, the increased p_{O_2} has become sufficiently high to prevent any slag/gas interface reduction of PbO taking place. The change in ZnO is sufficiently large to overcome the increased p_{O_2} and reduction occurs. Figure (19) shows the fluxes of species being reduced at the slag/gas interface. The PbO now displays the typical revertive behaviour associated with

Table 8. Equilibrium Constants of Species at 1200 °C and 1500°C.

Equilib. Constants	S P E C I E S .					
	$CuO_{0.5}$	NiO	SnO	PbO	ZnO	FeO
$E^{1200^{\circ}C}$	1.2×10^{1}	8.9×10^{3}	6.0×10^{4}	7.4×10^{3}	9.2×10^{5}	1.9×10^{6}
$E^{1500^{\circ}C}$	5.2×10^{0}	2.7×10^{2}	1.6×10^{3}	6.1×10^{1}	1.6×10^{1}	5.5×10^{4}
$\frac{E^{1500^{\circ}C}}{E^{1200^{\circ}C}}$	4.3×10^{-1}	3.0×10^{-2}	2.7×10^{-2}	8.2×10^{-2}	1.7×10^{-3}	2.9×10^{-2}

Figure 19. Flux Densities of Metal Being Reduced at the Slag/Gas Interface vs. Dimensionless Time. Temperature = 1500°C.

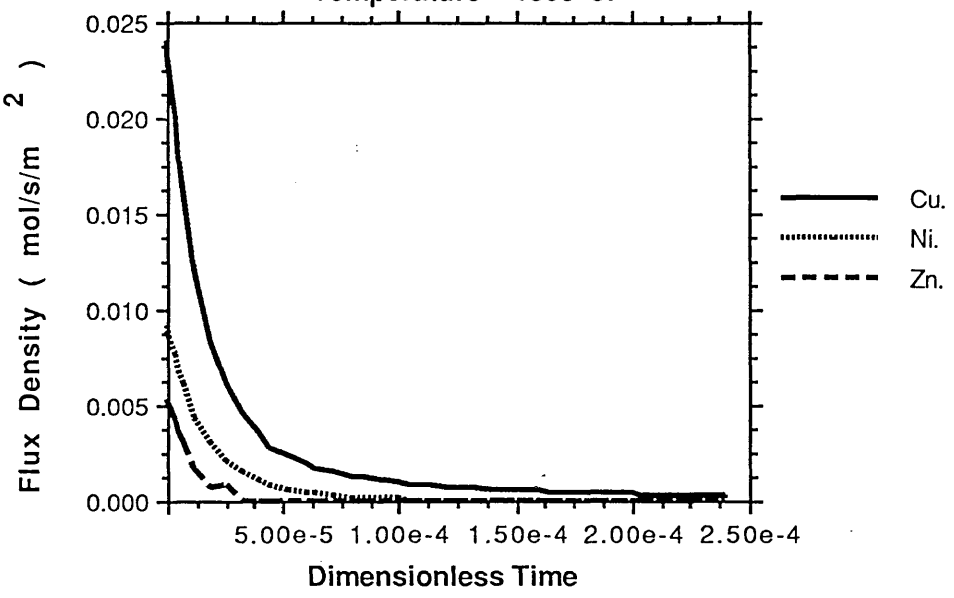
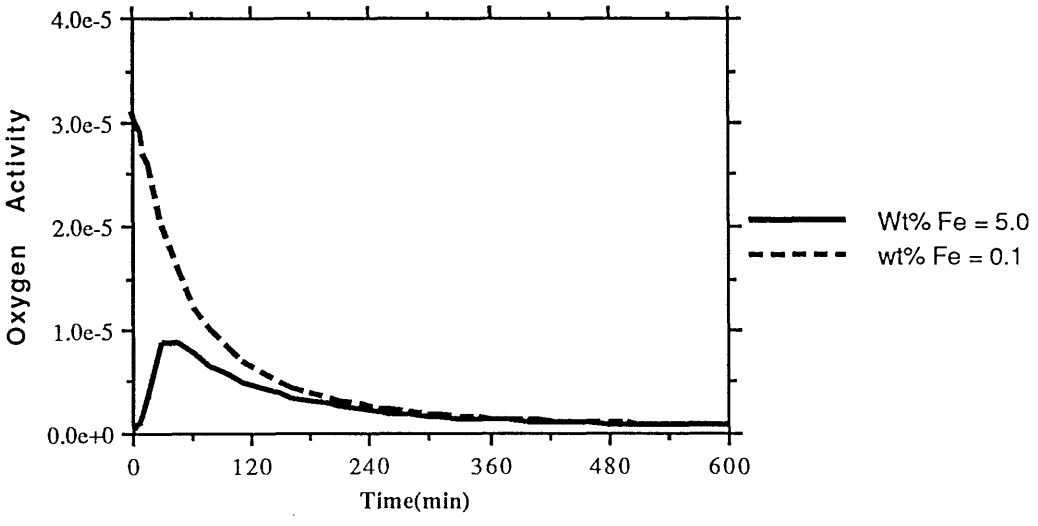


Figure 20. Oxygen Activity at the Slag/Gas Interface vs. Time with and without initial Fe.



oxides only reduced at the metal/slag interface. If removal of zinc is of primary importance, increasing the temperature yields better cleaning, but at the expense of higher losses of some other values. The volatility of Zn may result in losses to the gas phase if a large metal/gas interfacial area is present.

Note that although no work has been done to investigate the changes in kinetic conditions in this study, it is known that the reaction will proceed more rapidly (ie. 1 dimensionless time unit will convert to a shorter period of real time at higher temperatures than for the standard conditions).

6.1.5. The effect of low initial iron activity in the metallic phase.

Figure (20) shows the metal/slag interfacial oxygen potential with and without an initial high iron activity in the metallic phase. When little Fe is present, the metal/slag interfacial oxygen potential is high, meaning that little reduction occurs here, the majority of cleaning being carried out at the slag/gas interface. The absence of the rapid Fe driven reduction early in the simulation results in slower process kinetics. No revertive behaviour is found, due to the lack of the initial low metal/slag interfacial oxygen potential. The amount of iron oxide formed by the oxidation of Fe from the metallic phase is small relative to the amount present in the slag. Reducing the initial Fe content from 5.0 Wt% to 0.1 Wt% results in little change to the final slag composition. Thus, it is expected that the

final extent of cleaning, and Fe recontamination of the metal to be similar to that of the standard conditions.

6.1.6. The effect of increasing the metal/slag mass ratio.

Increasing the metal/slag mass ratio has a three-fold effect. Firstly, it provides more metallic iron per unit mass of slag. This results in the metal/slag interfacial oxygen potential remaining low throughout the entire process time, giving rapid thorough cleaning. Secondly, the large quantity of metal means that for the same extent of cleaning, the product values in the metallic phase will be more dilute. This aids the ease in which metal species can move into the bulk metal, enhancing cleaning. Thirdly, the mass of Fe entering the slag causes a significant change in slag composition, leading the process to a different final equilibrium.

Although the slag is very low in values, subsequent treatment of the dilute product metal will be more difficult. Also, because of the substantial change in slag composition, extreme caution must be exercised when considering these results.

6.2 Model Validity.

The validity of this model can be considered with respect to

(1) the general applicability of Robertson's treatment of multi-component metal/slag/gas reactions

and

(2) the specific applicability of this treatment to slag cleaning.

Incorporation of the following factors demands specific alterations to the general formulations

- chemical reaction control
- effects of interfacial tension changes during reactions on mass transfer coefficients and areas of contact
- analogous effects of reactions involving gas evolution on mass transfer coefficients and areas of contact.

Floyd and Mackey[1], in a review of the very limited number of studies on the kinetics and mechanisms of slag reduction reactions, have concluded that any of the following processes can be rate determining.

(1) interfacial adsorption and desorption of reactants and/or products.

(2) nucleation and growth of solid, gaseous or liquid products.

(3) mass transport of species in metal, slag, and gas phases.

The possibility of other than mass transport control therefore cannot be neglected and further experimental studies are an essential prerequisite to adequate process modelling. Complications due to gas evolution via either CO

or SO_2 evolution may arise during slag cleaning reactions. Many of the flaws in the present model, resulting from the lack of fundamental data and over-simplification of reality, have been mentioned earlier in section 1.3 and 3.5 .

In addition, the assumption that the reducing conditions may be represented by simply considering that some given oxygen potential is established at the slag/gas interface may represent a serious over-simplification of the true state of affairs. Such an approximation may be reasonable when only gaseous reductants are employed, but in many practical cases solid reductants such as coke or coal are also used. In this case, entrainment of solid reductants in the slag phase and their subsequent reaction to liberate gas may provide local slag/gas interfaces at oxygen potentials different to the main slag/gas interface. The importance of such considerations has long been recognized in studies of the fuming of zinc oxide by submerged injection of reductants where different Zn removal rates are commonly achieved when using either CH_4/O_2 or alternatively coal/O_2 to provide the reducing conditions. Recent studies by Richards and co-workers[25-27] have indicated that in such zinc fuming operations, up to 33% of the injected coal may be entrained in the slag phase at any time, and that this entrained coal contributes significantly to the rates of zinc reduction and fuming.

6.3 Model Development

The reservations expressed about the complete applicability of the present model to slag cleaning and the lack of fundamental kinetic data for slag cleaning conditions and reactions under known controlled conditions indicate that any future programme of model development must be performed in parallel with a laboratory scale experimental programme of slag reductions. Further bench top scale experiments on FeO - SiO_2 based slags seems a sensible path for further investigation, followed by experiments with these simple slags fluxed with Al_2O_3 and/or CaO, for example. Once sufficient reduction data is collected with the simple gas phase reduction, more complex solid phase reductants could be considered. The resultant collection of information under known oxygen partial pressures, achieved by various reductants, and known interfacial areas should provide better estimates of the required kinetic and thermodynamic inputs to the present model and should permit a fundamental understanding of particular aspects of slag cleaning. Expansion of the model to allow for these more complex circumstances could be performed in parallel. A model that produced predictions of interfacial areas as a function of process parameters, along with predictions about the nature of entrained reductants, evolved or injected gases, and dispersed metal droplets would be exceedingly difficult to create without relying heavily on emperical relationships or making many simplifications. However, once interfacial areas

are estimated, the model can be applied to every interface(eg. slag/metal droplet, metal/gas bubble) and solved in exactly the way described here. In this way, a wide variety of process configurations and conditions could be modelled.

Finally, application and tuning of the adapted model to either pilot plant or full scale slag cleaning reactors would allow a more complete description of industrial operations. Incorporation of heat balances into the process modelling would permit consideration of non-isothermal conditions resulting from either exothermic reactions or deliberately programmed change in reaction temperature. Also, as the reaction occurs at interfaces, a model that takes into account the thermal gradients to and from these interfaces would enable better estimation of the actual interfacial reaction temperature and thus avoiding the need to approximate to the bulk temperature.

SECTION TWO.

THE DECOPPERING OF LIQUID LEAD BULLION BY ELEMENTAL SULPHUR ADDITIONS.

7.0 Introduction.

The refining of liquid lead bullion product from the lead blast furnace involves numerous refining stages aimed at either removing impurities for their intrinsic value or because of their deleterious effects on the properties of lead. Copper removal is affected in two stages,

(1) cooling and separation of a copper rich matte phase and

(2) addition of elemental sulphur at temperatures close to the melting point of lead and the preferential formation of copper sulphides.

This second stage, variously referred to as sulphur drossing, cold drossing, or fine decoppering is the subject of this work.

The first stage of copper removal(matte separation) typically results in a final copper level of around 0.05 Wt% Cu. The sulphur drossing stage is remarkable in that equilibrium calculations indicate that for copper levels of less than 0.05 Wt% Cu, lead sulphide would be anticipated to form preferentially to chalcocite(Cu_2S) or covellite(CuS).

In industrial practice however, copper levels more than an order of magnitude lower than this are regularly achieved initially, but in time copper reverts to the lead to the equilibrium value of 0.05 Wt% Cu.

Recent articles[28,29] give details of the numerous previous fundamental and applied investigations of the sulphur drossing of lead bullion. Previous investigations have

typically been involved with system thermodynamics[31,32], identification of phases formed during the decoppering process[32-34], elucidation of the decoppering mechanism[35-38], laboratory and pilot plant studies of the effect of process variables on the extent of decoppering[39-41], and the development and model simulation of batch wise and continuous sulphur drossing operations[29,42,43].

It seems clear that kinetic considerations must be applied to explain the observed excessive decoppering. The observation that

(1) the presence of very small quantities of silver in the lead melt result in more extensive and more rapid decoppering and

(2) that the intermediate formation of covellite occurs during decoppering appear to be particularly pertinent.

PbS formation is initially kinetically suppressed allowing a transient low level of copper in the lead to be achieved. The suppression of PbS formation has been attributed to

(1) chemical kinetics being slow, especially in the presence of Ag which, it has been suggested, acts as a surface active "anti-catalyst" or

(2) transport limitations on the growth of PbS, the silver in this case altering the defect structure and transport properties of solid PbS.

In this work, based on the detailed observations of Clarke and co-workers[32,33], and observations made by the author and co-workers, it has been assumed that sulphur droplets

stirred into the lead bullion are instantly encased in solid sulphides. Transport of reacting species through these solid layers then allows the continued growth of PbS and copper sulphides. A model has been developed, assuming that the decoppering process is controlled by diffusion through such sulphide layers separating the liquid lead and liquid sulphur, which shows agreement with observed reaction rates, and sulphide layer thicknesses and morphology for both initial decoppering and subsequent reversion.

However, the lack of critical fundamental data relating to diffusion rates in sulphides and the inconsistency of values quoted in literature(See table(9)) highlighted the necessity for experimental determination of this information. A series of simple experiments to determine the growth kinetics of solid sulphides was undertaken. The results of these experiments were implemented in a computer model when final comparisons and contrasts were drawn with observed decoppering practice.

Table (9). Published Diffusion Coefficients. ($cm^2.s^{-1}$)

Note that these values relate to species diffusing through perfect sulphide crystals.

SULPHIDE MATRIX	DIFFUSION COEFF. ($cm^2.s^{-1}$)			TEMP. (K)	Reference Number.
	Pb	Cu	S		
PbS	1.05×10^{-14}			773	44
PbS	4.27×10^{-13}			733	52
PbS		1.40×10^{-1}		600	36
PbS		1.24×10^{-1}		600	45
PbS		4.35×10^{-3}		600	51
PbS			6.80×10^{-15}	773	48
$CuS_{0.s}$		$4.20\times10^{+01}$		673	49
$CuS_{0.s}$		$1.50\times10^{+00}$		500	50
$CuS_{0.s}$		8.70×10^{-01}		450	53

8.0 Theoretical Considerations.

8.1 Basis of Model

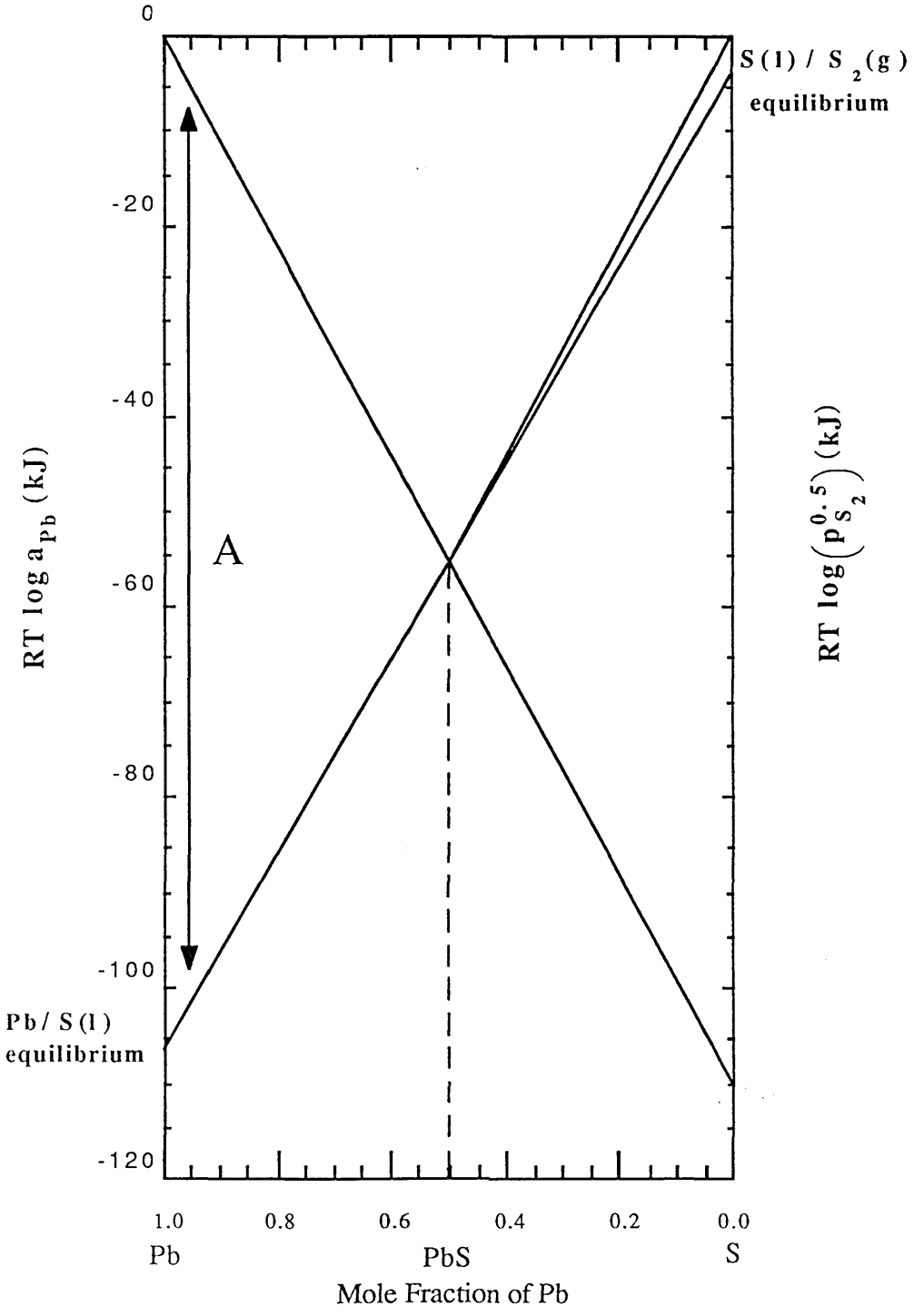
Consideration of the partial Gibb's free energy of mixing in the Pb/S system(see figure(21)) indicates that when liquid S is contacted with liquid Pb, solid PbS will form instantly, assuming no delay in phase nucleation. This results in a solid PbS layer forming between Pb liquid and S liquid, and diffusion of reacting species through the PbS layer is required if further growth of PbS and consumption of S is to occur. Sulphur and lead activity gradients exist across the PbS layer. These gradients, assumed linear for lack of any reliable information to indicate otherwise, provide the driving force for diffusion through the layer and hence growth of the PbS layer.

Investigations by Simkovich and Wagner[44] into the diffusion of Pb through n-type PbS concluded that diffusion in pure PbS crystals takes place because Frenkel point defects give rise to mobile interstitial Pb ions which carry single positive charges(Pb_i^+). Bloem and Kroger[45,46] suggested that the major mobile species in p-type PbS was singly positively charged vacancies(V_c^+). The diffusion of Pb in solid PbS is quite slow, whilst the diffusion of S ions is so slow as to allow them to be considered immobile(see Table (9)). Thus, once the initial PbS layer forms, further growth of the PbS layer will be slow. Bloem and Kroger also found that the diffusion of copper ions through PbS was much faster than Pb

Figure 21. ΔG° for the Pb/S System at 330°C.

Pb Activity and S Potential in Equilibrium with PbS also shown .

A - Initial PbS Layer Growth 'Driving Force'.



diffusion due to the small Cu^{+} ionic radius(9.6 nm) compared with the Pb^{++} ionic radius(13.2 nm) and $S^{=}$ ionic radius(17.4 nm).

Thus,with Cu rapidly diffusing through PbS, the Cu potential at the PbS/S(liquid) interface will climb to a point where copper sulphides will form preferentially to PbS. Consideration of the partial Gibb's free energy of mixing in the Cu/S system(see figure(22)) indicates that CuS will be the first copper sulphide that will form at these high S potentials, giving rise to decoppering.

8.2 The Effect of Silver.

PbS will change from n-type to p-type, that is from Pb_i^{+} and electrons as the mobile species to V_c^{+} and electron holes when a critical S potential is exceeded. In pure PbS, this is the S potential in equilibrium with roughly stoichiometric PbS. If the S potential is lower, PbS will be Pb rich, and diffusion occurs via Pb_i^{+} ions. If the critical S potential is exceeded, PbS will be S rich, and diffusion occurs due to V_c^{+} migration. Thus, when pure Pb is contacted with pure S, the layer will be n-type when adjacent to the Pb and p-type at the PbS/S(liquid) adjacency.

Somewhere within the layer, the critical S potential and thus the p-n junction exists, all PbS above this point being p-type, all below being n-type(see figure (23)).

According to Bloem and Kroger[45], the influence of Ag is to dramatically reduce this critical S potential. This results

FIGURE 22. ΔG° for the CuS/S System at 330°C.
The Lines Show Cu Activities and S potentials
in Equilibria with CuS and CuS .

A - Decoppering 'Driving Force'
B - CuS Layer Growth 'Driving Force'

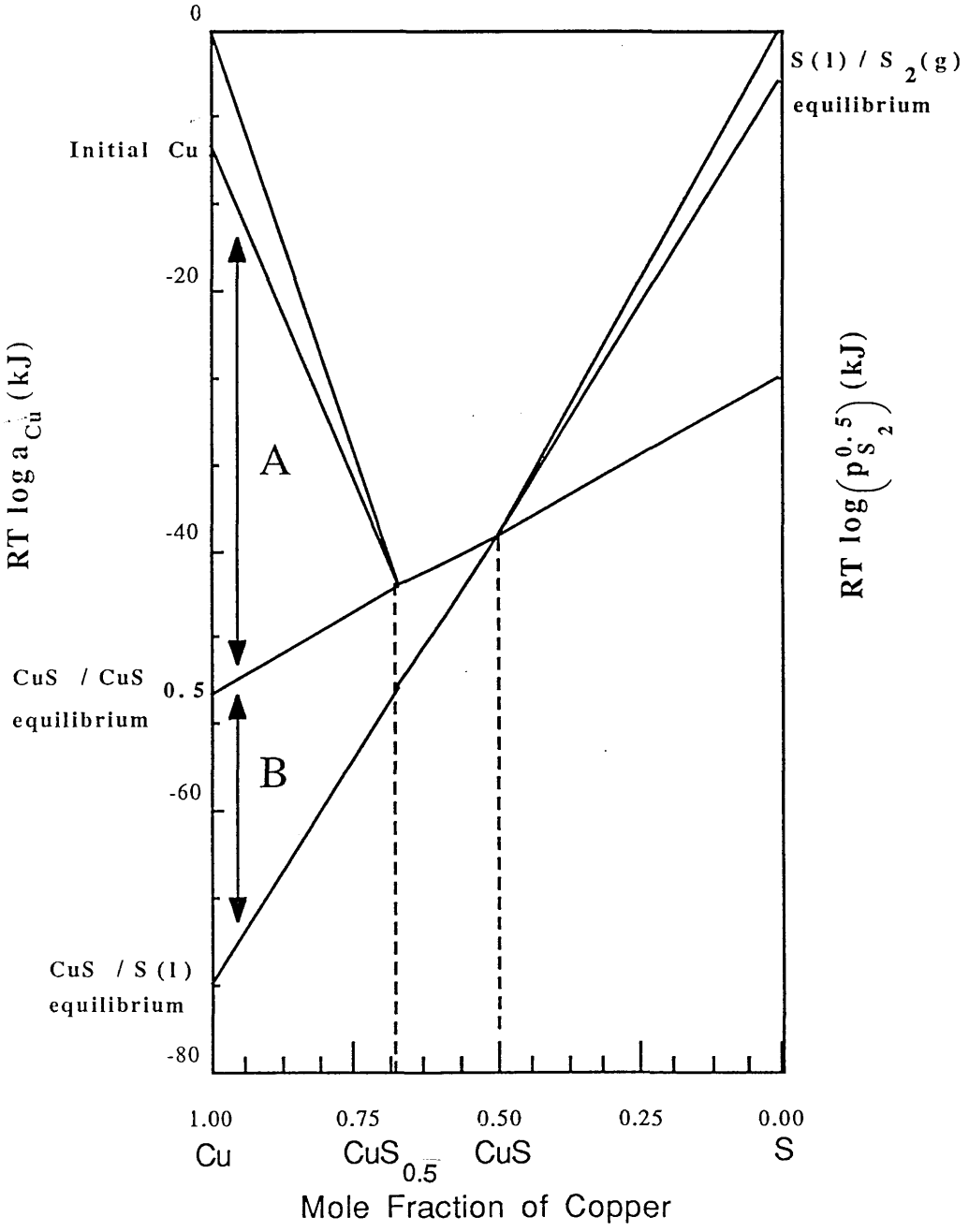
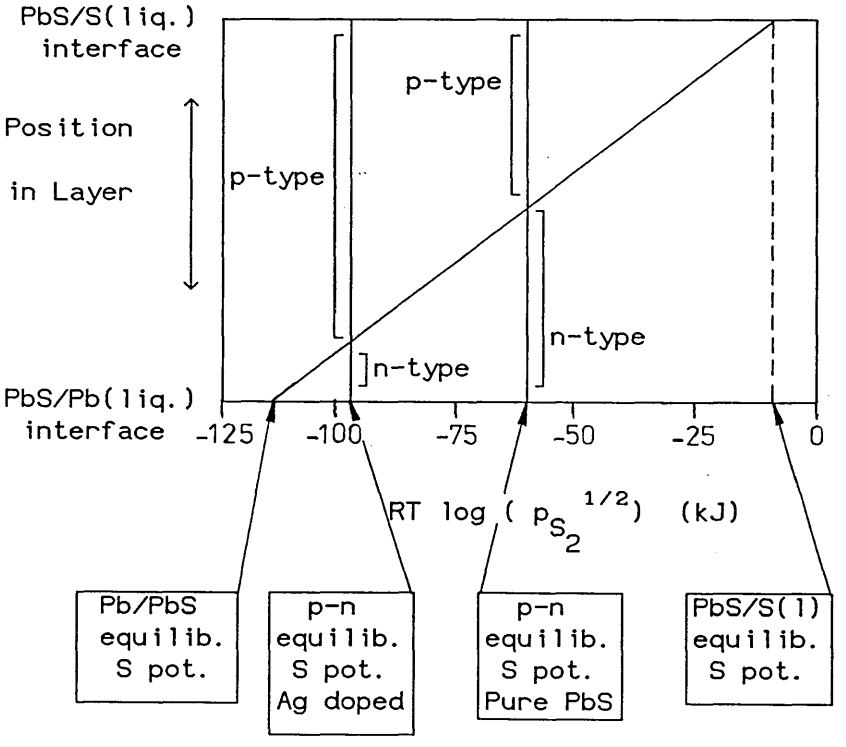


Figure 23. Schematic Representation of the Effect of Ag on the PbS layer, showing the roughly equal proportions of p-type and n-type when PbS is pure, and the vastly greater proportions of p-type expected when Ag is present. (Note that it is possible that no n-type at all is present if the p-n equililbrium S potential falls below that of the Pb/PbS equilibrium potential.)



in a far greater proportion of the PbS layer being p-type. Assuming that V_c^+ diffuse more slowly than Pb_i^+, the overall resistance to mass transport of Pb across PbS will be increased in the presence of silver. Thus, Ag contamination of the bulk may be very beneficial for good decoppering because when PbS is p-type, it forms so slowly that there is an opportunity for Cu transport through a thin PbS layer well before all the sulphur is consumed by reaction with lead. On the other hand, when Ag is absent, a PbS layer forms rapidly consuming the majority of the sulphur.

9.0 Kinetic Model for Decoppering

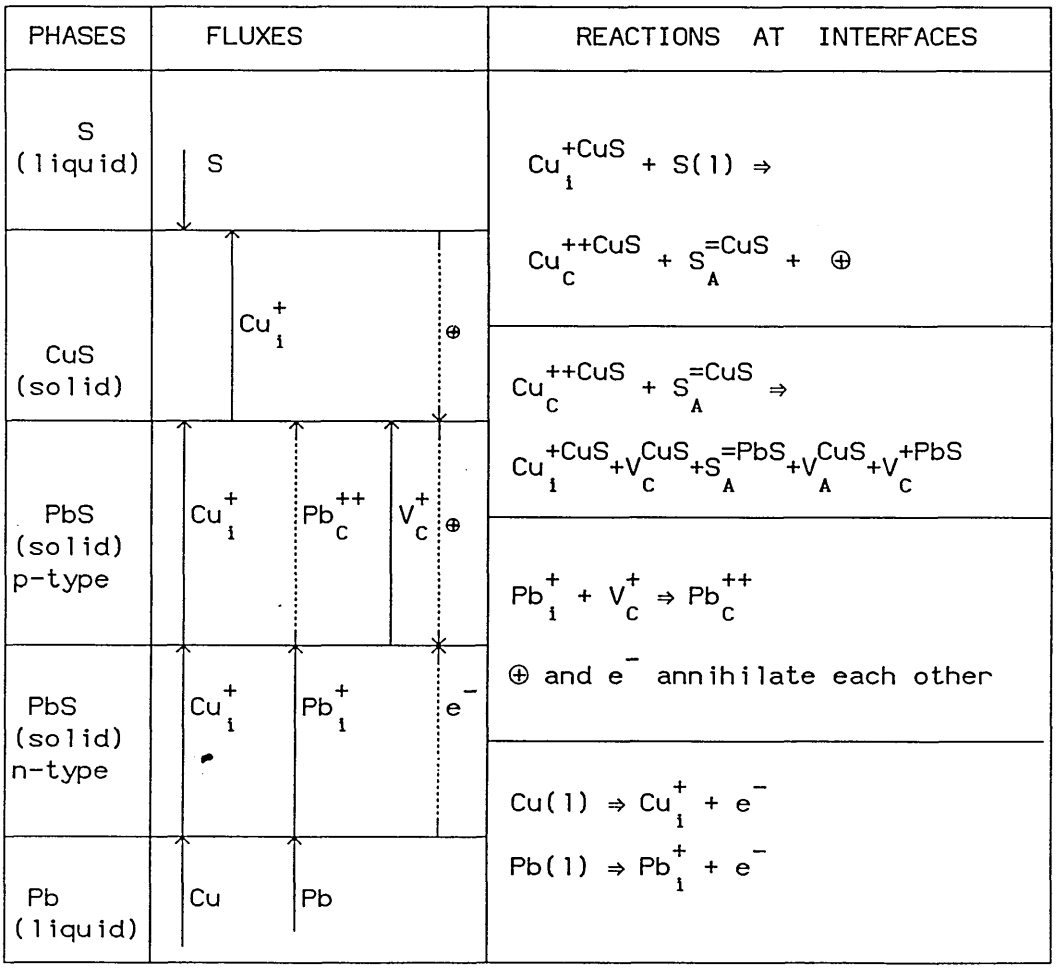
9.1 Decoppering

The above considerations lead to the construction of the kinetic model pictured in figure(24). This configuration exists when the Cu potential at the PbS/CuS interface is not high enough for $CuS_{0.5}$ to form. The rate of growth of the CuS layer depends on the rate of Cu ion diffusion to the liquid sulphur through the liquid Pb bullion, the solid PbS layer and the CuS layer.

Transport equations for each phase are detailed in the following section, and show that the rate of growth is inversely related to the thickness of each layer. Here, due to the self-dependence of the growth rate, iterative numerical methods are used to calculate the growth of the layers, assuming that for each of a series of small time intervals, each layer thickness is constant at a particular value for that interval and is incremented for each subsequent time step. Similar assumptions are applied to inter-facial and bulk activities.

As the CuS layer thickens, the copper activity at the PbS/CuS interface increases, due to increased resistance to diffusion across the thickening CuS layer, causing a build-up of copper activity approaching that of the bulk bullion. At some point in time, the copper activity has climbed sufficiently high to cause the formation of $CuS_{0.5}$, hence a layer of $CuS_{0.5}$ forms between the PbS and CuS phases. The model then becomes as

Figure 24. Schematic Model of the Reaction Products which are formed and the transport Paths followed when Liquid Sulphur comes into Contact with Liquid Lead. It can be seen that adjacent to the liquid lead are n and p type layers of solid PbS which are instantaneously formed on contact of S liquid with Pb and then a solid CuS layer which forms by Cu diffusion to the liquid sulphur interface through the solid PbS layers. The reaction taking place at each interface are also shown.

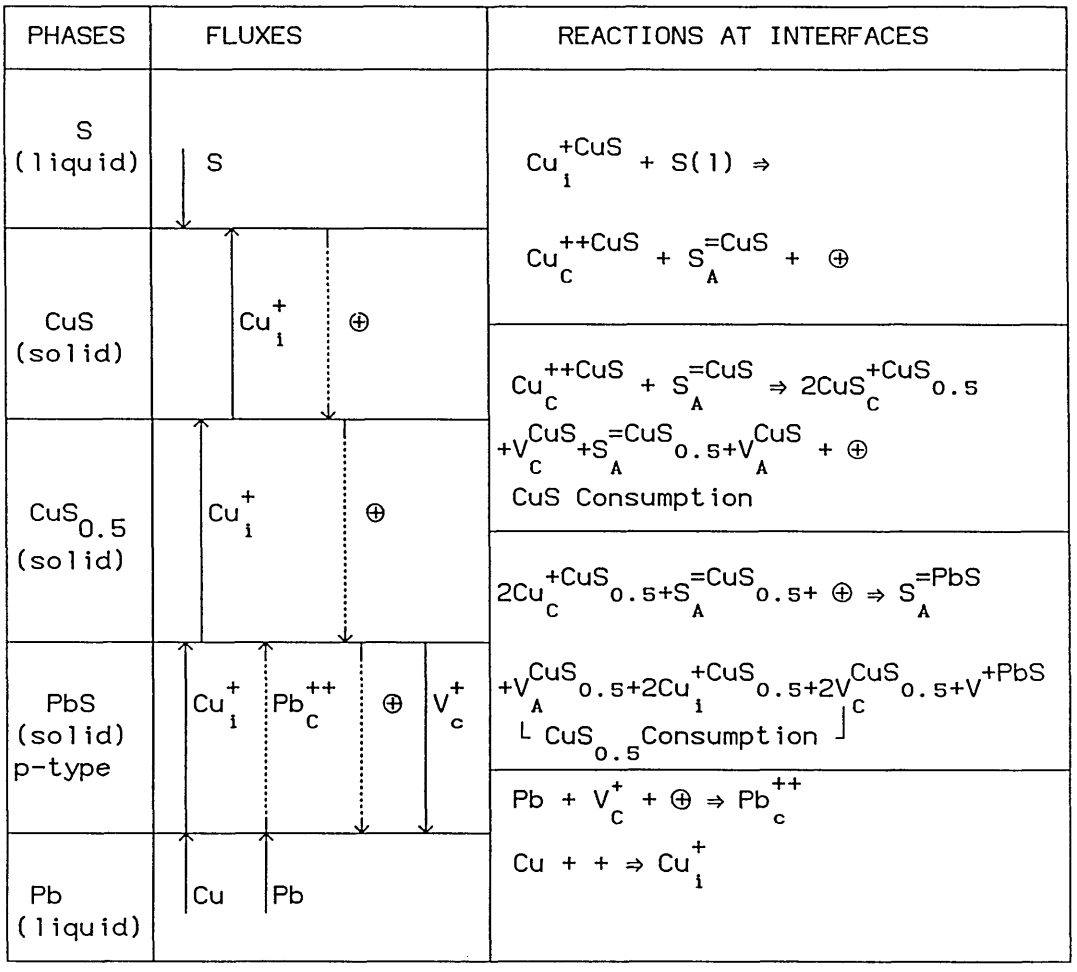


shown in figure(25). $CuS_{0.5}$ growth proceeds as copper continues to diffuse through the solid layers at the expense of the CuS layer, that is, as the CuS layer grows into the liquid sulphur, the $CuS_{0.5}$ layer grows into the CuS . While liquid sulphur provides a high S potential and thus a low Cu potential at the CuS/S interface, copper will diffuse away from the bulk Pb. The overall driving force decreases with time as the bulk concentration of Cu in liquid Pb decreases and the activity gradient is further reduced as the intervening solid layers become thicker. At the time when all the S liquid is consumed, the Cu potential at the top of the CuS must rise rapidly from its value in equilibrium with liquid S to its value in equilibrium with $CuS_{0.5}$. The CuS layer will continue to be consumed by the advancing $CuS_{0.5}$ layer and the copper ion flux in the CuS will be negligible because there is no source of, or sink for, copper at the front surface of the CuS. Note that decoppering will still be occurring during this period after all the S liquid is consumed but before the whole copper sulphide layer exists as $CuS_{0.5}$.

9.2 Reversion

Once the copper sulphide layer is entirely $CuS_{0.5}$ and all the CuS is consumed, the Cu potential at the front interface will rise from the $CuS/CuS_{0.5}$ equilibrium value to the $PbS/CuS_{0.5}$ equilibrium value, that is, there will be negligible flux of copper ions through the $CuS_{0.5}$ layer due to the lack of a

Figure 25. Schematic Model as in Figure 24, But also showing the $CuS_{0.5}$ Layer which forms between the PbS and CuS layers.



source or sink for copper ions at the top surface of the $CuS_{0.5}$. Figure(26) shows the expected configuration.

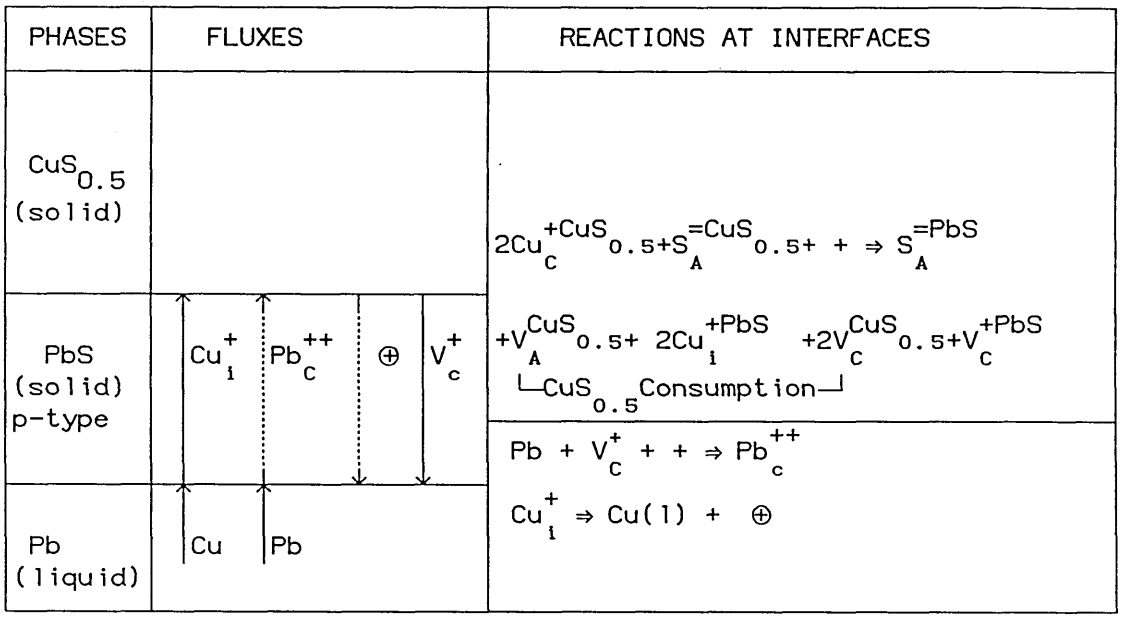
Interstitial lead ions will still be diffusing through the PbS layer slowly. On arriving at the $CuS_{0.5}$ layer, they will dislodge two Cu^{+} ions to form the more thermodynamically stable PbS. The Cu^{+} ions diffuse freely back through the PbS layer to the now low Cu potential bulk metal, and thus produces reversion. The reversion rate is limited by the speed at which lead can diffuse through PbS and will be very slow, especially when PbS has built up to a substantial thickness.

9.3 Model Applicability

The processes described in the previous two sections have been subjected to a computer simulation on the basis of the general multi-component transport control theory of Robertson described earlier.

It seems pertinent to critically examine the model applicability at this stage. The diffusion equations relating mass transport to activity differences across solid sulphide layers assume constant average values for the diffusion coefficients of individual species across each sulphide layer. The possible effects of porosity and rapid diffusion paths along grain boundaries are therefore implicitly incorporated in the values chosen for the species diffusion coefficients and layer thicknesses. Variations of activity coefficients of individual species across each layer

Figure 26. Schematic Representation of the Decoppering System after the CuS Consumes all the CuS and Reversion has commenced.
0.5



have also been neglected. All interfacial areas have been assumed constant and thus represent a planar cross section on an imaginary lead bath initially covered with sulphur. Each phase is therefore assumed to be in perfect contact with the adjacent phase and no intermixing of phases occurs. There is no reduction in interfacial area or additional mass transport resistance present at any phase boundary. The sulphide phases have been assumed to have constant densities, a reasonable assumption in view of their limited range of stoichiometry. The model does not consider any contribution of chemical resistance to the overall process rate and any delays in phase nucleation have been neglected.

9.4 Mathematical Formulation

The mathematical formulation employs the same general principles used in the slag cleaning model, except that the system has many layers, some of which are solid. Equilibria are still assumed at all interfaces and the thin film diffusion theory is applied to the liquid phases. However, a new form of equation is needed to describe mass transport across the solid layers.

The equation selected is,

$$N = D.C.(a_{top} - a_{bottom}) / (\gamma.\tau)$$

where N is the flux density ($mole.s^{-1}.m^{-2}$)

D is the diffusion coefficient ($m^2.s^{-2}$)

C is the total molar concentration ($mole.m^3$)

a_{top} is the activity of the diffusing species at the top interface

a_{bottom} is the activity of the diffusing species at the bottom interface

γ is the activity coefficient

τ is the layer thickness

This equation implicitly requires the activity coefficient to remain constant across the layer. Examining the more fundamental equation (as quoted by Schmalzried[47]),

$$N_i = \frac{- D_i c_i}{R.T} \frac{d \mu_i}{d x}$$

where $\mu_i = R.T.\ell n\ a_i$

c_i = local concentration of diffusing species, i

x = distance through the layer

leads to,

$$N_i = -D_i\ c_i\ \frac{d\ \ell n\ a_i}{d\ x}$$

$$= -D_i\ c_i\ \frac{d\ ln\ a_i}{d\ a_i}\ \frac{d\ a_i}{d\ x}$$

Now,

$$\frac{d\ \ell n\ a_i}{d\ a_i} = 1/\ a = 1/(X_i.\gamma_i)$$

where X_i = the local molar concentration of diffusing species, i.

Assuming constant γ_i with X_i,

$$N_i = \frac{-D_i}{X_i} \frac{c_i}{\gamma_i} \frac{d\, a_i}{d\, x}$$

Now,

$c_i / X_i = C_i$, the bulk molar concentration

So,

$$N_i = \frac{-D_i . C_i}{\gamma_i} \frac{d\, a_i}{d\, x}$$

Assuming a linear activity gradient across the layer,

$$\frac{d\, a_i}{d\, x} = (a_{top} - a_{bottom}) / \tau$$

The conservation equations relating change in bulk concentration to flux remain the same as previously used. However, equations relating the change in layer thickness to flux are of the form,

$$d\tau/dt = (N_{in} - N_{out}) / C$$

where τ = layer thickness (m)

t = time (s)

N = flux density ($mole.s^{-1}.m^{-2}$)

C = bulk molar concentration ($mole.m^{-3}$)

The full description of the mathematical formulation can be found in appendix(4).

10.0. Experimental Procedure and Results

10.1 Aim of Experimental Programme

As mentioned in section 7.0, a lack of fundamental diffusion data prevented confident application of the model. Thus, it was necessary to perform experiments to evaluate the required diffusion coefficients. As it was the diffusion of Pb through PbS that was considered critical, this was the focus of the investigation. Controlled sulphide growth experiments were carried out, data relating reaction time and layer thickness collected, from which diffusion coefficients were determined following the procedure laid out in the following sections.

10.2 Determination of Diffusion Coefficients

The flux equations selected for this model were of the form,

$J = A.C.D.(a_{top} - a_{bottom}) / (\gamma.\tau)$ (equation 1)

where

J = flux of diffusing species($mole.s^{-1}$)

A = interfacial area(m^2)

C = bulk molar concentration($mole.m^{-3}$)

D = effective diffusion coefficient($m^2.s^{-1}$)

a_{top} = activity at the top surface of the layer

a_{bottom} = as a top at the bottom

γ = $\frac{\text{activity}}{\text{coefficient}}$

τ = layer thickness(m)

In the experiments, A, C, and γ are all known or estimated. a_{top} equals the Pb activity in equilibrium with S(l) and PbS(s) at the PbS/S interface, while a_{bottom} equals the activity of Pb at the Pb/PbS interface, assumed to be unity.

The conservation equation used for the model was of the form,

$$(J_{in} - J_{out}) = A.C.\ d\tau/dt \qquad \text{(equation 2)}$$

Seeing that all the the PbS that diffuses through the PbS layer reacts with sulphur to form PbS, $J_{out} = 0$.

Equating equations 1 and 2, then rearranging gives,

$$\tau_{Pb}^{PbS}\, d\tau_{Pb}^{PbS} = D_{Pb}^{PbS}(1 - a_{Pb}^{Pb/S}) / \gamma_{Pb}^{PbS} dt$$

Integrating,

$$\tau_{Pb}^{PbS^2}/2 = t\, D_{Pb}^{PbS}(1 - a_{Pb}^{Pb/S})/\gamma_{Pb}^{PbS} + C_1$$

At $t = 0$, $\tau = 0$, so $C_1 = 0$.

Also, $_{Pb}(1-a^{Pb/S})$ equals one to a very good approximation.

Thus,

$$\tau_{Pb}^{PbS^2} = (D_{Pb}^{PbS}.\gamma_{Pb}^{PbS})/2t$$

γ_{Pb}^{PbS} is assumed to be one. Thus, by plotting $\tau_{Pb}^{PbS^2}$ versus 2t, the slope equals the diffusion coefficient.

10.3 Preparation of Pb/Ag pellets.

One kilogram of "chemical A" grade Pb[55] was melted in a stainless steel container. A quantity of finely ground

silver was added and the melt stirred rapidly. The liquid was chill cast into a steel mould (see Figure (27)) which produced approximately 100 cylindrical pellets of 10 grammes each. A random selection of pellets were analysed to guarantee uniform composition across the batch.

A further quantity of "chemical A" lead was melted. A number of pellets were added to the melt and stirred. This again was chill cast into pellets. This procedure of dilution was repeated to provide batches of pellets at a series of compositions. These compositions are listed in Table(10).

10.4 Sulphide Layer Growth Experiments.

A vertical tube furnace (see figure (28)) was constructed. A temperature profile at a series of set point temperatures were performed with a differential thermocouple and a uniform hot zone 5 cm in length was found. The temperature variation with time was less than one degree celsius. A pellet was slid into a crucible (actually a pyrex test tube) and then placed into a crucible holder. This was introduced from the bottom of the furnace tube. The furnace was flushed with argon to prevent surface oxidation of the lead and combustion of the sulphur. The support rod was pushed up to locate the sample in the middle of the hot zone. Once the sample temperature reached that of its surroundings, sulphur powder was added from above. Only a small drop in temperature was observed, due to the small thermal mass of the sulphur relative to the sample and surroundings.

Figure 27. Steel Mould for Casting Pb Alloy Pellets.
Mould Held Together With G- Clamps.
Metal Rapidly Poured into Mould, Then
Excess Scraped Off Top.

+ G-clamp mounting points.

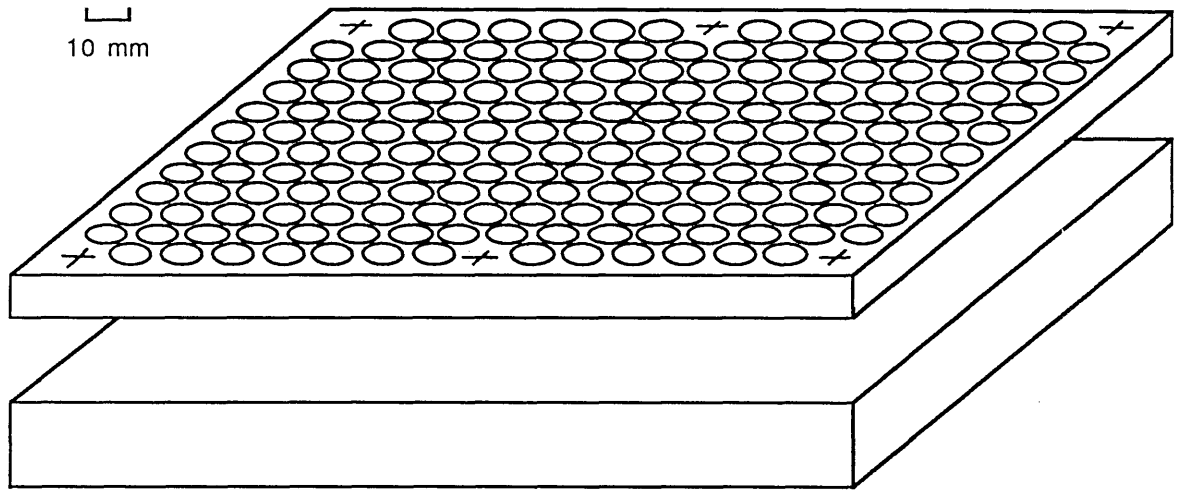
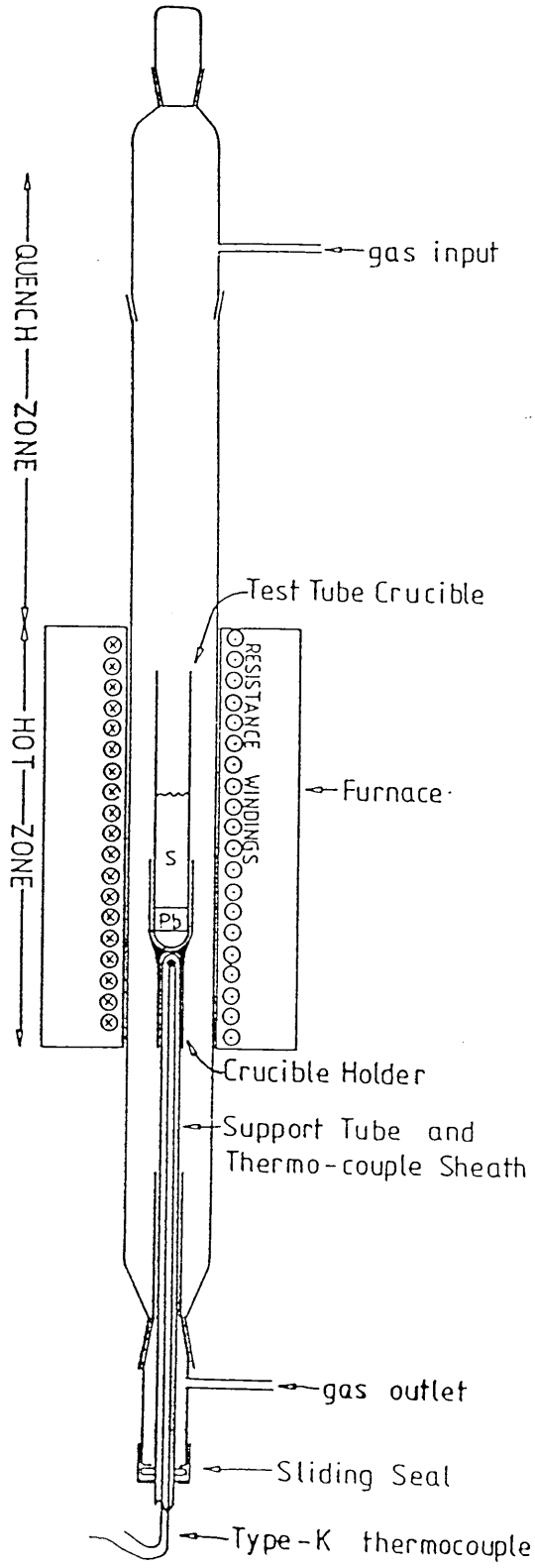


Table 10. Chemical Analysis Of Lead Pellets.

BATCH No.	Ag CONCENTRATION wt% Ag
1	0.10470
2	0.01400
3	0.00095
4	0.00060
5	0.00048
6	0.00038
7	0.00032
8	<0.00005

Figure 28. Vertical Tube Furnace Used For Layer Growth Experiments.



After various reaction times, the pellets were quenched, removed from the crucible, sectioned, and mounted in "Araldite 2003" mounting resin. This particular resin was used after trials with many other mounting media proved unsuccessful due to reaction with sulphur and the softness of the lead. Careful polishing to avoid smearing of the lead and fracture of the brittle sulphides followed. Scratch free samples were virtually impossible to produce.

Optical microscopy offered sufficient magnification and resolution to perform layer thickness measurements. Due to the non-uniformity of the layers, large numbers of measurements were taken and averaged for every sample. A example set of raw data is presented in appendix (5).

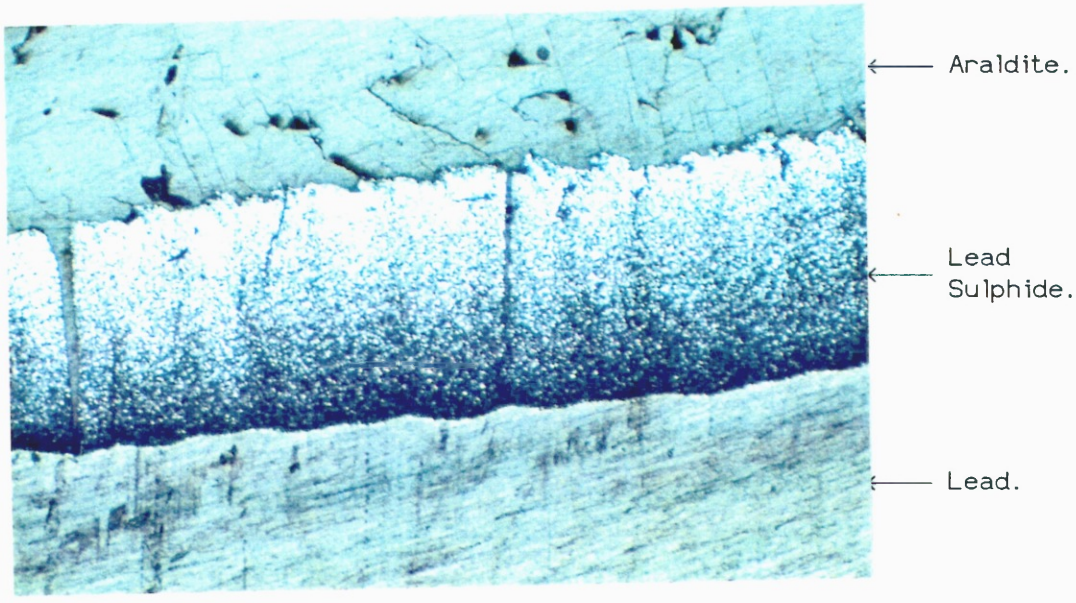
Also, experiments were usually done in triplicate to check for consistency. The actual number of readings varied with the quality of the sample(that is, some samples were of exceptional quality and did not require many measurements to determine the layer thickness). An eye-piece mounted graticule that was independently calibrated was used to perform the measurements.

Both the effect of variation of Ag content and temperature were studied independently. A small number of similar experiments were carried out with pellets of pure copper. Plate 1(a) shows the large PbS layer that grows on low Ag lead pellets, plate 1(b) shows the fine PbS layer that grows on high Ag lead pellets, and plate 2(a) shows the CuS and $CuS_{0.5}$ layer that grows on a copper pellet.

Plate 1. Micrograph Of The Phases Found During The Layer Growth Experiments On Pure Pb And A Pb/Ag Alloy.

Magnification = 4000 X

a) Layers Found When Liquid Sulphur Is Contacted With Pure Solid Lead Pellets For 2 Hours At 285°C.



b) Layers Found When Liquid Sulphur Is Contacted With Solid Lead Pellets Containing 0.1047 Wt% Ag For 48 Hours at 285°C.

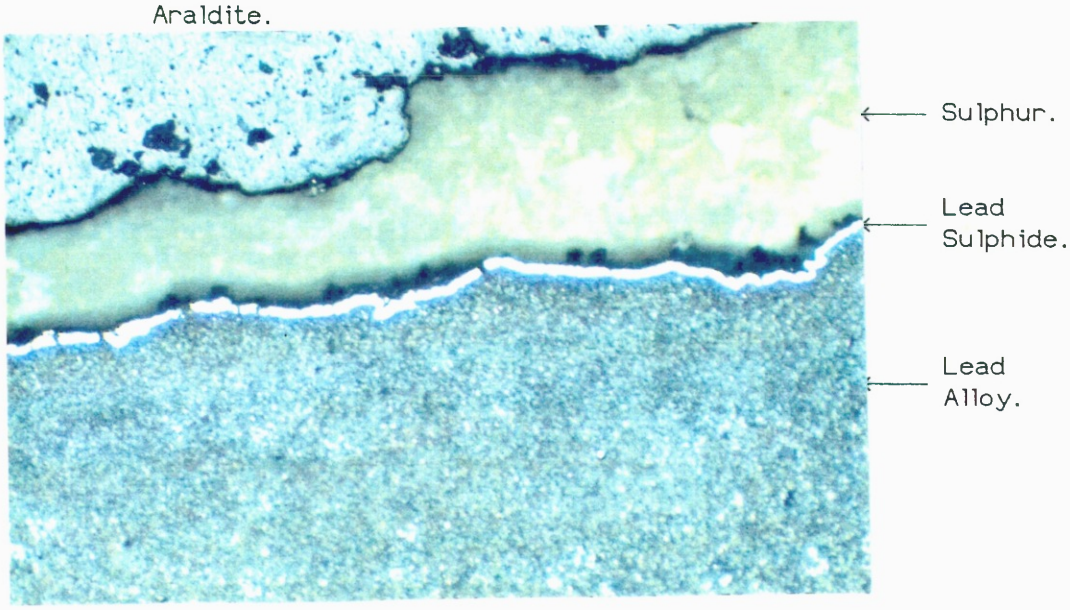
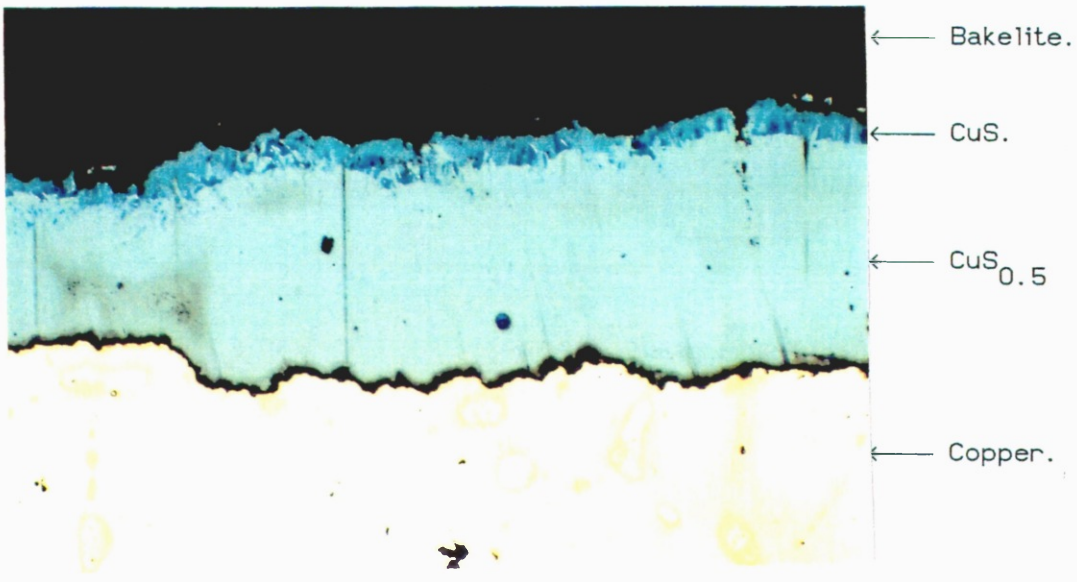


Plate 2. Micrograph Of The Phases Found During The Layer Growth Experiments On Pure Copper..

Magnification = 4000 X

a) Layers Found When Liquid Sulphur Is Contacted With Pure Solid Copper Pellets For 2 Hours At 285°C.



10.5 Experimental Development

Initial experiments above the melting point of lead met with limited success. The liquid sulphur and liquid lead unexpectedly mixed together, forming a very irregular interface. This resulted in a complex sulphide layer geometry which made legitimate measurement of layer thickness impossible, and prevented reasonable estimates of interfacial area, a fundamental input into the decoppering model. Thus, it was decided to limit experimental temperature to below the melting point. In this way, a planar interface and known interfacial area can be maintained. The draw-back to experiments below the lead melting point was that decoppering proved impossible. The increased resistance to Cu diffusion through solid Pb caused the Pb/PbS interfacial Cu activity to be low. This meant that a high enough driving force for Cu diffusion through the PbS layer, and thus copper sulphide formation, was not achieved. Thus, only simple single layer diffusion experiments were carried out.

Two groups of experiments were performed. The first group kept all process parameters constant and varied the temperature. The second group kept all process parameters constant including temperature, but varied the silver content of the reaction pellets.

10.6 The effect of temperature

A summary of the results for this series of experiments are

tabulated in table(11). The Ag content of the Pb was 0.1047 wt% Ag. The voluminous quantity of raw data and intermediate calculation have been omitted for the sake of brevity, but a sample calculation can be found in appendix (5). Diffusion coefficients were deduced by linear regression of the results. The correlation coefficients in all cases are satisfactory.

It was assumed that the relationship between the diffusion coefficient and temperature could be described by an equation of the form,

$D = D_0 \exp(- \Delta H/RT)$

Plotting ℓn D against 1/T (see figure (29)) gave the following results.

$D_0 = 3.7 \times 10^{-9} (m^2.s^{-1})$

$\Delta H = 4.066$ kcal/mole

10.7 The Effect of Silver Concentration

A summary of the results for this series of experiments are tabulated below in table(12) and shown graphically in figure(30). The temperature for all these experiments was 285^0C. It was intended to perform the trials at 300^0C, but an error in set point in the controller was not detected until an advanced stage of the experimental series, so it was decided to continue at 285^0C.

Correlation for the results where layer growth was quite slow was poorer than for other tests, but still well within acceptable limits.

Figure 29. Log Diffusion Coefficient in PbS versus Inverse Temperature.
Ag Concentration = 0.1047 wt%

ΔH = 15.99 kcal/mol

$D_o = 3.7 \times 10^{-9}$ m^2 / sec

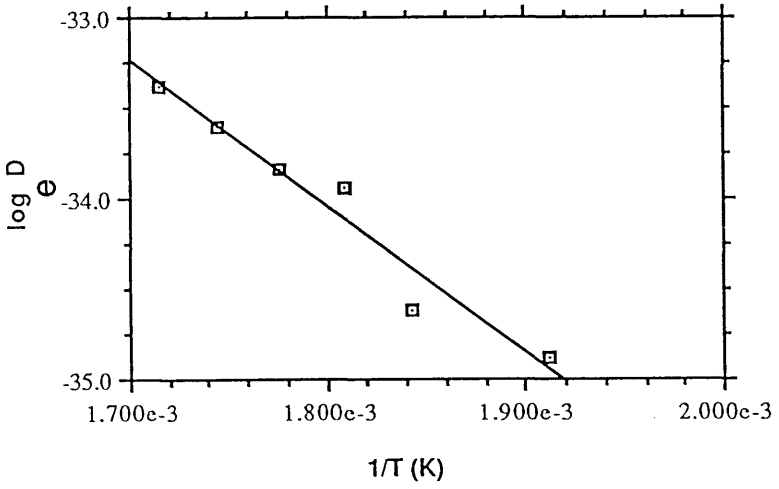


Table 11. Pb in PbS Diffusion Coefficient versus Temperature.

TEMP. C^0	Diffusion Coefficient ($m^2.s^{-1}$)	Correlation Coefficient (dimensionless)
250	7.08×10^{-16}	0.956
270	9.20×10^{-16}	0.989
280	1.82×10^{-15}	0.948
290	2.02×10^{-15}	0.988
300	2.55×10^{-15}	0.996
310	3.20×10^{-15}	0.977

FIGURE 30. The Variation in the Effective Diffusion Coefficient of Lead Through PbS with Silver Concentration of Bulk Pb. Temperature = 285°C.

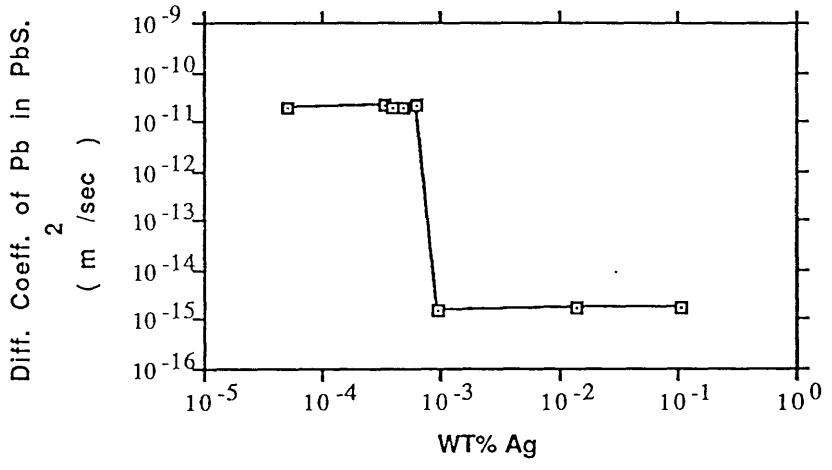


Table 12. Pb in PbS Diffusion Coefficient versus Silver Concentration.

COMPOSITION wt% Ag	DIFFUSION COEFF. ($m^2.s^{-1}$)	CORRELATION COEFF. (dimensionless)
0.10470	1.68×10^{-15}	0.987
0.01400	1.63×10^{-15}	0.986
0.00095	1.47×10^{-15}	0.990
0.00060	2.12×10^{-11}	0.910
0.00048	1.90×10^{-11}	0.942
0.00038	1.88×10^{-11}	0.925
0.00032	2.12×10^{-11}	0.983
<0.00005	1.97×10^{-11}	0.997

10.8 Model Output

An input file for the model was compiled using diffusion coefficients determined by the current experiments and those published in literature, published thermodynamic and activity data, process parameters matching the experimental conditions described by Clarke et al.(32), with the remaining unknowns being estimated as closely as possible. A full list of the input file with explanatory notes can be found in appendix(6). The most significant values are mentioned below. The diffusion coefficients used were from literature where ever available.

$D^{Pb}_{PbS} = 1.0 \times 10^{-14}$ cm^2/s

$D^{Cu}_{PbS} = 1.0 \times 10^{-5}$ cm^2/s

$D^{Cu}_{CuS_{0.5}} = 1.0 \times 10^{-3}$ cm^2/s

D^{Cu}_{CuS} was set at 1.0×10^{-3} cm^2/s, no other better information being available. One layer growth experiment was performed (see plate (2)), which confirmed this estimate to be reasonable.

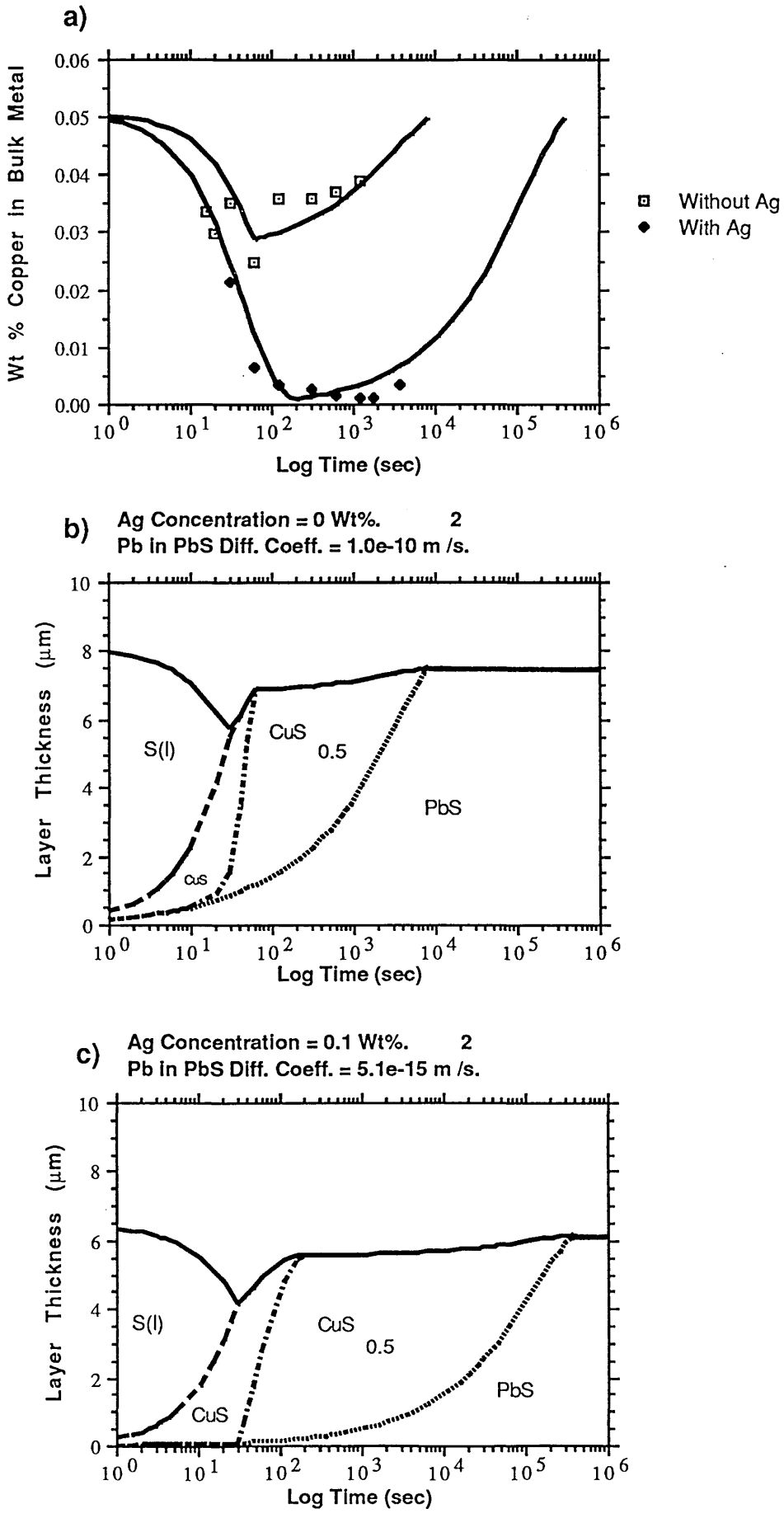
D^{Pb}_{PbS} (Ag doped) was estimated to be 5.1×10^{-19} cm^2/s using the equation relating temperature to diffusion coefficients resultant from the current experiments.

Initial layer thicknesses were set as thin as possible at 0.01 μm. If a smaller value was input, the simulation diverged (very large fluxes highlighted the short-comings of the quasi-steady state assumption). The surface area to volume ratio is set such that the sulphur droplets in the

melt would be approximately 10 to 20 μm in diameter, corresponding to the observations of Clarke, Baker and Jenkins[32,33].

Figure 31 shows the the output from the model. Figure 31(b) shows the layer thicknesses predicted when adding sulphur to bullion containing no silver, while figure 31(c) shows these thicknesses when silver is present. Figure 31(a) shows the decoppering curve that would result if these layers were uniform over the surface of the melt. Clarke et al.[32,33] added sulphur to bench scale liquid lead samples, the lead both containing silver and being silver free, then quenched the samples at various intervals to allow micro-examination of the sulphides formed during various stages of the decoppering process. Plates (3), (4), and (5) show micrographs of sulphides present as a result of adding sulphur to Ag contaminated lead after 30 seconds, 180 seconds, and 3600 seconds respectively. Note that computer aided image enhancement was used to improve the quality of the reproduction of these published micrographs by increasing the contrast.

Figure 31. Copper Concentration and Layer Thickness versus Log Time
For Both Silver Free and Silver Contaminated Cases.
Temperature = 330°C.



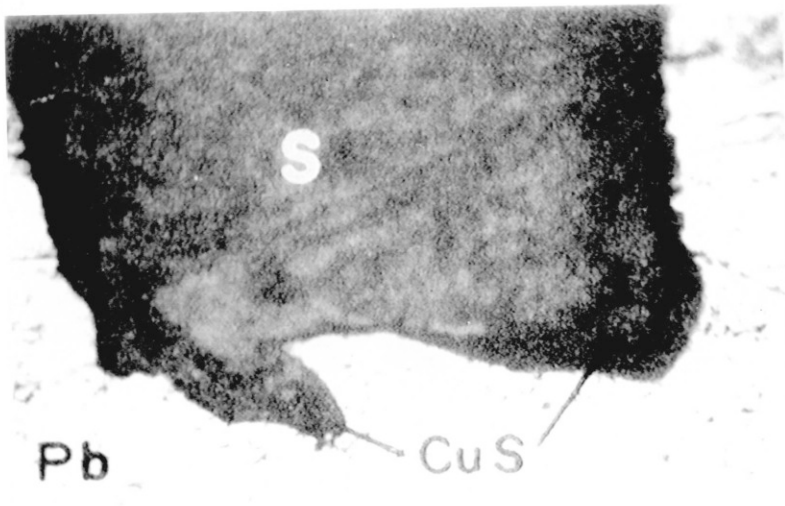


Plate 3. CuS Phase at Interface between S and Pb in Pb + Cu + 0.1 Wt% Ag Stirred at 1000 rpm with 0.05 Wt% S for 30 secs.

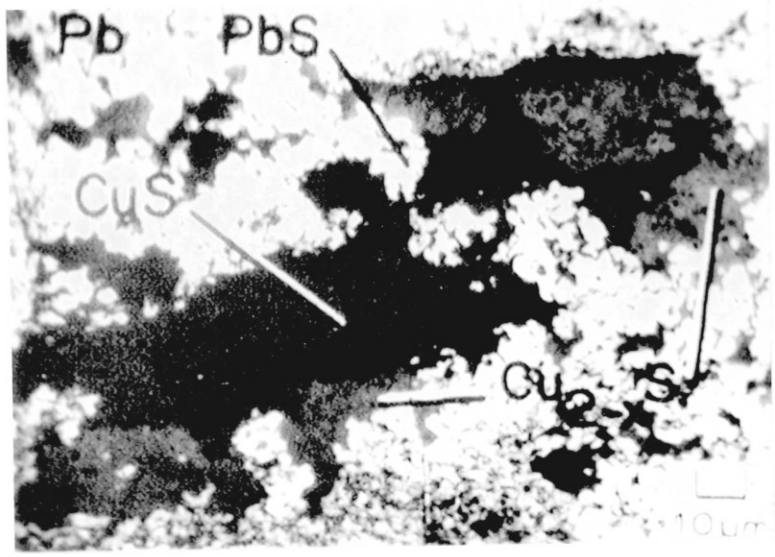


Plate 4. Moderate Size Sulphide Area Showing Roughly Equal Portions of CuS and $Cu_{2-x}S$, 3 mins after S was stirred in to Pb + Cu + Ag melt.

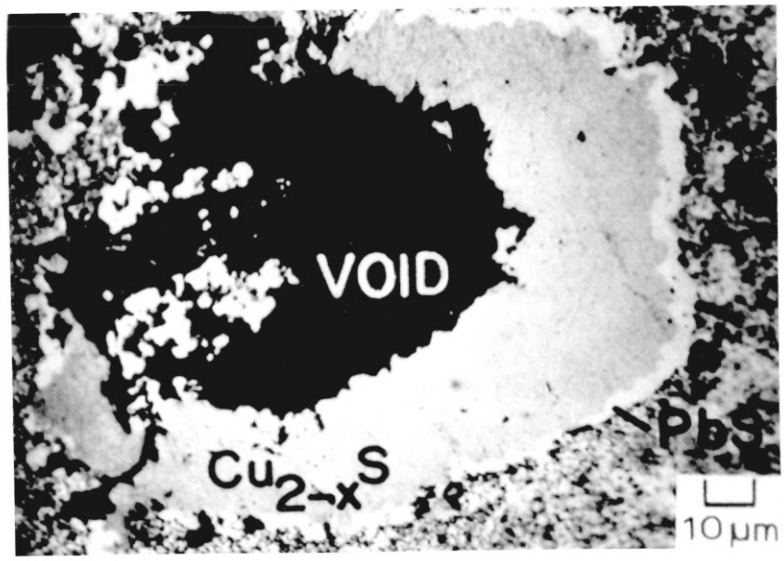


Plate 5. Void Essentially Surrounded by Thick Layer of $Cu_{2-x}S$ and Thin Shell of PbS in Pb + Cu + Ag Melt Reacted with Sulphur For 60 mins.

11.0. Discussion

When the value for the diffusion coefficient measured in the current experiments is used in the model, excellent agreement with the observations of Clarke, Baker and Jenkins[32,33], both with respect to the occurence and thickness of layer with time and the copper content of the bullion at any moment, is found.

First we will consider the case where Ag is present. Plate (2) shows the morphology of sulphides present 30 seconds after sulphur was added to copper contaminated liquid Pb. A CuS layer averaging around 5 microns thick adjacent to sulphur with no apparent PbS is depicted. As stated before, it is possible that the PbS layer is undetectably thin at this time. Examining the corresponding model output in figure 31(c), at 30 seconds, virtually no PbS and only CuS and liquid sulphur is predicted. The model expects the CuS layer to be around 5 microns which is in excellent agreement with observations.

Plate (3) shows that after 3 minutes (180 secs), PbS, CuS, and mostly $CuS_{0.5}$ is seen. Again, the model displays very similar characteristics, with large quantities of $CuS_{0.5}$ apparent, visible amounts of PbS, and no sulphur remaining. It varies only in that the CuS layer has already been consumed, but only a very short period of time before. This can be considered to display a very high level of agreement.

Plate (4) shows the morphology of the sulphides after one hour (3600 secs), when reversion is well underway. The PbS

layer has now grown to a substantial thickness, while $CuS_{0.5}$ is the sole copper sulphide present, in close concurrence with model predictions.

Similar close correspondence is found between the model output and the observations of Clarke and co-workers when the bullion is free of silver. Unfortunately, sufficiently good quality reproduction of their published micrographs was not achieved, even with the aid of computer assisted image enhancement, and have therefore not been included.

Examining figure 31(a), it can be seen that excellent agreement between the predicted and experimentally measured decoppering curves occurred. This very good fit was achieved by inputting into the model a critical value for the initial sulphur layer thickness, and thus the amount of sulphur available for decoppering. If a lower value is input, less overall decoppering takes place, and reversion commences earlier. If a larger value is input, the decoppering will continue down to a level corresponding to a bulk copper activity of 3.9×10^{-5}. This is the theoretical limit for decoppering, being the $CuS_{0.5}$/CuS equilibrium Cu activity. This is the lowest Cu activity towards which copper in the bulk can diffuse. The very low Cu activity at the CuS/S(l) interface is always shielded from the bullion by the $CuS_{0.5}$/CuS interface, except in the very earliest stages of decoppering. The copper flux away from the bullion is controlled by the difference in activity between the bulk and the $CuS_{0.5}$/CuS interface. When the bulk Cu activity reaches the $CuS_{0.5}$/CuS interfacial Cu activity, the decoppering flux

goes to zero, and the limit has been reached.

In laboratory tests, or indeed industrial applications, it is unlikely that this theoretical limit will be reached as there will always be imperfect stirring in the melt, leaving some copper tied up in whatever "dead-space" is present. It is also unlikely that that there will be a uniform sulpur potential throughout, leaving local volumes at low sulphur potentials where premature reversion could be occurring.

The model also predicts a slower rate of reversion than has been observed experimentally. This may be explained by the possibility of a direct $Pb/CuS_{0.5}$ reaction, of which the model takes no account, aiding the $PbS/CuS_{0.5}$ reversion mechanism.

The model developed here relies on the premise that Pb finds it much more difficult to diffuse through PbS than does Cu. This characteristic is represented in the model by giving the PbS layer a much higher resistance to diffusion for Pb than for Cu.

Values for the diffusion coefficients resulting from the current series of experiments and used in the model give excellent agreement with reality. However, these values are higher than the published diffusion coefficients. This can be explained when one considers that the diffusion coefficients quoted in literature are those relating to diffusion through perfect crystals. However, these values are of little relevance to the decoppering process, as the sulphide layers will be highly flawed due to rapid formation rates, continuing shearing stresses placed on the layers by

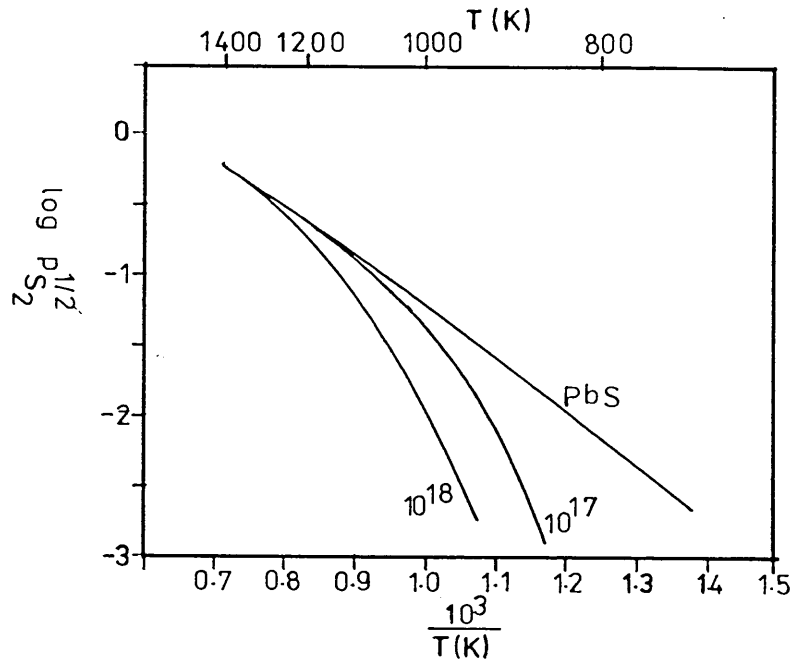
mixing, and the multi-granular nature of the layers. There will be many paths for fast diffusion, along grain boundaries for example, and although the experimental procedure is very simple, the results provided are more pertinent than those collected under more rigorously controlled conditions.

11.1 The Effect of Silver

Measurements made by Clarke et al[32,33] indicated that the concentration of silver in the bulk Pb bullion was similar to that found within the PbS layer. If we assume this approximate relationship holds, we can relate the Ag concentration in the bullion to the results of experiments studying diffusion behaviour in PbS crystals with various levels of Ag doping.

Figure(32),reproduced from Bloem and Kroger[45] shows the occurrence of the p-n junction for pure and Ag doped PbS as a function of sulphur potential and temperature. Although the diagram does not quite extend down to decoppering temperatures, it can readily seen that an Ag doping of 10^{18} atoms per cc(which corresponds to a silver concentration of 7.5×10^{-4} wt% Ag) is likely to produce a PbS layer that is entirely p-type at any sulphur potential encountered during decoppering. This corresponds very closely with the critical silver concentration at which the diffusion coefficient decreases dramatically(see figure(30)), the decrease being determined experimentally to lie between 6.0×10^{-4} and 9.5×10^{-4} wt% Ag. However, although this accurately

Figure 32. Boundaries between p- and n- type Regions for Undoped PbS and PbS Doped with Various Ag Concentrations over a Range of Sulphur Potentials and Temperatures. Concentrations of Ag are in Atoms/cc.



determines the minimum silver doping to result in good decoppering, it does little to help explain why there is such a sudden change in the ease of diffusion of Pb through PbS.

Re-examining fig(23) in section 8.2, a linear sulphur potential gradient across the layer has been assumed. As the p-n junction equilibrium sulphur potential is reduced by Ag doping, the PbS layer will become steadily more p-type, and thus steadily more resistant to Pb diffusion. This would suggest a smooth, although possible quite rapid, change in diffusivity, rather than the quite abrupt change observed.

One possible explanation for the sudden move from n-type to p-type is that the sulphur potential profile across the layer is not linear. If the majority of the sulphur potential gradient was confined to a small part of the layer, most of the layer could change from n-type to p-type with only a small change in critical sulphur potential.

It is also possible that the PbS layer is not uniformly doped with Ag. If an Ag concentration gradient existed across the PbS, being higher at the Pb/PbS interface, a more abrupt change from n-type to p-type would be expected.

Another explanation places doubt on the entire theory of solid state diffusion limitation of PbS growth as a mechanism for decoppering. This argument centres around the possibility that Ag acts as a surface active agent, preventing rapid PbS growth. There is some support for this argument when it is considered that Clarke and co-workers() did sometimes find higher Ag concentrations adjacent to the Pb/PbS interface. Surface activity also has difficulty in

providing a mechanism to explain the rapidity in change of PbS growth rate.

When small amounts of sulphur were dropped onto the surface of hot Ag doped Pb, rapid reaction occurred. This suggests little resistance to reaction at the interface, good surface contact being achieved instantaneously. Also, this eliminates difficulty of nucleation of PbS as a cause for delayed PbS formation. However, it does not eliminate the possibility of surface activity effects preventing the continued growth of PbS. During the earliest stages of lead sulphide formation, the growth mechanism is completely different to that expected later. As the initial PbS layer grows, pure Pb and pure S are in contact with each other at a low energy site at the edges of the spreading PbS film, encouraging rapid reaction. This spreading growth could explain the initial rapid appearance of PbS and ,thus, this behaviour cannot be used to draw conclusions about surface active effects.

The sudden change from n-type to p-type occurs when the silver concentration reaches a concentration of 10^{18} atoms/cm^3 of PbS. This value also equals the concentration of positive cationic vacancies expected under these conditions. For p-type PbS to offer much more resistance to diffusion than n-type, V_c^+ must be for more immobile than Pb_i^+. The presence of interstitial silver ions is unlikely to have any great effect on the diffusion of lead ions through the lattice as they interfere with only an extreme minority of possible diffusion paths. If, however, interstitial silver

ions were to diffuse to, and occupy, the cation vacancies within the lattice, it is conceivable that they pin the vacancy in position and greatly reduce vacancy mobility. The critical Ag concentration is equal to the number of available cation vacancy sites. However, the current experiments can provide no proof of this proposed mechanism.

12.0 Conclusions.

12.0 Slag Cleaning.

Successful modelling of two groups of bench top scale experiments investigating simple systems related to slag cleaning practice has been achieved. Good agreement was found in both cases with the same set of kinetic data. Modelling of complex systems more similar to those expected in slag cleaning practice gave the following conclusions.

1) Maintaining a high iron activity in the metallic phase keeps the metal/slag interfacial oxygen activity low which aids decoppering.

2) Increasing temperature will be beneficial with regard to improved kinetics, but in most cases, the beneficial shift in equilibria is matched by the detrimental increase on oxygen potential needed to avoid FeO reduction.

3) Decreasing FeO activity in the slag will result in a lower final Fe contamination of the metal phase and will allow the use of a lower oxygen pressure.

Use of this type of model has the advantage of making much information, such as interfacial activities and transfer rates of species available.

However, this work emphasised the many short-comings of the model in its current form. These are,

1) Solution thermodynamic and mass transport data is very limited, mass transport data being specific to the mixing conditions of the reactor under consideration. Establishing

a descriptive matrix of activity coefficients and interaction parameters to allow for the numerous species is, at best, a large undertaking.

2) The current model makes no allowances for multi-refractory slags. Oxide complexes formed by fluxes, contaminants ,or the feed oxides themselves, requires extensions to the model to be made.

3) Solid reductants, gas bubbles, and entrained metal droplets cannot be modelled because of the lack of ability to predict interfacial areas. However, this imformation being known, the modification required to allow for these occurrence is readily achieveable.

4) The model makes no allowances for change in surface tensions or interfacial areas during reaction.

5) Kinetic effects of temperature change are not considered.

6) Imperfect phase contact, surface active species, delays in phase nucleation and ionic diffusion have all been ignored.

12.2 Decoppering.

Simple experiments revealed unusual growth characteristics which led to the proposal of a new mechanism to explain the non-thermodynamically justifyable decoppering of lead. The critical Ag concentration to achieve the change in PbS growth characteristics lies between 6.0 and 9.5 x 10^{-4} Wt% Ag.

The theoretical limit to which current decoppering practice

can reach is to a bulk copper activity of 3.9×10^{-5}, which is the $CuS_{0.5}$/CuS equilibrium copper activity. The only way to achieve more thorough decoppering is to avoid $CuS_{0.5}$ formation, and make use of the CuS/S(l) equilibrium copper activity of 2.84×10^{-7}. This is unlikely as $CuS_{0.5}$ will form within 10 to 100 seconds of S addition. The beneficial effect of multiple sulphur additions can be readily explained by considering decoppering in the light of the proposed mechanism because the first stage of decoppering with CuS only present (when sulphide layers are thin and the decoppering driving force is large) is repeatedly caused. Attempting very violent local stirring to break up sulphide particles and expose encased sulphur to the bullion may be beneficial, but this will also cause direct bullion/copper sulphide contact accelerating reversion.

A continuous process where bullion is fed to a small highly agitated reactor that has only a brief residence time, whereupon the bullion containing sulphide particle is immediately left to stand and allow sulphide particles to rise to the surface to be skimmed may give good results. This will produce large S(l) interfacial areas, make use of the low CuS/S(l) copper activity, allow only thin layers which guarantee rapid diffusion, and lower process times to avoid any reversion. Note that the sulphide particles will still contain sulphur, so a separate process to recover sulphur from the dross would be required.

BIBLIOGRAPHY.

1. J.M. Floyd and P.J. Mackey

   Developments in Pyrometallurgical Treatments of Slag:

   A Review of Current Technology and Physical Chemistry.

   Extraction Met.81 IMM 1981 pp.345-375

2. S.C. Barnett

   The Methods and Economics of Slag Cleaning.

   Mining Magazine 1979(Jan.) pp.408-417

3. W.R.N. Snelgrove and John C. Taylor

   The Recovery of Values from Non-ferrous Smelter Slags.

   Can. Met. Quart. Vol. 20, No.2, 1981. pp. 231-240

4. D.G.C. Robertson, B. Deo, and S. Ohguchi

   Multicomponent Mixed-Transport Control Theory for Kinetics of Couples Slag/Metal and Slag/Metal/Gas Reactions: Application to De-sulphurizion of Molten Iron.

   Iron Making and Steel Making. Vol. 11, No.1, 1984. pp. 41-56

5. S. Ohguchi

   Ph.D. Thesis, Imperial College, London, 1983.

6. B. Deo

   D.I.C. Thesis, Imperial College, London, 1983.

7. Y. Kawai and K. Mori

Tetsu To Hagane, Vol. 68(2), 1982 p. A21 (In Japanese)

8. T. Okazaki

Ph.D. Thesis, Imperial College, London, 1985.

9. E.T.Turkdogan

Physical Chemistry of High Temperature Technology.

Academic Press , 1980.

10. JANAF Tables

U.S. Dept. of Commerce, Bureau of Standards, (2nd Ed.)

11. M. Nagamori and P.J. Mackey

Thermodynamics of Copper Matte Converting: Part II. Distribution of Au, Ag, Pb, Zn, Ni, Se, Te, Bi, Sb, and As between Copper, Matte and Slag in the Noranda Process.

Met. Trans. B., Vol. 9B, 1978 pp. 567-579

12. G.K. Sigworth and J.F.E. Elliott

The Thermodynamics of Dilute Liquid Copper Alloys.

Can. Met. Quart., Vol. 21, No.3, 1982, pp. 221-260

13. P.J. Mackey

The Physical Chemistry of Copper Smelting Slags - A Review.

Can. Met. Quart., Vol. 21, No. 3, 1982, pp. 221 - 260.

14. F.D. Richardson

Physical Chemistry of Melts in Metallurgy

Academic Press. 1974. p.252

15. D.B. Butrymowicz

Diffusion Rate Data and Mass Transport Phenomena in Copper Systems.

INCRA Monograph V. The INCRA series on the Metallurgy of Copper. 1981.

16. T.R.A. Davey

Phase Systems Concerned with Copper Drossing of Lead.

Trans. IMM., Vol. 22, 1963, pp. 553 - 620.

17. T. Azakami

Nippon Kogyo Kaishi. Vol 86, 1970, pp. 865 - 869.(In Japanese)

18. M. Hagashi et al.

J. Japan. Inst. Metals. Vol. 90, 1974, pp. 55 - 66. (In Japanese)

19. Y. Chang et al.

Phase Diagrams and Thermodynamic Properties of Ternary Copper-Metal Systems.

INCRA Monograph IV. The INCRA series on the Metallurgy of Copper. 1979.

20. J.B. See and W.J. Rankin.

Effect of Al_2O_3 and CaO on the solubility of Copper in Silica-Unsaturated Iron Silicate Slags at 1300^{o}C.

Trans. IMM C Vol. 92, 1983, pp. C9 - C13.

21. M. Nagamori and P.J. Mackey

Thermodynamics of Copper Matte Converting : Part 1. Fundamentals of the Noranda Process.

Met. Trans. B., Vol. 13B, 1982 pp. 319 - 329.

22. M. Nagamori and P.C. Chaubal

Thermodynamics of Copper Matte Converting : Part III. Steady Volatilization of Au, Ag, Pb, Zn, Ni, Se, Te, Bi, Sb, and As from Slag, Matte and Metallic Copper.

Met. Trans. B., Vol 13B, 1982, pp. 319 - 329.

23. M. Nagamori and P.C. Chaubal

Thermodynamics of Copper Matte Converting : Part IV. A Priori Predictions of the Behaviour of Au, Ag, Pb, Zn, Ni, Se, Te, Bi, Sb, and As in the Noranda Process Reactor.

Met. Trans. B., Vol. 13B, 1982, pp. 331 - 338.

24. T. Quaarm

Physical Chemistry and Pyrometallgy

Trans. IMM C , Vol. 89, 1980 pp. C139 - C144.

25. G.C. Richards, J.K. Brimacombe, and G.W. Toop

Kinetics of Zinc Slag-Fuming Process : Part I. Industrial Measurement.

Met. Trans. B., Vol. 16B, 1985, pp. 513 - 527.

26. G.C. Richards and J.K. Brimacombe

Kinetics of Zinc Slag-Fuming Process : Part II. Mathematical Model.
Met. Trans. B., Vol. 16B, 1985, pp. 529 - 539.

27. G.C. Richards and J.K. Brimacombe
Kinetics of the Zinc Slag-Fuming Process : Part III. Model Predictions and Analysis of Process Kinetics.
Met. Trans. B., Vol. 16B, 1985, pp.540-549.

28. T.R.A. Davey
The Physical Chemistry Of Lead Refining.
Lead-Zinc-Tin 80 TMS-AIME, 1980, pp. 477 - 507.

29. H.A. Simson and F. Lawson
Mathematical Model for the Fine Decoppering of Lead.
Trans. IMM C , Vol. 94, 1985, pp. C83 - C88.

30. R.F. Blanks and G.M. Willis
Physical Chemistry of Process Metallurgy Part 2.
G.R. St.Pierre (Ed.), New York Interscience, 1961.

31. T.R.A. Davey
Phase Systems Concerned with the Decoppering of Lead.
Trans. IMM, Vol 72, 1962-3, pp. 553 - 620.

32. I.R.S. Clarke, L.A. Baker, and A.E. Jenkins.
Decoppering of Lead Alloys with Sulphur : 1 - Reactions in the Pb + Cu System.
Trans. IMM C, Vol. 81, 1972, pp. C195 - C203.

33. I.R.S. Clarke, L.A. Baker, and A.E. Jenkins

Decoppering of Lead Alloys with Sulphur : 2 - Reactions in the Pb + Cu + Ag and Pb + Cu + Sn Systems.

Trans IMM C, Vol. 82, 1973, pp. C1 - C9.

34. D. Pollard

Phases Formed During Sulphur Treatment of Lead.

Trans. IMM C, Vol. 88, 1979, pp. C131 - C132.

35. F. Belis, W. Verwimp and J.R. Roos

Decopering Lead with Sulphur. Influence of Deficient Sulphides.

Met. Trans. B.,Vol. 7B, 1976, pp. 149 - 150.

36. C. Pin and J.B. Wagner Jr.

The Removal of Copper from Liquid Lead by Lead Sulphide Containing Controlled Atomic Defects.

Trans. Met. Soc. AIME., Vol. 227, 1963, pp. 1275-1281.

37. G. Simcovich

Point Defects in PbS and their Effect in the Decopperization of Lead with Sulphur.

Met. Trans. B., Vol. 9B, 1978, pp. 527 - 529.

38. G.M. Willis

Refining Metals with Sulphur.

Proc. AUS IMM, No. 237, 1971, pp.11-21.

39. R.J. McClincy and A.H. Larson

The Removal of Copper from Lead with Sulphur.

Trans. Met. Soc. AIME., Vol. 245, 1969, pp. 193 - 196.

40. T.R.A. Davey and J.V. Happ

The Decoppering of Lead, Tin, and Bismuth By Stirring with Elemental Sulphur.

Proc. AUS IMM, No. 237, 1971, pp. 23 - 31.

41. T.R.A. Davey, G. Jensen, and E.R. Segnit

Decoppering of Lead and Hard Lead by Stirring with Sulphur and Pyrites.

Australia Japan Extractive Met. Symp., Sydney, 1980.

AUS IMM 1980, pp. 301 - 312.

42. F. Lawson.

Continuous Sulphur Drossing of Lead.

Advances in Extractive Met., 1977, M.J. Jones (Ed.), IMM 1977, pp. 185 - 189.

43. J.F. Castle and J.H. Richards

Lead Refining : Current Technology and a New Continuous Process. Advances in Extractive Met.,1977, M.J. Jones (Ed.), IMM 1977, pp. 217 - 234.

44. G. Simcovich and J.B. Wagner Jr.

Self-Diffusion of Lead 210 in Single Crystals of Lead Sulphide as a Fucntion of Stoichiometry and Doping Additions.

J. Chemical Physics, Vol. 38, 1963, pp. 1368 - 1375.

45. J. Bloem and F.A. Kroger

Interstitial Diffusion of Copper In PbS Single Crystals.

Phillips Research Reports, Vol. 12, 1957, pp. 281 - 302.

46. J. Bloem

Controlled Conductivity in Lead Sulphide Single Crystals.

Phillips Research Reports, Vol. 11, 1956, pp. 273 - 336.

47. H. Schmalzreid

Solid State Reactions.

Academic Press 1974.

48. M.S. Seltzer ans J.B. Wagner Jr.

Diffusion of Sulphur 35 in Single Crystals of Lead Sulphide as a Function of Stoichiometry and Doping Additions.

J. Physical Chemistry (Solids), Vol. 26, 1965, pp. 233 - 250.

49. T.A. Ramanaraganar and P.D. Rose

Investigations of Diffusion and Non-Stoichiometry in Cuprous Sulpide.

J. Electrochem. Soc., Vol. 125(10), 1978, pp. 1684 - 1689.

50. N.F. Lugakov, A.S. Lyashevich, E.A. Movchanskii, I.I. Dokrovskii, and I.E. Shimanovich.

Dolk. Akad. Nawk. B., SSR, 1974, Vol. 18(9), pp. 825 - 827.

51. V.S. Andramov, N.S. Bargshev, and I.S. Aver'yanov

Soviet Phys.(Solid State), Vol. 4, 1963, p. 1626.

52. J.S. Anderson and J.R. Richards.
The Self-Diffusion of Lead in Lead Sulphide.
J. Chem. Soc., Part 1, 1946, pp.537 - 542.

53. I. Bartkovicz, E. Fryt, and S. Mrowee
Zesz. Nawk. Akad. Gorn-Hutn Krakowie, Ceram., Vol. 14, 1969, pp. 19 - 34.

54. T. Nakamura, B.Chan, and J.M. Toguri
The Effect of Iron Activity and Oxygen Pressure on Copper and Iron Transfer in Fayalite Slag at 1200^{o}C.
CIM Bulletin, Vol. 78, 1985, pp 119 to 130.

55. W.Ryan (Ed)
Non-Ferrous Extractive Metallurgy in the United Kingdom.
1968.

APPENDIX 1. Slag Cleaning Model Mathematical Formulation.

Section A : Algebraic Development of Metal/Slag Interface.

The flux equation for the metal species in the metallic phase is as follows

$$J_M = A^{M/S} C^M k_M (a_M^b - a_M^i)/\gamma_M$$

Substituting equilibrium equation,

$$J_M = A^{M/S} C^M k_M (a_M^b - a_{MO_\sigma} / (K_{MO_\sigma} P_{O_2}^{(1/2\sigma)}) / \gamma_M$$

Using the metal species conservation equation,

$$J_M = J_{MO_\sigma} = A^{M/S} C^S k_{MO_\sigma} (a_{MO_\sigma}^i - a_{MO_\sigma}^b) / \gamma_{MO_\sigma}$$

$$= a^M C^M k_M (a_M^b - a_{MO_\sigma}^i / (K_{MO_\sigma} P_{O_2}^{i\ (1/2\sigma)}))/\gamma_M$$

Rearranging,

$$a_{MO_\sigma}^i \left[\frac{C^S k_{MO_\sigma}}{\gamma_{MO_\sigma}} + \frac{C^M k_M}{\gamma_M} + \frac{1}{K_{MO_\sigma} P_{O_2}^{(1/2)}} \right]$$

$$= a_M^b C^M k_M/\gamma_M + a_{MO_\sigma}^b C^S k_{MO_\sigma} / \gamma_{MO_\sigma}$$

EQUATION 1.

$$a^{i}_{MO_\sigma} = \frac{a^{b}_{MO_\sigma} + a^{b}_{M}\left[\dfrac{C^{M}\, k_{M}\, \gamma_{MO_\sigma}}{C^{S}\, k_{MO_\sigma}\, \gamma_{M}}\right]}{1 + \dfrac{1}{K_{MO}\; p_{O}^{i\,(1/2\,\sigma)}}\;\dfrac{C^{M}\, k_{M}\, \gamma_{MO_\sigma}}{C^{S}\, k_{MO_\sigma}\, \gamma_{M}}}$$

This equation holds for each metal and its oxide.

The flux equation for oxygen in the metallic phase is as follows,

$$J_O = A^{M/S}\, C^{M}\, k_O\, (\, a^{b}_{O} - a^{i}_{O}\,) \,/\, \gamma_O$$

Substituting in the oxygen disolution equilibrium equation,

$$J_O = A^{M/S}\, C^{M}\, k_O\, (\, a^{b}_{O} - p^{i\,(1/2)}_{O_2}/K_O\,) \,/\, \gamma_O$$

Using the oxygen conservation equation,

$$J_O = \Sigma\, \sigma\, J_{MO_\sigma}$$

$$= A^{M/S}\, C^{M}\, k_O\, (\, a^{b}_{O} - p^{i\,(1/2)}_{O_2} \,/\, K_O\,) \,/\, \gamma_O$$

$$= \Sigma\, \sigma\, A^{M/S}\, C^{S}\, k_{MO_\sigma}\, (\, a^{i}_{MO_\sigma} - a^{b}_{MO_\sigma}\,) \,/\, \gamma_{MO_\sigma}$$

Substitution of equation one into the above equation for each species gives an equation in p_{O_2} only, which can be solved numerically.

Section B : Algebraic Development of the Slag/Gas Interface.

The flux equation for the slag species in the slag phase is as follows,

$$J^{S}_{MO_\sigma} = A^{S/G}\, C^{S}\, k^{S}_{MO_\sigma} \left(a^{b}_{MO_\sigma} - a^{i}_{MO_\sigma} \right) / \gamma^{S}_{MO_\sigma}$$

Similarly, in the gas phase, the slag species flux is,

$$J^{G}_{MO_\sigma} = A^{S/G}\, C^{G}\, k^{G}_{MO_\sigma} \left(p^{i}_{MO_\sigma} - p^{b}_{MO_\sigma} \right) / p_{total}$$

As there will be a substantial gas flow across the surface of the slag clearing away any accumulation of oxide (or metal) vapour, $p^{b}_{MO_\sigma}$ can be assumed to be zero. p_{total} will only be considered when atmospheric, and equal to one.

The equilibrium equations are,

$$K_{MO_\sigma} = a_{MO_\sigma} / \left(a_M\, p_{O_2}^{(1/2\sigma)} \right)$$

$$K^{S/G}_{MO_\sigma} = p_{MO_\sigma} / a_{MO_\sigma}$$

The conservation equations are,

1. For oxygen,

$$\Sigma\, \sigma\, R = - J_{CO} = J_{CO_2}$$

2. For Metal Oxides,

$$J^{S}_{MO_\sigma} = R + J^{S}_{MO_\sigma}$$

We have two entirely different sets of possible behaviours at the slag/gas interface, namely volatilization or reduction. Simultaneous volatilization and reduction is unlikely for the following reasons. If reaction is occuring at the slag/gas

interface, CO with be going to CO_2, thus the oxygen potential will be higher at the interface than in the bulk. Thus, if an oxide were to volatilize, it would travel away into a lower oxygen potential region where it would be reduced. The rate at which the oxide concentration drops as distance from the interface increases is likely to be significantly less than tha rate at which the oxygen potential decreases because oxide transport would be expected to be slower than that of either CO or CO_2. Thus, any oxide arriving at the interface should be reduces if any reduction is taking place. As the model does not take into account the settling of dispursed metal droplets back through the slag, all reduced metal is simply put back into the metallic phase.

I. Volatilization.

The metal oxide conservation equation becomes,

$$J^S_{MO_\sigma} = J^G_{MO_\sigma}$$

Substituting in the flux equations and relevent equilibrium equations,

$$C^S k^S_{MO_\sigma} (a^b_{MO_\sigma} - a^i_{MO_\sigma}) / \gamma^S_{MO_\sigma}$$

$$= C^G k^G_{MO_\sigma} (K^{S/G}_{MO_\sigma} a^i_{MO_\sigma})$$

$$a^{i}_{MO_\sigma} = \frac{C^S \, k^S_{MO_\sigma} \, a^b_{MO_\sigma} \, / \, \gamma_{MO_\sigma}}{C^G \, k^G_{MO_\sigma} \, K^{S/G}_{MO_\sigma} \, / \, \gamma_{MO_\sigma}}$$

II. Reduction.

At some critical oxygen potential, reduction occurs and metal is produced. Looking at the relevent equilibrium equation reveals that if we know the oxygen potential and the activity at which the metal is formed (assumed to be unity), we know the interfacial oxide activity. From this we can calculate the flux of oxide to the interface. The equivalent metal flux is added to the metallic phase, the oxygen being carries off as CO_2. The oxide flux equation becomes,

$$J^S_{MO_\sigma} = R$$

Substituting into the flux equation and relevent equilibrium equation,

$$R = A^{S/G} \, C^S \, k^S_{MO_\sigma} \, (\, a^b_{MO_\sigma} - K_{MO_\sigma} \, p^{i\,(1/2\sigma)}_{O_2} \,) \, / \, \gamma/MO_\sigma$$

Section C : Algebraic Development of the Metal/Gas Interface.

The conservation equation for this volatilization reaction is,

$$J_M^M = J_M^G$$

Substituting flux equations and the relevent equilibrium equation,

$$A^{M/G}\, C^M\, k_M^M\, (\, a_M^b - a_M^i\,) \,/\, \gamma_M^M = A^{M/G}\, C^G\, k_M^G\, (\, a_M^i\, K_M^{M/G}\,)$$

Rearranging,

$$a_M^i = \frac{C^M\, k_M^M\, a_M^b \,/\, \gamma_M^M}{C^G\, k_M^G\, K_M^{M/G} + C^M\, k_M^M \,/\, \gamma_M^M}$$

Appendix 2. Slag Cleaning Model FORTRAN Code.

```
      PROGRAM SCM(SCMDAT,O,CU,FE,NI,SN,PB,ZN,
     +          SIO2,CU05,FEOX,NIO,SNO,PBO,ZNO,
     +          FO,FCU,FFE1,FFE2,FNI,FSN,FPB,FZN,E,
     +          TAPE1=SCMDAT,
     +          TAPE11=O,TAPE13=CU,TAPE15=FE,TAPE16=NI,TAPE17=SN,
     +           TAPE18=PB,TAPE19=ZN,TAPE21=SIO2,TAPE23=CU05,
     +          TAPE25=FEOX,TAPE26=NIO,TAPE27=SNO,
     +           TAPE28=PBO,TAPE29=ZNO,TAPE30=FO,TAPE31=FCU,
     +           TAPE32=FFE1,TAPE33=FFE2,TAPE34=FNI,TAPE35=FSN,
     +           TAPE36=FPB,TAPE37=FZN,TAPE38=E)
      CHARACTER DUMMY
      REAL K(40),X(40),Z(40),E(30),DH(30),DS(30),AC(20),MW(20),A(40,6)
      REAL METAL(10),SLAG(10),XN(50),R(10),WTPC(40)
      REAL NIO,MOLMET,MOLSLAG
C*****************************************************************
C*                                                               *
C*            D A T A   E N T R Y                                *
C*                                                               *
C*****************************************************************
C
C  MASS TRANSFER COEFFICIENTS ------------------------------------
C
      READ(1,10)DUMMY
      DO 100 I=1,10
            READ(1,20)K(I),K(I+10),K(I+20),K(I+30)
  100 CONTINUE
C
C   BULK CONCENTRATIONS ------------------------------------------
C
      READ(1,10)DUMMY
      DO 200 I=1,10
            READ(1,20)WTPC(I),WTPC(I+10),WTPC(I+20),WTPC(I+30)
  200 CONTINUE
C
C   STOICHIOMETRY ------------------------------------------------
C
      READ(1,10)DUMMY
      DO 300 I=1,10
            READ(1,20)Z(I),Z(I+10),Z(I+20),Z(I+30)
  300 CONTINUE
C
C   DH'S ---------------------------------------------------------
C
      READ(1,10)DUMMY
      DO 400 I=1,10
            READ(1,30)DH(I),DH(I+10),DH(I+20)
  400 CONTINUE
C
C   DS'S ---------------------------------------------------------
C
      READ(1,10)DUMMY
      DO 500 I=1,10
            READ(1,30)DS(I),DS(I+10),DS(I+20)
  500 CONTINUE
C
C   ACTIVITY COEFFICIENTS ----------------------------------------
C
      READ(1,10)DUMMY
      DO 600 I=1,10
            READ(1,40)AC(I),AC(I+10)
  600 CONTINUE
C
C MOLECULAR WEIGHTS -------------------------------------------
```

```
C
 READ(1,10)DUMMY
 DO 700 I=1,10
        READ(1,40)MW(I),MW(I+10)
 700 CONTINUE
C
C INTERFACIAL AREAS,TEMP,PHASE MASSES,C6,VOLUMES,DENSITIES,AND DT
C
 READ(1,10)DUMMY
 READ(1,*)AMS,AMG,ASG,T,TOTMET,TOTSLAG,C6,ROEMET,ROESLAG,DT
C
C NUMBER OF ELEMENTS ----------------------------------------
C
 READ(1,10)DUMMY
 READ(1,*)N,FINISH,BULKFEO
C
C*****************************************************************
C*                                                               *
C* P R E L I M I N A R Y   C A L C U L A T I O N S               *
C*                                                               *
C*****************************************************************
C
C EQUILIBRIUM CONSTANTS ---------------------------------------
C
 DO 800 I=1,30
        E(I)=EXP((T*DS(I)-DH(I))/(1.987*T))
 800 CONTINUE
C
C INITIALIZATIONS ---------------------------------------------
C
 I10=50
 TIME=0.0
 MOLMET=0.0
 MOLSLAG=0.0
 DO 850 I=1,40
        DO 855 J=1,6
            A(I,J)=0.0
        855 CONTINUE
        XN(I)=0.0
        XN(I+10)=0.0
 850 CONTINUE
C
C CALCULATE INITIAL PHASE VOLUMES ----------------------------------
C
 V1=TOTMET/ROEMET
 V4=TOTSLAG/ROESLAG
C
C INITIALIZE FLUXES,FUMES,AND"RESISTANCES",AND CALCULATE
C SPECIES MASSES AND TOTAL MOLES OF SLAG AND METAL ----------------
C
 DO 860 I=1,N
        R(I)=0.0
        METAL(I)=TOTMET*WTPC(I)/100.0
        SLAG(I)=TOTSLAG*WTPC(I+10)/100.0
        MOLMET=MOLMET+METAL(I)/MW(I)
        MOLSLAG=MOLSLAG+SLAG(I)/MW(I+10)
 860 CONTINUE
C
C CALCULATE INITIAL MOLE FRACTIONS AND ACTIVITIES IN THE BULK ----
C
 DO 870 I=1,N
        X(I)=METAL(I)/(MW(I)*MOLMET)
        X(I+10)=SLAG(I)/(MW(I+10)*MOLSLAG)
        A(I,1)=X(I)*AC(I)
        A(I+10,4)=X(I+10)*AC(I+10)
```

```
870 CONTINUE
A(15,4)=BULKFEO
SIO2FEO=X(11)/X(15)
C
C CALCULATION OF BULK MOLAR CONCENTRATIONS ----------
C
 C1=MOLMET/V1
 C4=MOLSLAG/V4
C
C INITIAL GUESS OF M/S INTERFACIAL OXYGEN POTENTIAL
C
 X1=(X(13)*AC(13)/(X(3)*AC(3)*E(3)))**2.0
 A(1,5)=WTPC(31)
C*****************************************************************
C*                                                               *
C*        METAL/SLAG INTERFACE SOLUTION                          *
C*                                                               *
C*****************************************************************
998 CONTINUE
AI=ACU05(A,AC,E,K,C1,C4,X1)
BI=AFEO(A,AC,E,K,C1,C4,X1)
CI=ANIO(A,AC,E,K,C1,C4,X1)
DI=ASNO(A,AC,E,K,C1,C4,X1)
EI=APBO(A,AC,E,K,C1,C4,X1)
FI=AZNO(A,AC,E,K,C1,C4,X1)
Y=YVAL(A,AC,E,K,C1,C4,AI,BI,CI,DI,EI,FI,X1)
IF(Y.LT.0.0)THEN
X1=X1*2.0
GOTO 998
END IF
1000 CONTINUE
X2=X1/2.0
X1LOG=ALOG10(X1)
X2LOG=ALOG10(X2)
1001 CONTINUE
A2=ACU05(A,AC,E,K,C1,C4,X2)
B2=AFEO(A,AC,E,K,C1,C4,X2)
C2=ANIO(A,AC,E,K,C1,C4,X2)
D2=ASNO(A,AC,E,K,C1,C4,X2)
E2=APBO(A,AC,E,K,C1,C4,X2)
F2=AZNO(A,AC,E,K,C1,C4,X2)
Y=YVAL(A,AC,E,K,C1,C4,A2,B2,C2,D2,E2,F2,X2)
IF(Y.GT.0.0)THEN
X1LOG=X2LOG
X2LOG=X2LOG-2.0
X1=10.0**X1LOG
X2=10.0**X2LOG
GOTO 1001
END IF
IF(Y.LT.0.0)THEN
1100 CONTINUE
XNEWLOG=(X1LOG+X2LOG)/2.0
XNEW=10.0**XNEWLOG
ANEW=ACU05(A,AC,E,K,C1,C4,XNEW)
BNEW=AFEO(A,AC,E,K,C1,C4,XNEW)
CNEW=ANIO(A,AC,E,K,C1,C4,XNEW)
DNEW=ASNO(A,AC,E,K,C1,C4,XNEW)
ENEW=APBO(A,AC,E,K,C1,C4,XNEW)
FNEW=AZNO(A,AC,E,K,C1,C4,XNEW)
YNEW=YVAL(A,AC,E,K,C1,C4,ANEW,BNEW,CNEW,DNEW,ENEW,FNEW,XNEW)
IF(YNEW.GT.0.0)X1LOG=XNEWLOG
IF(YNEW.LT.0.0)X2LOG=XNEWLOG
IF(ABS(YNEW).LT.1.0E-06)GOTO 2000
GOTO 1100
END IF
```

```
2000 CONTINUE
PO2I=XNEW
CU05=ANEW
FEO=BNEW
NIO=CNEW
FE2O3=E(4)*FEO*PO2I**0.25/E(5)
SNO=DNEW
PBO=ENEW
ZNO=FNEW
XN(1)=C1*K(1)*(A(1,1)-PO2I**0.5/E(1))/AC(1)
XN(13)=C4*K(13)*(CU05-A(13,4))/AC(13)
XN(14)=C4*K(14)*(FE2O3-A(14,4))/AC(14)
XN(15)=C4*K(15)*(FEO-A(15,4))/AC(15)
XN(16)=C4*K(16)*(NIO-A(16,4))/AC(16)
XN(17)=C4*K(17)*(SNO-A(17,4))/AC(17)
XN(18)=C4*K(18)*(PBO-A(18,4))/AC(18)
XN(19)=C4*K(19)*(ZNO-A(19,4))/AC(19)
A(1,2)=PO2I**0.5/E(1)
A(3,2)=CU05/(E(3)*PO2I**0.25)
A(5,2)=FEO/(E(5)*PO2I**0.5)
A(6,2)=NIO/(E(6)*PO2I**0.5)
A(7,2)=SNO/(E(7)*PO2I**0.5)
A(8,2)=PBO/(E(8)*PO2I**0.5)
A(9,2)=ZNO/(E(9)*PO2I**0.5)
A(13,2)=CU05
A(14,2)=FE2O3
A(15,2)=FEO
A(16,2)=NIO
A(17,2)=SNO
A(18,2)=PBO
A(19,2)=ZNO
XN(3)=C1*K(3)*(A(3,1)-A(3,2))/AC(3)
XN(5)=C1*K(5)*(A(5,1)-A(5,2))/AC(5)
XN(6)=C1*K(6)*(A(6,1)-A(6,2))/AC(6)
XN(7)=C1*K(7)*(A(7,1)-A(7,2))/AC(7)
XN(8)=C1*K(8)*(A(8,1)-A(8,2))/AC(8)
XN(9)=C1*K(9)*(A(9,1)-A(9,2))/AC(9)
C*************************************************************
C*                                                           *
C* SLAG/GAS INTERFACE SOLUTION                               *
C*                                                           *
C*************************************************************
 DO 2222 I=3,N
          A(I+10,5)=E(I)*A(1,5)**(Z(I)/2.0)
          XN(40+I)=C4*K(I+10)*(A(I+10,4)-A(I+10,5))/AC(I+10)
          R(I)=XN(40+I)
          IF(A(I+10,4).LT.A(I+10,5))THEN
          A(I+10,5)=C4*K(I+10)*A(I+10,4)/AC(I+10)/
+                 (C6*K(30+I)*E(20+I)+C4*K(30+I)/AC(10+I))
          XN(40+I)=C6*K(I+30)*A(10+I,5)*E(20+I)
          R(I)=0.0
 IF(I.EQ.4.OR.I.EQ.5)THEN
 A(15,5)=(K(14)*A(14,4)/AC(14)+K(15)*A(15,4)/AC(15))/
+      (K(15)/AC(15)+K(14)*E(4)*A(1,5)**0.25/(E(5)*AC(14)))
 A(14,5)=E(4)*A(15,5)*A(1,5)**0.25/E(5)
 XN(44)=C4*K(14)*(A(14,4)-A(14,5))/AC(14)
 XN(45)=C4*K(15)*(A(15,4)-A(15,5))/AC(15)
 END IF
          END IF
 2222 CONTINUE
```

```
C#*************************************************************
C*                                                           *
C* METAL/GAS  INTERFACE  SOLUTION*
C*                                                           *
C*************************************************************
 DO 3333 I=3,N
         A(I,3)=(C1*K(I)*A(I,1)/AC(I))/(C6*K(20+I)*E(10+I)
+              +C1*K(I)/AC(I))
         XN(I+20)=C1*K(I)*(A(I,1)-A(I,3))/AC(I)
 3333 CONTINUE
C*************************************************************
C*
C* CONSERVATION  EQUATIONS       *
C*                                                           *
C*************************************************************
 METAL(1)=METAL(1)-XN(1)*DT*MW(1)*AMS
 METAL(3)=METAL(3)+(R(3)*ASG-AMS*XN(3))*DT*MW(3)
 METAL(5)=METAL(5)+(R(5)*ASG-AMS*XN(5))*DT*MW(5)
 METAL(6)=METAL(6)+(R(6)*ASG-AMS*XN(6))*DT*MW(6)
 METAL(7)=METAL(7)+(R(7)*ASG-AMS*XN(7))*DT*MW(7)
 METAL(8)=METAL(8)+(R(8)*ASG-AMS*XN(8))*DT*MW(8)
 METAL(9)=METAL(9)+(R(9)*ASG-AMS*XN(9))*DT*MW(9)
CSLAG(1)=SLAG(5)*SIO2FEO*MW(11)/MW(15)
 SLAG(3)=SLAG(3)+(XN(13)*AMS-ASG*XN(43))*DT*MW(13)
 SLAG(4)=SLAG(4)+(XN(14)*AMS-ASG*XN(44))*DT*MW(14)
 SLAG(5)=SLAG(5)+(XN(15)*AMS-ASG*XN(45))*DT*MW(15)
 SLAG(6)=SLAG(6)+(XN(16)*AMS-ASG*XN(46))*DT*MW(16)
 SLAG(7)=SLAG(7)+(XN(17)*AMS-ASG*XN(47))*DT*MW(17)
 SLAG(8)=SLAG(8)+(XN(18)*AMS-ASG*XN(48))*DT*MW(18)
 SLAG(9)=SLAG(9)+(XN(19)*AMS-ASG*XN(49))*DT*MW(19)
 TOTMET=METAL(1)+METAL(3)+METAL(5)+METAL(6)+METAL(7)+METAL(8)+METAL(9)
 TOTSLAG=SLAG(1)+SLAG(3)+SLAG(4)+SLAG(5)+SLAG(6)+SLAG(7)+SLAG(8)+
+       SLAG(9)
 MOLMET=METAL(1)/MW(1)+METAL(3)/MW(3)+METAL(5)/MW(5)+
+      METAL(6)/MW(6)+METAL(7)/MW(7)+METAL(8)/MW(8)+METAL(9)/MW(9)
 MOLSLAG=SLAG(1)/MW(11)+SLAG(3)/MW(13)+SLAG(4)/MW(14)+SLAG(9)/MW(19)
+      +SLAG(5)/MW(15)+SLAG(6)/MW(16)+SLAG(7)/MW(17)+SLAG(8)/MW(18)
 X(1)=METAL(1)/(MW(1)*MOLMET)
 X(3)=METAL(3)/(MW(3)*MOLMET)
 X(5)=METAL(5)/(MW(5)*MOLMET)
 X(6)=METAL(6)/(MW(6)*MOLMET)
 X(7)=METAL(7)/(MW(7)*MOLMET)
 X(8)=METAL(8)/(MW(8)*MOLMET)
 X(9)=METAL(9)/(MW(9)*MOLMET)
 X(11)=SLAG(1)/(MW(11)*MOLSLAG)
 X(13)=SLAG(3)/(MW(13)*MOLSLAG)
 X(14)=SLAG(4)/(MW(14)*MOLSLAG)
 X(15)=SLAG(5)/(MW(15)*MOLSLAG)
 X(17)=SLAG(7)/(MW(17)*MOLSLAG)
 X(18)=SLAG(8)/(MW(18)*MOLSLAG)
 X(19)=SLAG(9)/(MW(19)*MOLSLAG)
 X(16)=SLAG(6)/(MW(16)*MOLSLAG)
 A(1,1)=X(1)*AC(1)
 A(3,1)=X(3)*AC(3)
 A(5,1)=X(5)*AC(5)
 A(6,1)=X(6)*AC(6)
 A(7,1)=X(7)*AC(7)
 A(8,1)=X(8)*AC(8)
 A(9,1)=X(9)*AC(9)
 A(13,4)=X(13)*AC(13)
 A(14,4)=X(14)*AC(14)
 A(16,4)=X(16)*AC(16)
 A(17,4)=X(17)*AC(17)
 A(18,4)=X(18)*AC(18)
 A(19,4)=X(19)*AC(19)
```

```
V1=TOTMET/ROEMET
V4=TOTSLAG/ROESLAG
C1=MOLMET/V1
C4=MOLSLAG/V4
WTPC(11)=SLAG(1)*100.0/TOTSLAG
WTPC(13)=SLAG(3)*100.0/TOTSLAG
WTPC(14)=SLAG(4)*100.0/TOTSLAG
WTPC(15)=SLAG(5)*100.0/TOTSLAG
WTPC(16)=SLAG(6)*100.0/TOTSLAG
WTPC(17)=SLAG(7)*100.0/TOTSLAG
WTPC(18)=SLAG(8)*100.0/TOTSLAG
WTPC(19)=SLAG(9)*100.0/TOTSLAG
WTPC(1)=METAL(1)*100.0/TOTMET
WTPC(3)=METAL(3)*100.0/TOTMET
WTPC(5)=METAL(5)*100.0/TOTMET
WTPC(6)=METAL(6)*100.0/TOTMET
WTPC(7)=METAL(7)*100.0/TOTMET
WTPC(8)=METAL(8)*100.0/TOTMET
WTPC(9)=METAL(9)*100.0/TOTMET
C*************************************************************
C*                                                           *
C* OUTPUT RESULTS                                            *
C*                                                           *
C*************************************************************
 IF(I10.GE.50)THEN
 TMIN=TIME/60.0
 I10=0
 WRITE(11,40)TMIN,WTPC(1)
 WRITE(13,40)TMIN,WTPC(3)
 WRITE(15,40)TMIN,WTPC(5)
 WRITE(16,40)TMIN,WTPC(6)
 WRITE(17,40)TMIN,WTPC(7)
 WRITE(18,40)TMIN,WTPC(8)
 WRITE(19,40)TMIN,WTPC(9)
 WRITE(21,40)TMIN,WTPC(11)
 WRITE(23,40)TMIN,WTPC(13)
 WRITE(25,30)TMIN,WTPC(14),WTPC(15)
 WRITE(26,40)TMIN,WTPC(16)
 WRITE(27,40)TMIN,WTPC(17)
 WRITE(28,40)TMIN,WTPC(18)
 WRITE(29,40)TMIN,WTPC(19)
 WRITE(38,90)TMIN,E(1),E(3),E(4),E(5),E(6),E(7),E(8),E(9)
 WRITE(30,90)TMIN,A(1,1),XN(1),A(1,2),A(1,5),TOTMET,TOTSLAG
 WRITE(31,90)TMIN,A(3,1),XN(3),A(3,2),A(13,2),A(13,4),XN(43),R(3)
 WRITE(32,90)TMIN,A(14,2),XN(14),A(14,4),XN(44),A(14,5)
 WRITE(33,90)TMIN,A(5,1),XN(5),A(5,2),A(15,2),XN(15),A(15,4),XN(45)
 WRITE(34,90)TMIN,A(6,1),XN(6),A(6,2),A(13,2),A(16,4),XN(46),R(6)
 WRITE(35,90)TMIN,A(7,1),XN(7),A(7,2),A(17,2),A(17,4),XN(47),R(7)
 WRITE(36,90)TMIN,A(8,1),XN(8),A(8,2),A(18,2),A(18,4),XN(48),R(8)
 WRITE(37,90)TMIN,A(9,1),XN(9),A(9,2),A(19,2),A(13,4),XN(43),R(9)
 END IF
 I10=I10+1
 X1=PO2I*1000.0
 IF(TIME.GE.1.000)DT=0.1
 IF(TIME.GE.10.00)DT=1.0
 IF(TIME.GE.100.0)DT=5.0
 IF(TIME.GE.1000.0)DT=20.0
 TIME=TIME+DT
 IF(TMIN.LT.FINISH)GOTO 1000
 10 FORMAT(A1/)
 20 FORMAT(4E12.4)
 30 FORMAT(3E12.4)
 40 FORMAT(2E12.4)
 50 FORMAT(E12.4)
 60 FORMAT(I10)
```

```
 70 FORMAT(6A1)
 80 FORMAT(F7.1)
 90 FORMAT(9E9.2)
 95 FORMAT(8E10.3)
 9999 END
C*****************************************************************
C*****************************************************************
C*****************************************************************
C*****************************************************************
C*****************************************************************
 FUNCTION ACU05(A,AC,E,K,C1,C4,PO2I)
 REAL A(40,6),AC(20),E(30),K(40)
 ACU05=(A(3,1)+A(13,4)*C4*K(13)*AC(3)/(C1*K(3)*AC(13)))
+     /(1.0/(E(3)*PO2I**0.25)+C4*K(13)*AC(3)/(C1*K(3)*AC(13)))
 END
 FUNCTION AFEO(A,AC,E,K,C1,C4,PO2I)
 REAL A(40,6),AC(20),E(30),K(40)
 AFEO=(C1*K(5)*A(5,1)/AC(5)+C4*K(15)*A(15,4)/AC(15)+C4*K(14)*A(14,4)
+    /AC(14))/(C1*K(5)/(AC(5)*E(5)*PO2I**0.5)+C4*K(15)/AC(15)+
+    C4*K(14)*E(4)*PO2I**0.25/(AC(14)*E(5)))
 END
 FUNCTION ANIO(A,AC,E,K,C1,C4,PO2I)
 REAL A(40,6),AC(20),E(30),K(40)
 ANIO=(A(16,4)*C4*K(16)/AC(16)+A(6,1)*C1*K(6)/AC(6))
+    /(C4*K(16)/AC(16)+C1*K(6)/(AC(6)*E(6)*PO2I**0.5))
 END
 FUNCTION ASNO(A,AC,E,K,C1,C4,PO2I)
 REAL A(40,6),AC(20),E(30),K(40)
 ASNO=(A(17,4)*C4*K(17)/AC(17)+A(7,1)*C1*K(7)/AC(7))
+    /(C4*K(17)/AC(17)+C1*K(7)/(AC(7)*E(7)*PO2I**0.5))
 END
 FUNCTION APBO(A,AC,E,K,C1,C4,PO2I)
 REAL A(40,6),AC(20),E(30),K(40)
 APBO=(A(18,4)*C4*K(18)/AC(18)+A(8,1)*C1*K(8)/AC(8))
+    /(C4*K(18)/AC(18)+C1*K(8)/(AC(8)*E(8)*PO2I**0.5))
 END
 FUNCTION AZNO(A,AC,E,K,C1,C4,PO2I)
 REAL A(40,6),AC(20),E(30),K(40)
 AZNO=(A(19,4)*C4*K(19)/AC(19)+A(9,1)*C1*K(9)/AC(9))
+    /(C4*K(19)/AC(19)+C1*K(9)/(AC(9)*E(9)*PO2I**0.5))
 END
 FUNCTION YVAL(A,AC,E,K,C1,C4,CU05,FEO,NIO,SNO,PBO,ZNO,PO2I)
 REAL A(40,6),AC(20),E(30),K(40),NIO
 YVAL=C1*K(1)*(PO2I**0.5/E(1)-A(1,1))/AC(1)+
+    0.5*C4*K(13)*(CU05-A(13,4))/AC(13)+
+    C4*K(15)*(FEO-A(15,4))/AC(15)+
+    1.5*C4*K(14)*(E(4)*PO2I**0.25*FEO/E(5)-A(14,4))/AC(14)+
+    C4*K(16)*(NIO-A(16,4))/AC(16)+
+    C4*K(17)*(SNO-A(17,4))/AC(17)+
+    C4*K(18)*(PBO-A(18,4))/AC(18)+
+    C4*K(19)*(ZNO-A(19,4))/AC(19)
 END
```

Appendix 3(a) Data file for Toguri Simulation.

MASS TRANSFER COEFFICIENTS(cm/s)

METAL	SLAG	GAS	GAS	
0.00015	0.00010	0.000	0.000	O
0.00015	0.00010	0.000	0.000	
0.00015	0.00010	0.000	0.000	Cu CuO0.5
0.00015	0.00010	0.000	0.000	Fe FeO1.5
0.00015	0.00010	0.000	0.000	Fe FeO
0.00015	0.00010	0.000	0.000	
0.00015	0.00010	0.000	0.000	
0.00015	0.00010	0.000	0.000	
0.00015	0.00010	0.000	0.000	
0.00015	0.00010	0.000	0.000	

BULK CONCENTRATIONS IN WEIGHT PERCENT

METAL	SLAG	GAS	GAS			
1.0E-05	40.0	1.0E-07	1.0E-07	O	SiO2	pO2
0.0	0.0	0.0	0.0			
99.49999	4.80	0.0	0.0	Cu	CuO0.5	
0.0	5.2	0.0	0.0		FeO1.5	
0.50	50.0	0.0	0.0	Fe	FeO	
0.0	0.0	0.0	0.0			
0.0	0.0	0.0	0.0			
0.0	0.0	0.0	0.0			
0.0	0.0	0.0	0.0			
0.0	0.0	0.0	0.0			

STOICHIOMETRY

METAL	SLAG	GAS	GAS	
0.0	0.0	0.0	0.0	
0.0	0.0	0.0	0.0	
1.0	0.5	0.0	0.0	CuO0.5
1.0	1.5	0.0	0.0	FeO1.5
1.0	1.0	0.0	0.0	FeO
0.0	0.0	0.0	0.0	
0.0	0.0	0.0	0.0	
0.0	0.0	0.0	0.0	
0.0	0.0	0.0	0.0	
0.0	0.0	0.0	0.0	

HEATS OF FORMATION (IN CALORIES)

M/S	M/G	S/G	
-20500.0	0.0	0.0	1/2 (O2) = [O]
-67150.0	0.0	0.0	CO + 1/2 O2 = CO2
-14190.0	0.0	0.0	Cu(l) + 1/4 O2 = CuO0.5
-97290.0	0.0	0.0	Fe(l) + 3/4 O2 = FeO1.5
-61200.0	0.0	0.0	Fe(l) + 1/2 O2 = FeO
0.0	0.0	0.0	
0.0	0.0	0.0	
0.0	0.0	0.0	
0.0	0.0	0.0	
0.0	0.0	0.0	

ENTROPIES (IN CALORIES)

M/S	M/G	S/G	
-10.9	0.0	0.0	1/2 (O2) = [O]
-20.37	0.0	0.0	CO + 1/2 O2 = CO2
-4.72	0.0	0.0	Cu(l) + 1/4 O2 = CuO0.5
-24.48	0.0	0.0	Fe(l) + 3/4 O2 = FeO1.5
-12.83	0.0	0.0	Fe(l) + 1/2 O2 = FeO
0.0	0.0	0.0	
0.0	0.0	0.0	
0.0	0.0	0.0	

ACTIVITY COEFFICIENTS

METAL	SLAG		
0.34	0.0	O	
0.0	0.0		
1.0	0.8	Cu	CuO0.5
15.95	1.5	Fe	FeO1.5
15.95	0.0	Fe	FeO
0.0	0.0		
0.0	0.0		
0.0	0.0		
0.0	0.0		
0.0	0.0		

MOLECULAR WEIGHTS (KG/MOLE)

METAL	SLAG		
0.016	0.060	0	SiO2
0.012	0.0	C	
0.0635	0.0747	Cu	CuO0.5
0.0558	0.0769	Fe	FeO1.5
0.0558	0.0771	Fe	FeO
0.0	0.0		
0.0	0.0		
0.0	0.0		
0.0	0.0		
0.0	0.0		

INTERFACIAL AREAS(sq.m),TEMPERATURE(K),PHASE MASSES(kg)
,C6(mole/cubic m),PHASE DENSITIES(kg/cubic m),AND TIME INCREMENT

4.0E-04	Met/Slag
0.0	Met/Gas
4.0e-04	Slag/Gas
1473.0	
0.10	
0.05	
10.0	
7500.0	
3500.0	
0.01	

NUMBER OF ELEMENTS PRESENT
(INTEGER)
5

Appendix 3(b) Data file for current experiment simulation.

MASS TRANSFER COEFFICIENTS(cm/s)

METAL	SLAG	GAS	GAS		
0.000015	0.000010	0.040	0.040	O	SiO2
0.000015	0.000010	0.000	0.000		
0.000015	0.000010	0.000	0.000	Cu	CuO0.5
0.000015	0.000010	0.000	0.000	Fe	FeO1.5
0.000015	0.000010	0.000	0.000	Fe	FeO
0.000015	0.000010	0.000	0.000	Ni	NiO
0.000015	0.000010	0.000	0.000		
0.000015	0.000010	0.000	0.000		
0.000015	0.000010	0.000	0.000		
0.000015	0.000010	0.000	0.000		

BULK CONCENTRATIONS IN WEIGHT PERCENT

METAL	SLAG	GAS	GAS			
1.0E-05	40.0	1.0E-07	1.0E-07	O	SiO2	pO2
0.0	0.0	0.0	0.0			
98.86999	0.1	0.0	0.0	Cu	CuO0.5	
0.0	10.0	0.0	0.0		FeO1.5	
0.12	45.10	0.0	0.0	Fe	FeO	
0.01	4.8	0.0	0.0	Ni	NiO	
0.0	0.0	0.0	0.0			
0.0	0.0	0.0	0.0			
0.0	0.0	0.0	0.0			
0.0	0.0	0.0	0.0			

STOICHIOMETRY

METAL	SLAG	GAS	GAS		
0.0	0.0	0.0	0.0		
0.0	0.0	0.0	0.0		
0.5	0.5	0.0	0.0	Cu	CuO0.5
1.50	1.50	0.0	0.0	Fe	FeO1.5
1.0	1.0	0.0	0.0	Fe	FeO
1.0	1.0	0.0	0.0	Ni	NiO
0.0	0.0	0.0	0.0		
0.0	0.0	0.0	0.0		
0.0	0.0	0.0	0.0		
0.0	0.0	0.0	0.0		

HEATS OF FORMATION (IN CALORIES)

M/S	M/G	S/G	
-20500.0	0.0	0.0	1/2 (O2) = [O]
-67150.0	0.0	0.0	CO +1/2 O2 = CO2
-14190.0	0.0	0.0	Cu(l) + 1/4 O2 = CuO0.5
-97290.0	0.0	0.0	Fe(l) + 3/4 O2 = FeO1.5
-61200.0	0.0	0.0	Fe(l) + 1/2 O2 = FeO
-60490.0	0.0	0.0	Ni(l) + 1/2 O2 = NiO
0.0	0.0	0.0	
0.0	0.0	0.0	
0.0	0.0	0.0	
0.0	0.0	0.0	

ENTROPIES (IN CALORIES)

M/S	M/G	S/G	
-10.9	0.0	0.0	1/2 (O2) = [O]
-20.37	0.0	0.0	CO +1/2 O2 = CO2
-4.72	0.0	0.0	Cu(l) + 1/4 O2 = CuO0.5
-30.00	0.0	0.0	Fe(l) + 3/4 O2 = FeO1.5
-12.83	0.0	0.0	Fe(l) + 1/2 O2 = FeO
-22.99	0.0	0.0	Ni(l) + 1/2 O2 = NiO
0.0	0.0	0.0	
0.0	0.0	0.0	

ACTIVITY COEFFICIENTS

METAL	SLAG	
0.34	0.0	O
0.0	0.0	
1.0	5.0	Cu CuO0.5
15.95	1.0	Fe FeO1.5
15.95	0.0	Fe FeO
2.11	4.26	Ni NiO
0.0	0.0	
0.0	0.0	
0.0	0.0	
0.0	0.0	

MOLECULAR WEIGHTS (KG/MOLE)

METAL	SLAG	
0.016	0.060	O SiO2
0.012	0.0	C
0.0635	0.0715	Cu CuO0.5
0.0558	0.0798	Fe FeO1.5
0.0558	0.0718	Fe FeO
0.0587	0.0747	Ni NiO
0.0	0.0	
0.0	0.0	
0.0	0.0	
0.0	0.0	

INTERFACIAL AREAS(sq.m),TEMPERATURE(K),PHASE MASSES(kg)
,C6(mol/cubic m),PHASE DENSITIES(kg/cubic m),AND TIME INCREMENT

4.0E-04	Met/Slag
0.0	Met/Gas
4.0e-04	Slag/Gas
1473.0	
0.020	
0.005	
10.0	
7500.0	
3500.0	
0.01	

NUMBER OF ELEMENTS PRESENT
(INTEGER)
6

Appendix 3(c). Data file for slag cleaning simulation.

```
MASS TRANSFER COEFFICIENTS(cm/s)
   METAL     SLAG      GAS       GAS
 0.000015  0.000010    0.0001    0.0001  O
 0.000015  0.000010    0.0001    0.0001
 0.000015  0.000010    0.0001    0.0001   Cu   CuO0.5
 0.000015  0.000010    0.0001    0.0001   Fe   FeO1.5
 0.000015  0.000010    0.0001    0.0001   Fe   FeO
 0.000015  0.000010    0.0001    0.0001   Ni   NiO
 0.000015  0.000010    0.0001    0.0001   Sn   SnO
 0.000015  0.000010    0.0001    0.0001   Pb   PbO
 0.000015  0.000010    0.0001    0.0001   Zn   ZnO
 0.000015  0.000010    0.0001    0.0001
BULK CONCENTRATIONS IN WEIGHT PERCENT
   METAL     SLAG      GAS       GAS
 1.6E-05     41.0    4.5E-14   4.5E-14       O    SiO2     pO2
   0.0       0.0       0.0       0.0
 90.999984     5.0       0.0       0.0           Cu  CuO0.5
   0.0       1.0       0.0       0.0               FeO1.5
   5.0      45.0       0.0       0.0             Fe  FeO
   1.0       2.0       0.0       0.0             Ni  NiO
   1.0       2.0       0.0       0.0             Sn  SnO
   1.0       2.0       0.0       0.0             Pb  PbO
   1.0       2.0       0.0       0.0             Zn  ZnO
   0.0       0.0       0.0       0.0
STOICHIOMETRY
   METAL     SLAG      GAS       GAS
   1.0       1.0       0.0       0.0           O
   0.0       0.0       0.0       0.0
   0.5       0.5       0.0       0.0         CuO0.5
   1.50      1.50      0.0       0.0         FeO1.5
   1.0       1.0       0.0       0.0         FeO
   1.0       1.0       0.0       0.0         NiO
   1.0       1.0       0.0       0.0         SnO
   1.0       1.0       0.0       0.0         PbO
   1.0       1.0       0.0       0.0         ZnO
   0.0       0.0       0.0       0.0
HEATS OF FORMATION ( IN CALORIES )
    M/S       M/G       S/G
    0.0       0.0       0.0
 -67150.0       0.0       0.0                CO + 1/2 O2 = CO2
 -14190.0   73650.0   1000000.0              CuO0.5   Cu(g)   CuO0.5(g)
 -97290.0 1000000.0   1000000.0              FeO1.5   Fe(g)   FeO1.5(g)
 -61200.0 1000000.0   1000000.0              FeO      Fe(g)   FeO(g)
 -60490.0 1000000.0   1000000.0              NiO      Ni(g)   NiO(g)
 -62690.0 1000000.0     57990.0              SnO      Sn(g)   SnO(g)
 -43300.0   43490.0     51270.0              PbO      Pb(g)   PbO(g)
-110000.0   28230.0   1000000.0              ZnO      Zn(g)   ZnO(g)
    0.0       0.0       0.0
ENTROPIES (IN CALORIES)
    M/S       M/G       S/G
    0.0       0.0       0.0
  -20.37      0.0       0.0                 CO + 1/2 O2 = CO2
   -4.72     26.02      0.0                  CuO0.5   Cu(g)   CuO0.5(g)
  -30.00      0.0       0.0                  FeO1.5   Fe(g)   FeO1.5(g)
  -12.83      0.0       0.0                FeO      Fe(g)   FeO(g)
  -22.99      0.0       0.0                NiO      Ni(g)   NiO(g)
  -20.69      0.0     -32.27               SnO      Sn(g)   SnO(g)
  -16.26     21.54     28.69                 PbO      Pb(g)   PbO(g)
  -47.40     23.96      0.0                  ZnO      Zn(g)   ZnO(g)
```

ACTIVITY COEFFICIENTS

METAL	SLAG		
0.34	0.0	O	
0.0	0.0		
1.0	3.0	Cu	CuO0.5
15.95	1.0	Fe	FeO1.5
15.95	1.3	Fe	FeO
2.11	4.26	Ni	NiO
0.058	0.78	Sn	SnO
4.37	0.07	Pb	PbO
0.165	1.8	Zn	ZnO
0.0	0.0		

MOLECULAR WEIGHTS (KG/MOLE)

METAL	SLAG		
0.016	0.060	O	SiO2
0.012	0.0	C	
0.0635	0.0715	Cu	CuO0.5
0.0558	0.0798	Fe	FeO1.5
0.0558	0.0718	Fe	FeO
0.0587	0.0747	Ni	NiO
0.1187	0.1347	Sn	SnO
0.2072	0.2232	Pb	PbO
0.0654	0.0814	Zn	ZnO
0.0	0.0		

INTERFACIAL AREAS(sq.m),TEMPERATURE(K),PHASE MASSES(kg),
C6(mol/cubic m),PHASE DENSITIES(kg/cubic m),AND TIME INCREMENT

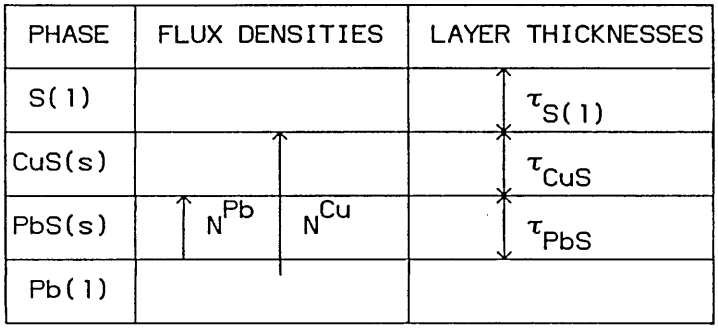
```
 4.0e-04
 4.0e-05
 4.0e-04
1473.0
 0.025
 0.010
 10.0
7500.0
3500.0
 0.01
```

NUMBER OF ELEMENTS PRESENT,
TOTAL PROCESS RUN-TIME (MINS.),AND BULK FEO ACTIVITY.

```
 9
600.0
0.4
```

Appendix 4. Decoppering Model Mathematical Formulation.

Layer Configuration One. Pb(l)/PbS/CuS/S(l).



$$N^{Cu} = k^{Cu}_{Pb}\, C_{Pb} \left(a^{Cu}_{Pb} - a^{Cu}_{Pb/PbS} \right) / \gamma^{Cu}_{Pb}$$

$$= D^{Cu}_{PbS}\, C_{PbS} \left(a^{Cu}_{Pb/PbS} - a^{Cu}_{PbSCuS} \right) / \left(\gamma^{Cu}_{PbS}\, \tau^{Cu}_{PbS} \right)$$

$$\approx D^{Cu}_{CuS}\, C_{CuS} \left(a^{Cu}_{PbS/CuS} - a^{Cu}_{CuS/S(l)} \right) / \left(\gamma^{Cu}_{CuS}\, \tau^{Cu}_{CuS} \right)$$

The approximate equality refers to the fact that N^{Cu} in CuS actually equals N^{Cu} in PbS plus N^{Pb}, each lead ion arriving dislodging a Cu ion which would diffuse towards the sulphur(and slightly change the interfacial Cu activity). However, we will assume N^{Pb} to be small.

Rearranging and adding,

$$a^{Cu}_{Pb} - a^{Cu}_{CuS/S(l)} =$$

$$N^{Cu} \left[\frac{\gamma^{Cu}_{Pb}}{k^{Cu}_{Pb}\, C_{Pb}} + \frac{\gamma^{Cu}_{PbS}}{D^{Cu}_{PbS}\, C_{PbS}} \tau^{PbS} + \frac{\gamma^{Cu}_{CuS}}{D^{Cu}_{CuS}\, C_{CuS}} \tau^{CuS} \right]$$

Let $R^{Cu}_{Pb} = \gamma^{Cu}_{Pb} / (k^{Cu}_{Pb} C_{Pb})$

$R^{Cu}_{PbS} = \gamma^{Cu}_{PbS} / (D^{Cu}_{PbS} C_{PbS})$

$R^{Cu}_{CuS} = \gamma^{Cu}_{CuS} / (D^{Cu}_{CuS} C_{CuS})$

Substitution gives,

$N^{Cu} = (a^{Cu}_{Pb} - a^{Cu}_{CuS/S(l)}) / (R^{Cu}_{Pb} + R^{Cu}_{PbS} \tau_{PbS} + R^{Cu}_{CuS} \tau_{CuS})$

$a^{Cu}_{CuS/PbS} = N^{Cu} R^{Cu}_{CuS} \tau_{CuS} + a^{Cu}_{CuS/S(l)}$

$a^{Pb}_{PbS/CuS} = a^{Cu}_{PbS/CuS} K^{CuS} / K^{PbS}$

$N^{Pb}_{PbS} = (1 - a^{Pb}_{PbS/CuS}) / (R^{Pb}_{PbS} \tau_{PbS})$

Conservation Equations

$d a^{Cu}_{Pb} / dt = N^{Cu} \text{ Area} / (C^{Pb} \text{ Vol})$

$d\tau^{PbS} / dt = N^{Pb} / C^{Pb}$

$d\tau^{CuS} / dt = N^{Cu} / C^{Cu}$

If $a^{Cu}_{PbS/CuS}$ becomes larger than the $CuS/CuS_{0.5}$ equilibrium copper potential, the $CuS_{0.5}$ will form.

Layer Configuration Two. $Pb(l)/PbS/CuS_{0.5}/S(l)$.

PHASE	FLUX DENSITIES	LAYER THICKNESSES
S(l)		$\tau_{S(l)}$
CuS(s)	N^{Cu}_{CuS}	τ_{CuS}
$CuS_{0.5}$(s)		$\tau_{CuS_{0.5}}$
PbS(s)	N^{Pb} N^{Cu}_{PbS}	τ_{PbS}
Pb(l)		

Solution of interfacial activities and fluxes in the Pb, PbS, and $CuS_{0.5}$ are similar to the previous layer configuration solution, only varying in that the resistances across the $CuS_{0.5}$ layer is different, and the $CuS_{0.5}$/CuS equilibrium Cu potential is higher than the CuS/S(l) equilibrium potential.

$$N^{Cu}_{Pb} = N^{Cu}_{PbS} = N^{Cu}_{CuS_{0.5}} =$$

$$a^{Cu}_{Pb} - \left(\frac{a^{Cu}_{CuS_{0.5}/CuS}}{R^{Cu}_{Pb} + R^{Cu}_{PbS}\,\tau_{PbS} + R^{Cu}_{CuS_{0.5}}\,\tau_{CuS_{0.5}}} \right)$$

$$N^{Cu}_{CuS} = \left(a^{Cu}_{CuS_{0.5}/CuS} - a^{Cu}_{CuS/S(l)} \right) / \left(R^{Cu}_{CuS}\,\tau_{CuS} \right)$$

$$a^{Cu}_{PbS/CuS_{0.5}} = N^{Cu}\,R^{Cu}_{CuS_{0.5}}\,\tau_{CuS_{0.5}} + a^{Cu}_{CuS_{0.5}/CuS}$$

$$a^{Pb}_{PbS/CuS_{0.5}} = \left(a^{Cu}_{PbS/CuS_{0.5}}\,K_{CuS_{0.5}} \right)^2 / E^{PbS}$$

$$N^{Pb}_{PbS} = \left(1 - a^{Pb}_{PbS/CuS_{0.5}} \right) / \left(R^{Pb}_{PbS}\,\tau_{PbS} \right)$$

Conservation Equations.

$$d\,a^{Cu}_{Pb} / dt = N^{Cu}_{Pb}\,Area / \left(C^{Pb}\,Vol \right)$$

$$d\tau_{PbS} / dt = N^{Pb} / C^{Pb}$$

$$d\,\tau_{CuS_{0.5}} / dt = \left(N^{Cu}_{CuS_{0.5}} - N^{Cu}_{CuS} \right) / C^{CuS_{0.5}}$$

$$d\tau_{CuS} / dt = 2\,N^{Cu}_{CuS} - N^{Cu}_{CuS_{0.5}}$$

If the sulphur runs out, we must go to another solution method.

Layer Configuration Three. $Pb(l)/PbS/CuS_{0.5}/CuS$.

PHASES	FLUX DENSITIES	LAYER THICKNESSES
CuS(s)		τ_{CuS}
$CuS_{0.5}(s)$		$\tau_{CuS_{0.5}}$
PbS(s)	N^{Pb} N^{Cu}	τ_{PbS}
Pb(l)		

This model is similar to the stage two model, differing only in that the copper flux through the CuS layer is negligible. There is no source or sink for diffusing copper ions at the top interface.

Layer Configuration Four. $Pb/PbS/CuS_{0.5}$.

PHASES	FLUX DENSITIES	LAYER THICKNESSES
$CuS_{0.5}(s)$		$\tau_{CuS_{0.5}}$
$PbS(s)$	N^{Pb} N^{Cu}	τ_{PbS}
$Pb(l)$		

There is no sink or source of Cu at the top interface. Thus, Pb arriving at the $PbS/CuS_{0.5}$ interface dislodges Cu, that diffuses back to the bullion giving reversion.

$$N^{Pb}_{PbS} = - 2N^{Cu} = - 2N^{Cu}_{Pb}$$

$$N^{Pb}_{PbS} = (1 - a^{Pb}_{PbS/CuS_{0.5}}) / (R^{Pb}_{PbS} \tau_{PbS})$$

$$N^{Cu}_{PbS} = (a^{Cu}_{Pb/PbS} - a^{Cu}_{PbS/CuS_{0.5}}) / (R^{Cu}_{PbS} \tau_{PbS})$$

$$N^{Cu}_{Pb} = (a^{Cu}_{Pb} - a^{Cu}_{Pb/PbS}) / R^{Cu}_{Pb}$$

$$a^{Pb}_{PbS/CuS_{0.5}} = (K_{CuS_{0.5}} a^{Cu}_{PbS/CuS_{0.5}}) / K_{PbS}$$

Solving these gives a quadratic in N^{Pb}_{PbS}.

$$4 N^{Pb}_{PbS} \left[(R^{Cu}_{Pb} + R^{Cu}_{PbS} \tau_{PbS})^2 + a^{Cu}_{Pb} (R^{Cu}_{Pb} + R^{Cu}_{PbS} \tau_{PbS}) \right] +$$

$$N^{Pb}_{PbS} \left[K^{PbS} R^{Pb}_{PbS} \tau_{PbS} / (K^{CuS_{0.5}})^2 \right] + (a^{Cu^2}_{Pb} + K^{PbS} / K^{CuS_{0.5}})$$

$$= 0$$

Conservation Equations.

$$d\,\tau_{CuS} / dt = -\,2\,N^{Pb}_{PbS} / C^{CuS}_{0.5}$$

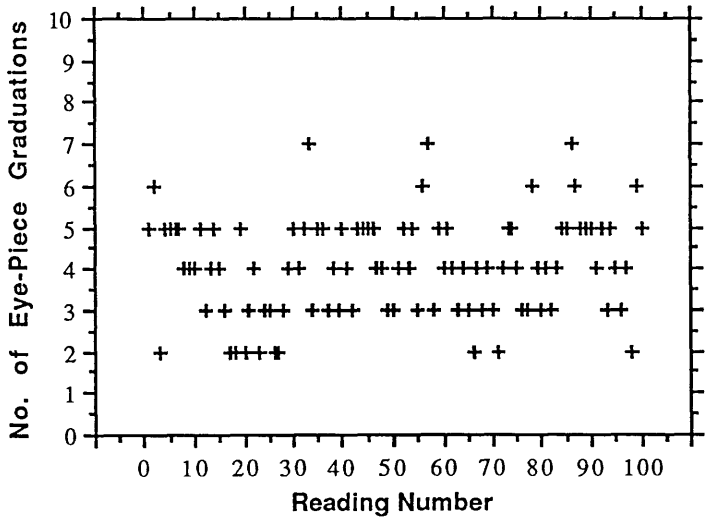
$$dx^{Cu}_{Pb} / dt = -\,2\,N^{Pb}_{PbS}\,(\,Area/Vol\,)\,/\,C^{Pb}$$

$$d\,\tau_{PbS} / dt = N^{Pb}_{PbS} / C^{PbS}$$

Appendix 5. Typical Layer Thickness Measurements and Explanation of Mathematical Manipulation.

The figure below shows a set of readings taken. Units of measurement are graduations on an eye-piece mounted grid. These measurements were converted to microns by calibration with a stage level graticule. The readings below are the worst set observed. A large number were taken to be sure the correlation was sufficiently high. Some difficulties were encountered as the limits of optical resolution were approached, as in this example.

Raw Data For Layer Thickness Measurements.
These represent the WORST set of data collected.



The highest and lowest value from each set were disguarded, then the remainder averaged. Sets of readings were taken from samples reacted for various times at some given conditions. Converting these values to centimeters, squaring them and ploting them against 2 x time (as described in section 10.2), linear regression was applied to find the line of best fit. The slope equals the effective diffusion coefficient.

The correlation coefficient was quoted in the results. Note that each experiment was repeated in triplicate. Reasonable agreement was always found between the three trials. Four reaction times were used, with three points at each time giving twelve points to regress. The intercept of the line of best fit was always close to the origin, indicating that the samples took little time to settle to the reaction temperature.

Appendix 6(a). Decoppering Model FORTRAN Code.

```
 PROGRAM DECOP(INPUT,OUTPUT,DECDAT,CU,LT,TAPE5=INPUT,
+       TAPE6= OUTPUT, TAPE2=CU,TAPE3=LT,TAPE1=DECDAT)
 CHARACTER DUMMY1,DUMMY2
 REAL LT,LAYER2
 DIMENSION XN(3,6),A(3,6),LT(6),C(6),D(3,6),E(4),AC(6),R(3,6)
C*************************************************
C*                                                *
C*            D A T A   E N T R Y                 *
C*                                                *
C*************************************************
 READ(1,10)DUMMY1,DUMMY2
 READ(1,*)((A(I,J),I=1,3),J=1,6)
 READ(1,10)DUMMY1,DUMMY2
 READ(1,*)((D(I,J),I=1,3),J=1,6)
 READ(1,10)DUMMY1,DUMMY2
 READ(1,*)(C(K),K=1,6)
 READ(1,10)DUMMY1,DUMMY2
 READ(1,*)(AC(J),J=1,6)
 READ(1,10)DUMMY1,DUMMY2
 READ(1,*)(LT(K),K=1,6)
 READ(1,10)DUMMY1,DUMMY2
 READ(1,*)(E(K),K=1,4)
 READ(1,10)DUMMY1,DUMMY2
 READ(1,*)AREA,VOL,DT
 10 FORMAT(A1)
C*************************************************
C*                                                *
C* P R E L I M I N A R Y   C A L C U L A T I O N S *
C*                                                *
C*************************************************
 TIME=0.0
 INT=10
 LAYER2=LT(2)*1000000.0
 PBCU05=(LT(2)+LT(3))*1000000.0
 ALL=(LT(2)+LT(3)+LT(4))*1000000.0
 THELOT=(LT(2)+LT(3)+LT(4)+LT(5))*1000000.0
 BULKCU=A(2,1)/3.226
CWRITE(6,200)TIME,A(2,1),LT(2),LT(3),LT(4),LT(5)
CWRITE(2,200)TIME,A(2,1),LAYER2,PBCU05,ALL,THELOT
 200 FORMAT(10E10.3)
 DO 20 J=1,6
        DO 30 I=1,3
              R(I,J)=AC(I)/(D(I,J)*C(J))
        30 CONTINUE
 20 CONTINUE
C*************************************************
C*                                                *
C*   SOLUTION OF PB/PBS/CUS/S(L) MODEL -- STAGE ONE *
C*                                                *
C*************************************************
 1111 CONTINUE
 XN(2,1)=(A(2,1)-A(2,5))/(R(2,1)+R(2,2)*LT(2)+R(2,4)*LT(4))
 A(2,3)=XN(2,1)*R(2,4)*LT(4)+A(2,5)
 A(1,3)=A(2,3)*E(4)/E(2)
 XN(1,2)=(1.0-A(1,3))/(R(1,2)*LT(2))
C  CONSERVATION EQUATIONS ----------------------------------------
 A(2,1)=A(2,1)-XN(2,1)*DT*AC(1)*AREA/(C(1)*VOL)
 LT(2)=LT(2)+XN(1,2)*DT/C(2)
 LT(4)=LT(4)+XN(2,1)*DT/C(4)
 LT(5)=LT(5)-(XN(2,1)+XN(1,2))*DT/C(5)
 TIME=TIME+DT
 IF(TIME.GE.DT*100.0)DT=DT*10.0
C OUTPUT RESULTS TO FILE "RESULT" -----------------------------
```

```
 LAYER2=LT(2)*1000000.0
 PBCU05=(LT(2)+LT(3))*1000000.0
 ALL=(LT(2)+LT(3)+LT(4))*1000000.0
 THELOT=(LT(2)+LT(3)+LT(4)+LT(5))*1000000.0
 BULKCU=A(2,1)/3.226
C TEST FOR CUS0.5 FORMATION ----------------------------------
 IF(A(2,3).GE.A(2,4))THEN
C                 WRITE(6,300)TIME
                  300 FORMAT('CUS0.5 FORMED AFTER',E10.3,' SECS')
                  GOTO 2222
 END IF
C TEST FOR S(L) DEPLETION
 IF(LT(5).LE.0.0)THEN
C                WRITE(6,400)TIME
                 400 FORMAT('SULPHUR GONE AFTER',E10.3,' SECS')
                 LT(5)=0.0
                 GOTO 3333
 END IF
 IF(INT.GE.10)THEN
 INT=0
 BULKCU=A(2,1)/3.226
CWRITE(6,200)TIME,A(2,1),LT(2),LT(3),LT(4),LT(5)
 WRITE(2,200)TIME,BULKCU
 WRITE(3,200)TIME,LAYER2,PBCU05,ALL,THELOT
 END IF
 INT=INT+1
 GOTO 1111
C*************************************************
C*                                                *
C*    SOLUTION TO PB/PBS/CUS0.5/CUS/S(L) MODEL -- STAGE TWO       *
C*                                                *
C*************************************************
 2222 CONTINUE
 XN(2,1)=(A(2,1)-A(2,4))/(R(2,1)+R(2,2)*LT(2)+R(2,3)*LT(3))
 A(2,2)=XN(2,1)*R(2,3)*LT(3)+A(2,4)
 A(1,2)=A(2,2)*E(3)*A(2,2)*E(3)/E(2)
 XN(1,2)=(1.0-A(1,2))/(R(1,2)*LT(2))
 XN(2,4)=(A(2,4)-A(2,5))/(LT(4)*R(2,4))
C  CONSERVATION EQUATIONS ---------------------------------------
 A(2,1)=A(2,1)-XN(2,1)*DT*AC(1)*AREA/(C(1)*VOL)
 LT(2)=LT(2)+XN(1,2)*DT/C(2)
 LT(3)=LT(3)+2.0*(XN(2,1)-XN(2,4))*DT/C(3)
 LT(4)=LT(4)+(2.0*XN(2,4)-XN(2,1))*DT/C(4)
 LT(5)=LT(5)-(XN(2,4)+XN(1,2))*DT/C(5)
 TIME=TIME+DT
 IF(TIME.GE.DT*100.0)DT=DT*10.0
C OUTPUT RESULTS TO FILE "RESULT" ------------------------------
 LAYER2=LT(2)*1000000.0
 PBCU05=(LT(2)+LT(3))*1000000.0
 ALL=(LT(2)+LT(3)+LT(4))*1000000.0
 THELOT=(LT(2)+LT(3)+LT(4)+LT(5))*1000000.0
 BULKCU=A(2,1)/3.226
C TEST FOR S(L) DEPLETION -------------------------------------
 IF(LT(5).LE.0.0)THEN
C                WRITE(6,400)TIME
                 LT(5)=0.0
                 GOTO 3333
 END IF
 IF(INT.GE.10)THEN
 INT=0
 BULKCU=A(2,1)/3.226
CWRITE(6,200)TIME,A(2,1),LT(2),LT(3),LT(4),LT(5)
 WRITE(2,200)TIME,BULKCU
 WRITE(3,200)TIME,LAYER2,PBCU05,ALL,THELOT
 END IF
```

```
 INT=INT+1
 GOTO 2222
C************************************************
C*                                                *
C*    SOLUTION TO PB/PBS/CUS0.5/CUS MODEL -- STAGE THREE          *
C*                                                *
C************************************************
 3333 CONTINUE
 XN(2,1)=(A(2,1)-A(2,4))/(R(2,1)+R(2,2)*LT(2)+R(2,3)*LT(3))
 A(2,2)=XN(2,1)*R(2,3)*LT(3)+A(2,4)
 A(1,2)=A(2,2)*E(3)*A(2,2)*E(3)/E(2)
 XN(1,2)=(1.0-A(1,2))/(R(1,2)*LT(2))
C  CONSERVATION EQUATIONS ----------------------------------------
 A(2,1)=A(2,1)-XN(2,1)*DT*AC(1)*AREA/(C(1)*VOL)
 LT(2)=LT(2)+XN(1,2)*DT/C(2)
 LT(3)=LT(3)+2.0*(XN(2,1)+XN(1,2))*DT/C(3)
 LT(4)=LT(4)-(XN(2,1)+4.0*XN(1,2))*DT/C(4)
 TIME=TIME+DT
 IF(TIME.GE.DT*100.0)DT=DT*10.0
C OUTPUT RESULTS TO FILE "RESULT" ------------------------------
 LAYER2=LT(2)*1000000.0
 PBCU05=(LT(2)+LT(3))*1000000.0
 ALL=(LT(2)+LT(3)+LT(4))*1000000.0
 THELOT=ALL
 BULKCU=A(2,1)/3.226
C TEST FOR CUS CONSUMPTION  ------------------------------------
 IF(LT(4).LE.0.0)THEN
C                 WRITE(6,500)TIME
                  500 FORMAT('CUS GONE AFTER',E10.3,' SECS')
                  LT(4)=0.0
                  GOTO 4444
 END IF
 IF(INT.GE.10)THEN
 INT=0
 BULKCU=A(2,1)/3.226
CWRITE(6,200)TIME,A(2,1),LT(2),LT(3),LT(4),LT(5)
 WRITE(2,200)TIME,BULKCU
 WRITE(3,200)TIME,LAYER2,PBCU05,ALL,THELOT
 END IF
 INT=INT+1
 GOTO 3333
C************************************************
C*                                                *
C*    SOLUTION OF PB/PBS/CUS0.5 MODEL -- STAGE FOUR               *
C*                                                *
C************************************************
 4444 CONTINUE
 A1=4.0*(R(2,1)+R(2,2)*LT(2))**2.0
 B1=4.0*A(2,1)*(R(2,1)+R(2,3)*LT(2))+E(2)*R(1,2)*LT(2)/E(3)**2.0
 C1=A(2,1)**2.0-E(2)/E(3)**2.0
 XN(1,2)=(-B1+(B1*B1-4.0*A1*C1)**0.5)/(2.0*A1)
C  CONSERVATION EQUATIONS ----------------------------------------
 A(2,1)=A(2,1)+2.0*XN(1,2)*DT*AC(1)*AREA/(C(1)*VOL)
 LT(2)=LT(2)+XN(1,2)*DT/C(2)
 LT(3)=LT(3)-2.0*XN(1,2)*DT/C(3)
 TIME=TIME+DT
 IF(TIME.GE.DT*100.0)DT=DT*10.0
C OUTPUT RESULTS TO FILE "RESULT" ------------------------------
 LAYER2=LT(2)*1000000.0
 PBCU05=(LT(2)+LT(3))*1000000.0
 ALL=PBCU05
 THELOT=ALL
 BULKCU=A(2,1)/3.226
C TEST FOR CUS0.5 CONSUMPTION  ---------------------------------
 IF(LT(3).LE.0.0)THEN
```

```
C               WRITE(6,600)TIME
                600 FORMAT('REVERSION COMPLETE AFTER ',E10.3,' SECS')
                LT(3)=0.0
                GOTO 9999
 END IF
 IF(INT.GE.10)THEN
 INT=0
 BULKCU=A(2,1)/3.226
CWRITE(6,200)TIME,A(2,1),LT(2),LT(3),LT(4),LT(5)
 WRITE(2,200)TIME,BULKCU
 WRITE(3,200)TIME,LAYER2,PBCU05,ALL,THELOT
 END IF
 INT=INT+1
 GOTO 4444
 9999 CONTINUE
CWRITE(6,200)TIME,A(2,1),LT(2),LT(3),LT(4),LT(5)
 WRITE(2,200)TIME,BULKCU
 WRITE(3,200)TIME,LAYER2,PBCU05,ALL,THELOT
CWRITE(6,200)TIME,A(2,1),LT(2),LT(3),LT(4),LT(5)
CWRITE(2,200)TIME,A(2,1),LAYER2,PBCU05,ALL,THELOT
 END
```

Appendix 6(b). Data input file for the Decoppering Model
(Case where Ag is present).

```
INITIAL ACTIVITIES
   LEAD   COPPER  SULPHUR
    0.0    0.163     0.0      Pb (bulk)
    1.0    0.150     0.0      Pb/PbS
    0.0     0.0      0.0
    0.0  3.90E-05    0.0      CuS0.5/CuS
    0.0  2.84E-07    0.439    CuS/S(l)
    0.0     0.0      0.439    S(l)/S2(g)
DIFFUSION AND MASS TRANSFER COEFFICIENTS(sq.m/sec)
   LEAD   COPPER  SULPHUR
    1.0   1.0E-05     1.0    Pb
 5.1E-15  1.3E-01     1.0    PbS
    1.0   1.0E+01     1.0    CuS0.5
    1.0   1.0E+01     1.0    CuS
    1.0     1.0       1.0    S(l)
    1.0     1.0     1.0E+01  S2(g)
BULK MOLAR
CONCENTRATIONS (mol/cubic m)
54831.0  Pb
31715.0  PbS
70625.0  CuS0.5
48750.0  CuS
31250.0  S(l)
 46.64   S2(g)
ACTIVITY COEFFICIENTS OF COPPER
( V.ROUGH ESTIMATES,MOSTLY )
 92.0  Pb
 1.0   PbS
 1.0   CuS0.5
 1.0   CuS
 0.0
 0.0
INITIAL LAYER
THICKNESS (m)
    1.0       Pb
 1.0E-08      PbS
 1.0E-08      CuS0.5
 1.0E-08      CuS
 0.64E-05     S(l)
    1.0       S2(g)
EQUILIBRIUM
CONSTANTS
    0.0
4.052E+09  Pb+1/2 S2(g) = PbS
3.689E+05  Cu+1/4 S2(g) = CuS0.5
5.513E+06  Cu+1/2 S2(g) = CuS
INTERFACIAL AREA(sq.cm), BULK VOLUME(l) AND
TIME INCREMENT (sec)
 0.1
 0.001
 0.05
```

Appendix 6(c) . Data input file for the Decoppering Model
(Ag Free Case)

```
ACTIVITIES
   LEAD   COPPER  SULPHUR
    0.0    0.163     0.0    Pb(bulk)
    1.0    0.150     0.0    Pb/PbS
    0.0     0.0      0.0
    0.0  3.90E-05    0.0    CuS0.5/CuS
    0.0  2.84E-07   0.439 CuS/S(l)
    0.0     0.0     0.439 S(l)/S2(g)
DIFFUSION AND MASS TRANSFER COEFFICIENTS (sq.m/sec)
   LEAD   COPPER  SULPHUR
    1.0    1.0E-05    1.0    Pb
 1.0E-10  1.3E-01    1.0    PbS
    1.0    1.0E+01    1.0    CuS0.5
    1.0    1.0E+01    1.0    CuS
    1.0     1.0       1.0    S(l)
    1.0     1.0     1.0E+01  S2(g)
BULK MOLAR
CONCENTRATIONS (mol/cubic m.)
54831.0    Pb
31715.0    PbS
70625.0    CuS0.5
48750.0    CuS
31250.0    S(l)
 46.64     S2(g)
ACTIVITY COEFFICIENTS OF COPPER
( V.ROUGH ESTIMATES,MOSTLY )
 92.0   Pb
  1.0   PbS
  1.0   CuS0.5
  1.0   CuS
  0.0
  0.0
INITIAL LAYER
THICKNESS (m)
    1.0     Pb
 1.0E-08  PbS
 1.0E-08  CuS0.5
 1.0E-08  CuS
 0.8E-05  S(l)
    1.0     S2(g)
EQUILIBRIUM
CONSTANTS
    0.0
4.052E+09   Pb + 1/2 S2 = PbS
3.689E+05   Cu + 1/4 S2 = CuS0.5
5.513E+06   Cu + 1/2 S2 = CuS
INTERFACIAL AREA(sq.cm), BULK VOLUME(l) AND
TIME INCREMENT(sec)
 0.1
 0.001
 0.05
```

ACKNOWLEDGEMENTS.

The author wishes to thank all those who have made this work possible, and in particular,

Dr. Brian Terry, for his supervision, understanding and support.

Prof. Paul Grieveson, for his advice and encouragement.

Prof. David Robertson, for initiating the work.

S.E.R.C. for financial support.

Members of the John Percy Group, and the J.P.D.C., for the help, hinderance, humour, comraderie and tolerance; most notably, Alex Neve, Dr. Charlie Marsden, Kev Douglas, John Durn, Rags, Jay, and Branimir.

Finally, to my family, who provided more support than they are aware.